UNCLASSIFIED

AD NUMBER

AD827107

NEW LIMITATION CHANGE

TO

Approved for public release, distribution unlimited

FROM

Distribution authorized to U.S. Gov't. agencies and their contractors; Administrative and Operational Use, Export Control; Dec 1967. Other requests shall be referred to the Air Force Materials Laboratory, Attn: MAYT, Wright-Paterson AFB, OH 45433.

AUTHORITY

AFML, per ltr 14 Jan 1969

THIS PAGE IS UNCLASSIFIED

AFML-TR-67-251

AD827107

INVESTIGATION OF RADIATION AND CONDUCTION HEAT TRANSFER IN FIBROUS HIGH TEMPERATURE INSULATIONS

EDMUND J. ROLINSKI
GEORGE V. PURCELL, CAPTAIN, USAF

TECHNICAL REPORT AFML-TR-67-251

DECEMBER 1967

This document is subject to special e: rt controls and each transmittal to foreign governments or foreign nati ls may be made only with prior approval of the Air Force Materials Laboratory (MAYT), Wright-Patterson Air Force Base, Ohio 45433.

AIR FORCE MATERIALS LABORATORY
RESEARCH AND TECHNOLOGY DIVISION
AIR FORCE SYSTEMS COMMAND
WRIGHT-PATTERSON AIR FORCE BASE, OHIO

DDC
RETRIEVED
FEB 21 1968
B

158

NOTICE

When Government drawings, specifications, or other data are used for any purpose other than in connection with a definitely related Government procurement operation, the United States Government thereby incurs no responsibility nor any obligation whatsoever; and the fact that the Government may have formulated, furnished, or in any way supplied the said drawings, specifications, or other data, is not to be regarded by implication or otherwise as in any manner licensing the holder or any other person or corporation, or conveying any rights or permission to manufacture, use, or sell any patented invention that may in any way be related thereto.

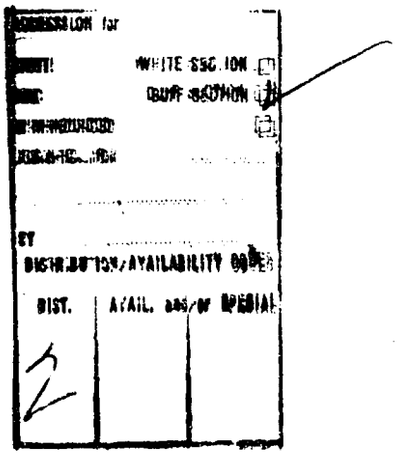

Copies of this report should not be returned unless return is required by security considerations, contractual obligations, or notice on a specific document.

300 - January 1968 - CO455 - 23-500

ABSTRACT

The experimental investigation was concerned with understanding the mechanisms by which fibrous insulations attenuate the transfer of thermal energy. Three fibrous insulation materials, Dynaquartz, Sapphire Wool, and Dynaflex, were evaluated for their usefulness in the high temperature environment. Effective thermal conductivities were measured in air, argon, and vacuum up to 2500°F. Transmission experiments were carried out to evaluate the relative contribution of radiation attenuation parameters for Dynaquartz.

(Distribution of this abstract is unlimited.)

AFML-TR-67-251

INVESTIGATION OF RADIATION AND CONDUCTION HEAT TRANSFER IN FIBROUS HIGH TEMPERATURE INSULATIONS

EDMUND J. ROLINSKI

GEORGE V. PURCELL, CAPTAIN, USAF

This document is subject to special export controls and each transmittal to foreign governments or foreign nationals may be made only with prior approval of the Air Force Materials Laboratory (MAYT), Wright-Patterson Air Force Base, Ohio 45433.

FOREWORD

This report was prepared jointly by the Materials Physics Division and the Materials Applications Division of the Air Force Materials Laboratory. The work was initiated under Project No. 7360, "The Chemistry and Physics of Materials," Task No. 736001, "Heat Transfer and Thermodynamics," and Project No. 7381, "Materials Application," Task No. 738103, "Materials Information Development, Collection, and Processing." The work was administered under the direction of the Air Force Materials Laboratory, Air Force Systems Command, Wright-Patterson Air Force Base, Ohio, with Mr. Edmund J. Rolinski (MAYT) and George V. Purcell, Capt, USAF (MAAE), Project Engineers.

This research was conducted during the period September 1965 to September 1967. Portions of this report were submitted to the Faculty of the Chemical Engineering Department, Ohio State University in June 1966 as the Master's Thesis of Edmund J. Rolinski. The report was submitted by the authors in July 1967 for publication as a technical report.

Mr. E. J. Rolinski gratefully acknowledges the guidance provided by his advisor at Ohio State University, Prof. Thomas L. Sweeney.

Appreciation is also extended to Dr. A. E. Wechsler of Arthur D. Little, Inc., and Dr. Emile Rutner and Mr. Raymond Prezecki, Materials Physics Division, Air Force Materials Laboratory, for their help and continued discussions, and to Ken Almon and others of the Johns-Manville Company for their cooperation in acquiring the Dynaquartz and Dynaflex samples used in this investigation.

All of the items compared in this report were commercial items that were not developed or manufactured to meet Government specifications, to withstand the tests to which they were subjected, or to operate as applied during this study. Any failure to meet the objectives of this study is no reflection on any of the commercial items discussed herein or on any manufacturer.

This technical report has been reviewed and is approved.

Albert O Olevitch

ALBERT A. OLEVITCH
Chief, Materials Engineering Branch
Materials Applications Division
Air Force Materials Laboratory

Hyman Marcus

HYMAN MARCUS
Acting Chief, Thermo and Chemical Physics Branch
Materials Physics Division
Air Force Materials Laboratory

TABLE OF CONTENTS

SECTION		PAGE
I	INTRODUCTION	1
II	THEORY	3
	1. Conduction	3
	a. Gas Conduction	3
	b. Solid Conduction	5
	2. Radiation	8
III	EXPERIMENTAL	14
	1. Spectral Transmission Experiments	15
	a. Description of Equipment	15
	b. Spectral Transmission Data	15
	c. Calculation of Integrated Transmission From Spectral Transmission Data	22
	2. Total Transmission Experiments	24
	a. Description of Equipment	24
	b. Calculation of Optical Scattering and Absorption Cross Sections	27
	3. Calculation of Radiation Cross Section From Electromagnetic Theory	33
	4. Discussion of Radiation Transmission Experiments	35
	5. Thermal Conductivity Experiments	37
	a. Description of Equipment	37
	b. Thermal Conductivity Measurements	44
	(1) Thermal Conductivity Measurements in Air	49
	(2) Thermal Conductivity Measurements in Vacuum	51
	(3) Thermal Conductivity Measurements in Argon	53
	(4) Summary of Thermal Conductivity Measurements on Dynaquartz	55
	c. Comparison of Thermal Conductivity Data	55
	(1) Dynaquartz in Air	60
	(2) Dynaquartz in Vacuum	60
	d. Discussion of Thermal Conductivity of Dynaquartz	63

TABLE OF CONTENTS (CONT)

SECTION		PAGE
	e. Thermal Conductivity of Sapphire Wool	66
	f. Thermal Conductivity of Dynaflex	66
IV	SUMMARY AND CONCLUSIONS	76
	1. Summary	76
	2. Conclusions	79
APPENDIXES		
I	Thermocouple Detector Sensitivity	81
II	Material Characteristics of Dynaquartz	87
III	Spectral Transmission and Integrated Transmission Calculations	89
IV	Error Analysis	96
V	Raw Data for Thermal Conductivity Measurements	99
VI	Correction for Zirconia Pins in Thermal Conductivity Measurements	125
REFERENCES		134-137
BIBLIOGRAPHY		138-139

ILLUSTRATIONS

FIGURE		PAGE
1.	Schematic of Insulation Sample	10
2.	Optical Path of Beckman IR-6 Single Beam Recording Spectrophotometer	16
3.	Spectral Transmission for Two Thicknesses of Dynaquartz	17
4.	Spectral Transmission for 0.045 Inch Thickness of Dynaquartz at Elevated Temperatures	18
5.	Spectral Transmission for 0.030 Inch Thickness of Dynaquartz at Elevated Temperatures	19
6.	Spectral Transmission for Three Thicknesses of Sapphire Wool	23
7.	Schematic Diagram of Experimental Apparatus for Total Transmission at 20°C Sample Temperature	26
8.	Schematic Diagram of Experimental Apparatus for Total Transmission at 400° and 600°C Sample Temperatures	29
9.	Schematic Diagram of Experimental Apparatus for Total Transmission at 700° and 800°C Sample Temperatures	30
10.	Overall View of Elevated Temperature Thermal Conductivity Apparatus	38
11.	Schematic Diagram of Test Stack	39
12.	Overall View of Test Stack	40
13.	Main and Guard Heater Configuration	41
14.	Bottom Dynaquartz Sample with Zirconia Pins	43
15.	Power and Control Circuits for Elevated Temperature Thermal Conductivity Apparatus	45
16.	Schematic Diagram of Hot Face Thermocouple Placement	46
17.	Schematic Diagram of Cold Face Thermocouple Placement	47

ILLUSTRATIONS (CONT)

FIGURE		PAGE
18.	Top Dynaquartz Sample and Thermocouple Placement with Differential, Main, and Guard Thermocouples	48
19.	Effective Thermal Conductivity of Dynaquartz (6.2 pcf) in Air Correcting for Zirconia Pins	50
20.	Effective Thermal Conductivity of Dynaquartz (6.2 pcf) in Vacuum Correcting for Zirconia Pins	52
21.	Effective Thermal Conductivity of Dynaquartz (6.2 pcf) in Argon (1 atm) Correcting for Zirconia Pins	54
22.	Effective Thermal Conductivity of Dynaquartz (6.2 pcf) in Air, Argon, and Vacuum at Elevated Temperatures	56
23.	Comparison of Effective Thermal Conductivity of Dynaquartz in Air	61
24.	Comparison of Effective Thermal Conductivity of Dynaquartz in Vacuum	62
25.	Logarithmic Plot of Effective Thermal Conductivity Versus Temperature for Dynaquartz	65
26.	Effective Thermal Conductivity of Dynaquartz by Superposition	67
27.	Thermal Conductivity of Sapphire Wool (1 pcf) in Air Corrected for Zirconia Pins	69
28.	Effective Thermal Conductivity of Dynaflex (8-10 pcf) in Air	74
29.	Dynaflex Samples (8-10 pcf) After Thermal Conductivity Measurements in Vacuum	75
30.	Schematic Diagram of Thermocouple Detector	82
31.	Thermocouple Response Versus Distance	83
32.	Linearity Plot of Thermocouple Detector	84

SYMBOLS

a	mathematical parameter defined by equation in Appendix IV
A	area of test section (see Appendix V), ft^2
A_1	mathematical constant in Equation 3
A_2	mathematical constant in Equation 5
A_3	empirical constant in Equation 51
A_c	area of fiber contact (see Equation 10), ft^2
A_d	area of detector (see Appendix I), cm^2
A_D	area of test sample subtracting zirconia pins (see Appendix VI), ft^2
A_h	area of black body emitting orifice (see Appendix I), cm^2
A_{pins}	area of zirconia pins in sample (see Appendix VI), 0.3125 $in.^2$
A_{total}	total area of sample with zirconia pins (see Appendix VI), 16 $in.^2$
A_o, A_n	scattering function (see Equation 39)
b	contact diameter (see Equation 12), ft
B	backward scattering component; fraction of scattered radiation scattered into a background hemisphere (see Equations 18 and 19), dimensionless
C_1	constant in Equation 30, $3.74(10^{-5})$ erg-cm^2/sec
C_2	constant in Equation 30, 1.439 cm-°K
C_c	compression load on fibers (see Equation 10), lb_f/ft^2
C_v	specific heat at constant volume, BTU/lb_m-°F
d	half width of gap separating the test area and guard heaters (see Appendix IV), inch
D_f	diameter of fiber (see Equations 15 and 40), microns

TABLES (CONT)

TABLE		PAGE
XVIII	Thermal Conductivity of Dynaflex (8-10 pcf) in Vacuum ($< 10^{-4}$ Torr)	72
XIX	Thermal Conductivity of Dynaflex (8-10 pcf) in Helium (1 atm)	73
XX	Least Square Parameters of Thermal Conductivity Data	77
XXI	Experimental Conditions of Thermal Conductivity Measurements	78
XXII	Thermocouple Detector Sensitivity	85
XXIII	Spectral and Integrated Transmission Data on Dynaquartz (6.2 pcf)	90-95
XXIV	Raw Data for Thermal Conductivity Using Guarded Hot Plate Apparatus	100-124
XXV	Correction for Zirconia Pins in Guarded Hot Plate Measurements	126-132

TABLES

TABLE		PAGE
I	Characteristics of Insulations Studied	2
II	Beckman IR-6 Room Temperature Transmission Data for Dynaquartz (6.2 pcf) Using Nernst Glower	20
III	Perkin-Elmer 12U Room Temperature Transmission Data for Dynaquartz (6.2 pcf) Using Filament Glower	21
IV	Values for Integrated Transmission Calculated From Spectral Transmission Data on Dynaquartz (6.2 pcf)	25
V	Total Transmission Data on Dynaquartz (6.2 pcf) (Sample at Room Temperature)	28
VI	Total Transmission Data on Dynaquartz (6.2 pcf) (Sample and Source Temperature Same)	31
VII	Calculated Cross Sections From Measured Total Transmission of Dynaquartz (6.2 pcf)	32
VIII	Calculated Values of Backscattered Energy and Scattering Cross Sections for Dynaquartz (6.2 pcf)	34
IX	Calculated Cross Sections From Integrated Total Transmission of Dynaquartz (6.2 pcf) Using Spectral Transmission Data	36
X	Comparison of Calculated Cross Sections of Dynaquartz (6.2 pcf) for Various Source Temperatures	36
XI	Chemical Analysis of Zirconia	44
XII	Thermal Conductivity of Dynaquartz (6.2 pcf) in Air, Composite Data	57
XIII	Thermal Conductivity of Dynaquartz (6.2 pcf) in Argon (1 atm)	58
XIV	Thermal Conductivity of Dynaquartz (6.2 pcf) in Vacuum ($<10^{-4}$ Torr)	59
XV	Thermal Conductivity of Sapphire Wool (1 pcf) in Air (1 atm)	68
XVI	Thermal Conductivity of Dynaflex (8-10 pcf) in Air	70
XVII	Thermal Conductivity of Dynaflex (8.2 pcf) in Air	71

SYMBOLS (CONT)

E	modulus of elasticity
E_{bb}	energy of black body emitted per unit time, σT^4, (see Appendix I), BTU/hr
$(E_{bb})_n$	black body energy emitted normal to cavity (see Appendix I), BTU/hr
$(E_{bb})_\theta$	energy of black body emitted per unit time per unit solid angle in a direction θ from normal (see Appendix I), BTU/hr
$(E_{bb})_\lambda$	energy of black body emitted per unit time per unit solid angle for monochromatic component (see Appendix III), BTU/hr
$E_n(r)$	energy incident on the detector normal to source at distance r from source (see Appendix I), watts
F	function in Equation 15
$g(\lambda, T)$	distribution function defined in Equation 30
G	load per contact (see Equation 12) $lb_f/in.^2$
h	thickness of test sample (Appendix IV), inch
H	integrated transmission (see Equation 31), dimensionless
i	current, amperes
I	transmitted intensity of radiant flux through sample
I_o	transmitted intensity of radiant flux in air
I_1	radiant flux density in the positive x direction (see Equations 18 and 19), $BTU/hr\text{-}ft^2$
I_2	radiant flux density in the negative x direction (see Equations 18 and 19) $BTU/hr\text{-}ft^2$
J	index of refraction (see Equations 27 and 51), dimensionless
J_i	imaginary part of complex index of refraction (see Equation 43)
J_r	real part of complex index of refraction (see Equation 43)

SYMBOLS (CONT)

k	thermal conductivity (see Equation 2), BTU-in./hr-ft^2-°F
$(k_{app})_s$	apparent thermal conductivity due to solid contact, BTU-in./hr-ft^2-°F
k_{BOT}	thermal conductivity of bottom specimen (see Appendix V), BTU-in./hr-ft^2-°F
k_D	thermal conductivity of sample corrected for zirconia pins (see Appendix VI), $\frac{\text{BTU-in.}}{\text{hr-ft}^2\text{-°F}}$
k_{eff}	effective or total thermal conductivity, BTU-in./hr-ft^2-°F
k_{gas}	thermal conductivity of gas phase, $\frac{\text{BTU-in.}}{\text{hr-ft}^2\text{-°F}}$
$(k_{gas})_p$	thermal conductivity of gas at pressure p, BTU-in./hr-ft^2-°F
$(k_{gas})_{p_o}$	thermal conductivity of gas at pressure p_o, BTU-in./hr-ft^2-°F
k_{pins}	thermal conductivity of zirconia pins (see Appendix VI), BTU-in./hr-ft^2-°F
k_r	thermal conductivity due to radiation (see Equation 28), BTU-in./hr-ft^2-°F
k_s	thermal conductivity due to solid conduction of matrix material, BTU-in./hr-ft^2-°F
k_{top}	thermal conductivity of top specimen (see Appendix V), BTU-in./hr-ft^2-°F
k_{total}	total thermal conductivity of a specimen including zirconia pins (see Appendix VI), BTU-in./hr-ft^2-°F
K	coefficient of thermocouple sensitivity (see Appendix I), $\mu v/\mu w$
K_a	absorption coefficient of a fiber (see Equation 42)

SYMBOLS (CONT)

K_s	backscattering coefficient of a fiber (see Equation 42)
L	specimen thickness taken in positive x direction (see Equations 26, 36, and 37), inches
L_g	effective interfiber distance (see Equations 3 and 4), microns
L_m	mean free path of gas molecules (see Equation 3), microns
L_{m_o}	mean free path of gas molecules at pressure p_o (see Equation 4), microns
m	slope of thermocouple sensitivity plot (see Appendix I), $\mu v/\mu w$
M	interception cross section per unit volume (see Equation 23) $inch^{-1}$
n	number of scatters per unit volume (see Equations 18 and 19)
N	scattering cross section per unit volume (see Equation 21), $inch^{-1}$
p	gas pressure (see Equation 4), $lb_f/in.^2$
p_o	gas pressure at temperature T_o (see Equation 4) $lb_f/in.^2$
P	absorption cross section per unit volume (see Equation 22), $inch^{-1}$
P_o, P_n	scattering function (see Equation 39)
pcf	lb/ft^3
q	heat flow, power (see Equation 1), BTU/hr
q_o	heat transfer directly across gap (see Appendix IV), BTU/hr-°F imbalance
q_{BOT}	heat flow or power transferred to bottom specimen (see Appendix V), BTU/hr
$(q_{BOT})_{total}$	total heat flow to bottom specimen (see Appendix V) BTU/hr

SYMBOLS (CONT)

q_{cond}	heat flow by mechanism of conduction, BTU/hr
q_{conv}	heat flow by mechanism of convection, BTU/hr
q_D	corrected heat flow or power to sample (see Appendix VI), BTU/hr
q_{eff}	effective heat flow or power, BTU/hr
q_{pins}	heat flow or power to zirconia pins (see Appendixes V and VI), BTU/hr
q_{rad}	heat flow by radiation, BTU/hr
q_{top}	heat flow or power transferred to top specimen (see Appendix V), BTU/hr
Q	total heat flux density for a constant cross section (see Equation 26 and 27), BTU/hr-ft^2
Q_{BOT}	heat flux density in bottom specimen (see Appendix V), BTU/hr-ft^2
Q_{top}	heat flux density in top specimen (see Appendix V), BTU/hr-ft^2
r	distance from source (see Appendix I), cm
R	fiber radius, microns
ΔR	compression of hemisphere end of contact unit (defined by Equation 7)
R_d	response of detector (see Appendix I), μv
S_a	absorption cross section per scatter (see Equations 18 and 19), in.^{2}
S_s	scattering cross section per scatter (see Equations 18 and 19), in.^{2}
T_o	temperature at defined condition, °F
T	temperature, absolute degrees or °F
T_m	mean temperature, °F
T_L	temperature at boundary x = L, °F

SYMBOLS (CONT)

ΔT	temperature difference, °F
V	voltage, volts
V_a	average molecular velocity, cm/sec
x	distance through insulation sample, inch
Δx	thickness of thermal conductivity sample, 1/2 inch
α	cylinder circumference (see Equation 40), microns
$1/\alpha^2$	opacity factor (see Equation 17)
β	fraction of fibers crossing fiber mat planes at average angle ϕ (see Equation 11), dimensionless
δ	void fraction or porosity of sample (see Appendix II), dimensionless
ϵ	emissivity (see Equation 16), dimensionless
ϵ_o	emissivity at boundary x = o (see Equations 26 and 27), dimensionless
ϵ_L	emissivity at boundary x = L (see Equations 26 and 27), dimensionless
ζ	number of fiber junctions per unit area (see Equations 6, 7, and 8), dimensionless
η	half of the linear dimension of test area of hot plate (see Appendix IV), inch
θ	angle with normal, degrees
λ	wavelength, microns
μ	Poisson's ratio (see Equation 10), symbol for microns
ξ	half the distance between fiber junctions (see Equation 6), microns
π	constant, 3.1416
ρ	bulk density, pcf (lb_m/ft^3)
ρ_g	gas density, lb_m/ft^3
ρ_s	solid material density, lb_m/ft^3

SYMBOLS (CONT)

σ	Stefan-Boltzmann constant, $0.174\ (10^{-8})\ \frac{BTU}{hr\text{-}ft^2\text{-}^\circ R^4}$
ϕ	angle at which fibers cross planes (see Equation 11), degrees
ψ	integral defined in Appendix IV
ω	mathematical constant (see Equation 4), dimensionless

SECTION I

INTRODUCTION

Thermal protection schemes for advanced reentry and hypersonic cruise vehicles have been undergoing investigation for some time (Reference 1). An outline of the various thermal protection requirements was reviewed at the Air Force Materials Laboratory Symposium in 1965. Some of these advanced concepts include ASSET, START, and the X-20 (Reference 2). The use of passive thermal protection schemes is particularly suited for hypersonic cruise vehicles, and studies for optimizing an efficient, lightweight, thermally protected structure are currently in progress (References 3, 4, 5, 6, 7, and 8).

Many thermal protection schemes are possible. These include hot and insulated structures, with and without integral fuel tanks. Thus, the combination of these four basic parameters, along with structural and aerodynamic parameters, make the analytical evaluation or design a formidable task.

Each trade-off study depends on specific vehicle requirements, but before these are undertaken and optimized, the thermophysical and chemical properties of the materials must be known with acceptable accuracy.

In the environments presented by aerospace applications, the thermal protection requirements become more demanding and effective thermal insulation materials capable of maintaining large temperature gradients at low heat flow are required for use over extended periods. Such applications include vehicle structure protection during reentry, but can also be used for minimization of heat flow from space power and propulsion components. Hence for aerospace applications, in addition to important factors of low weight and high thermal insulation efficiency at operating temperatures, insulations must have a very high reliability.

To meet the criteria outlined above, insulation components for use in high temperature thermal protection schemes require chemical, physical, and mechanical stability for many hours at high temperature. Incorporating these requirements in a commercially available material, Dynaquartz[1], which has several distinct advantages over other commercial insulations, was developed for the X-20 Dyna-Soar. Since Dynaquartz is a comparatively new material, and reliable thermal conductivity data were lacking, this investigation of its thermal properties was undertaken. Dynaquartz has the following desirable features:

(a) A low overall density. The material consists of randomly packed micron sized fibers. The specific density chosen for this study was the 6.2 pcf[2] because it represents an optimum material with respect to weight and mechanical integrity. Lower density Dynaquartz is extremely friable and high density does not substantially alter the heat transfer characteristics.

(b) Good mechanical stability. Dynaquartz exhibits 1% or less shrinkage at exposure to hot face temperatures of 2600°F or less.

(c) Maximum rated temperature of 2750°F; maximum use temperature of 2500°F.

---

[1] Dynaquartz is a heat stabilized (Type II) Microquartz insulation manufactured by Johns-Manville Company, (Reference 9).

[2] The notation for density to be used is shortened to pcf instead of lb/ft^3 because of custom.

(d) Good chemical stability. Silica has a low vapor pressure and is relatively unreactive with other insulation components.

(e) A small fiber diameter, ie, about 1.3 microns, is obtainable, and is characteristic of fibrous insulation. The small diameter reduces the contact area between the fibers, thus minimizing solid conduction. The small diameter fibers also attenuate thermal radiation thus decreasing the radiation component of heat transfer. This effect is particularly important at high temperatures where radiation effects dominate. The overall conduction can be further reduced by evacuating the sample to less than 10^{-2} torr and thus eliminate gas conduction.

Dynaquartz has several other properties which are a consequence of the fabrication techniques, and peculiar to silica. Dynaquartz is easily friable and must be handled delicately. It has a phase inversion temperature of about 400°F which transforms the crystal structure to that of Cristobalite so that cycling above 400°F reduces the efficiency of the material (Reference 10) and degrades its usefulness. Dynaquartz also has the undesirable feature of being susceptible to acoustical damage at 160 decibels after exposure to elevated temperatures (Reference 5). This characteristic is a consequence of a partial sintering of the fibers resulting in a brittle matrix. The material also has low mechanical strength (Reference 1).

The undesirable characteristics of Dynaquartz have resulted in an increased interest in Dynaflex[3] for aerospace systems (Reference 7). It is basically an alumina-silica fiber with chromia additive and it apparently possesses mechanical strength superior to Dynaquartz. Therefore, to complete the evaluation of high temperature fibrous insulations, Dynaflex and Sapphire Wool were also investigated. A summary of some of the important characteristics of the insulations evaluated in this study is shown in Table I. Dynaflex is undergoing extensive investigation (References 7, 12, and 13).

TABLE I

CHARACTERISTICS OF INSULATIONS STUDIED

	Dynaquartz	Dynaflex	Sapphire Wool
Maximum Rated Temp (°F)	2750	2800	3700
Density (pcf)	6.2	8-10	1.0
Fiber Diameter (microns)	1.3	3.5	1-3
Unidimensional Shrinkage After 2 hours	1.0% (2400°F)	2.9% (2600°F)	–
Chemical Composition	SiO_2 (99.0%)	SiO_2 (56.9%) Al_2O_3 (37.6%) Cr_2O_3 (4.5%)	Al_2O_3 (99.5%)
Manufacturer	Johns-Manville	Johns-Manville	Thermo-Kinetic Fibers, Inc.

[3]Dynaflex is manufactured by Johns-Manville Co.

SECTION II

THEORY

By assuming a superposition of solid conduction, gas conduction and radiation, by taking an energy balance and summing the heat transfer for each of the above mechanisms, we have at steady state

$$q_{eff} = q_{cond} + q_{conv} + q_{rad} \tag{1}$$

where

q_{eff} = effective heat flow, BTU/hr

q_{cond} = conduction heat flow, BTU/hr

q_{conv} = convection heat flow, BTU/hr

q_{rad} = radiation heat flow, BTU/hr

1. CONDUCTION

In fibrous insulations, there are two conduction mechanisms which must be considered: (a) conduction through the solid fibers and their contact points; and (b) the gas conduction through the void volume of the insulation. We can treat these two simultaneously by Fourier's law for one dimension

$$q_{cond} = -(k_s + k_{gas})\, A \,\text{grad}\, T \tag{2}$$

where k represents the thermal conductivity, A the area, and grad T the temperature gradient in the material.

a. Gas Conduction

Strong, et al (Reference 14) derived the following equation for the gas conduction contribution in a fibrous insulation

$$k_{gas} = A_1 \rho C_v V_a \frac{L_m L_g}{L_m + L_g} \tag{3}$$

where

A_1 = constant

ρ = density

C_v = specific heat at constant volume

V_a = average molecular velocity

L_m = mean free path of gas molecules

L_g = effective interfiber distance

In order to utilize Equation 3, the effective interfiber distance and packing distribution of the fibers must be assumed. Glaser, et al (Reference 15) modified Equation 3 and arrived at

$$\frac{(k_{gas})_{p,T}}{(k_{gas})_{p_o,T_o}} = \frac{1}{1 + \frac{p_o L_{m_o}}{p L_g}\left[\frac{T}{T_o}\right]^{\omega+1/2}} \tag{4}$$

where

$(k_{gas})_{p_o,T_o}$ = gas conductivity at pressure p_o, and temperature T_o

$(k_{gas})_{p,T}$ = gas conductivity at pressure p, and temperature T

L_{m_o} = mean free path of gas molecules at pressure p_o and temperature T_o

L_g = effective interfiber spacing

ω = constant, depending on the gas

Again the value of L_g must be determined from some assumptions as to the fiber arrangement. The effective interfiber distance represents the average distance a gas molecule can travel in the direction of heat flow before collision with a solid fiber. Schotte (Reference 16) modified the interfiber distance term to account for accommodation of energy at the surface of the fiber.

The influence of the gaseous conduction to the effective thermal conductivity of Dynaquartz can be examined from kinetic theory, which shows that the thermal conductivity of a gas is proportional to the density and the mean free path, ie

$$k_{gas} = A_2 \rho C_v V_a L_m \tag{5}$$

where A_2 is a constant, and the other terms have been defined previously. In general, since the interfiber spacing is much greater than the mean free path of the gas molecules at atmospheric pressure, the gas will diffuse as in a free gas volume. The value of the thermal conductivity of a gas at moderate pressure (10 to 1000 torr) is almost constant because two dominant effects cancel each other out, ie, density varies directly with pressure and, the mean free path inversely with the pressure. The net result is that the thermal conductivity of the gas varies only slightly with pressure in the pressure range noted above at constant temperature. Thus at moderate pressures, the thermal conductivity of the gas phase, which is continuous for Dynaquartz fibers, can be calculated from kinetic theory (Reference 17).

As the pressure of the gas is decreased, the mean free path increases until the average interfiber distance is reached and then the gaseous thermal conductivity again becomes pressure dependent for a constant temperature. Since the mean molecular path of the gas is greater than the interfiber distance, then the flux of molecules from fiber to fiber in the x-direction is directly proportional to the density. For a material like Dynaquartz, which has an average fiber diameter of 1.3 microns, the mean free path for the interfiber distance is 22.18 microns according to the calculation of Verschoor and Greebler (Reference 18). The pressure dependency effects of various insulations is well known and is described by Scott, (Reference 19) among others.

The gaseous conduction contribution to the heat transfer of Dynaquartz can be summarized as follows: at one atmosphere pressure, the influence of the Dynaquartz fiber spacing on the gaseous thermal conductivity is negligible; at 10 torr and below the dependence of effective mean free path on pressure and temperature becomes apparent.

The transition regime has been investigated by Ryan, et al (Reference 6) for Dynaquartz. Parametric plots of gaseous conduction contribution for various pressures and temperatures have been determined for nitrogen and helium using Equation 4.

Another important feature of Dynaquartz, or any other good fibrous insulation, is its small, effective interparticle spacing and thus the short mean free path between the fibers. For Dynaquartz, a reduction of the gas pressure to between 10^{-1} to 10^{-2} torr is sufficient to reduce gas conduction to less than 1% of the free gas value. In the thermal conductivity experiments, the pressure dependency effect was not investigated. Instead, the experiments were run in the two pressure independent regimes so that the effect of the gas conduction could be simply evaluated. Experiments were run in vacuum at pressures less than 10^{-4} torr and at one atmosphere pressure. Thus, the use of the term, k_{gas}, the thermal conductivity of the gas phase, is necessary for measurements in air or other gas environment, and excluded in the case of vacuum measurements.

b. Solid Conduction

Solid conduction heat transfer in fibrous insulations has been treated by various physical models. An important factor in the heat transfer is the nature of the solid-to-solid contact of the fibers. Several theoretical treatments for evaluating this factor have been proposed; all of these theories assume some highly ordered configuration to facilitate mathematical analysis. The actual configuration of fibrous insulation such as Dynaquartz is not highly ordered; the distribution of the fiber packing and arrangement is random, thus limiting the theoretical analysis to qualitative predictions. An added complexity to the solid-to-solid conduction is that it can affect the radiation transfer through scattering, and thus change the effective thermal conductivity. Hence, the most successful mathematical treatments should reflect the interaction between solid packing, and radiation conductivity where possible.

An analysis by Strong, et al (Reference 14) treated an idealized structure consisting of a symmetrical array of uniform fibers with the heat flow perpendicular to the fibers. This analysis yielded the following equation in terms of contact units:

$$q_s = \frac{4\pi R^2 k_s}{R \ln\left[\frac{4R}{\Delta R}\right] + 2\xi} \zeta \Delta T \qquad (6)$$

where

q_s = rate of heat flow per unit area across a contact unit thickness

R = fiber radius

k_s = solid conductivity of matrix material

ξ = half the distance between fiber junctions

ζ = number of fiber junctions per unit area

ΔT = temperature difference across the contact units

From a relation for the area of solid-to-solid contact and the area of the hemispherical end of the fibers, ΔR was found to be

$$\Delta R = \left[\frac{1.28}{4}\right]\left[\frac{G}{E}\right]^{2/3} R^{-1/3} \tag{7}$$

where

G = the load per contact

E = the modulus of elasticity

Hence the apparent thermal conductivity due to solid-to-solid conduction can be given by

$$\frac{(k_{app})_s}{k_s} = \frac{4\pi R^3 \zeta}{R \ln\left[\frac{4R}{\Delta R}\right] + 2\zeta} \tag{8}$$

where ζ can be calculated from the fiber density. The solid-to-solid contact resistance can be calculated from the loading, fiber size and mechanical properties of the matrix material. However, the loading is usually the most difficult to determine and Strong used the fact that each contact was under the force of atmospheric pressure. Strong's experimental data showed values of solid-to-solid conduction to be about one order of magnitude lower than predicted by his model.

A similar analysis of solid-to-solid contact between the fibers led Wang (Reference 20) to the following relation:

$$\frac{(k_{app})_s}{k_s} = \frac{1}{\ln\left[\frac{8\pi R^2}{A_c}\right] + \frac{\pi}{2(1-\delta)}} \quad \frac{3(1-\delta)^2}{\pi} \tag{9}$$

where A_c is the area of fiber contact.

$$A_c = \frac{\pi}{4} R^2 \left[\frac{3\pi^2(1-\mu^2) C_c}{E(1-\delta)^2}\right]^{2/3} \tag{10}$$

where

C_c = compression of the fibers

μ = Poisson's ratio

δ = void volume; for 6.2 pcf Dynaquartz, the value is 0.954.

It should be noted that both analyses predict a logarithmic dependence on the contact radius. This implies that a large change in the contact radius is reflected in a small change in apparent solid-to-solid conductivity.

In a further analysis of the solid-to-solid conduction process by Wechsler and Glaser (Reference 1), several types of parallel axial packings and cross packing arrangements were investigated. For a random array of fibers including parallel axial and cross packings, the general relation was developed

$$\frac{(k_{app})_s}{k_s} = \beta \sin\phi\,(1-\delta) + (1-\beta)\,\frac{3}{7}\left[\frac{(1-\delta)}{\ell n\,\frac{4R}{b}}\right] + \frac{3}{7}(1-\beta)\,\frac{4(1-\delta)^2}{\pi\,\ell n\left[\frac{6.72R}{b}\right]} + \frac{\pi^2}{32(1-\delta)} \tag{11}$$

where β = fraction of fibers crossing the fiber mat planes at an average angle ϕ

b = contact diameter defined by

$$b = 2.26\left[\frac{GR}{E}\right]^{1/3} \tag{12}$$

where G is again the load per contact, R the fiber radius, and E the modulus of elasticity.

In the preceding analysis, a three-dimensional array of fibers was treated and the following assumptions were made: (1) most of the fibers were in the XZ plane, (2) fibers cross the XZ plane at small angles, (3) XZ plane fibers were arranged in a random fashion, and (4) most of the fibers were not curled. The first term in the expression accounts for four coaxial heat transfer modes in the x and y directions and the second term for the three cross packed modes in the y direction. The whole expression was modified by the contribution to total heat transfer by the fraction of fibers which cross consecutive layers at some angle with XZ plane. Thus, it is possible to calculate some solid-to-solid conduction contributions if the values for β, ϕ, and the mechanical properties can be found from examination of the matrix material.

Utilizing this approach of Wechsler and Glaser (Reference 1), Ryan, et al (Reference 5) have estimated the solid-to-solid conduction contribution to effective thermal conductivity of Dynaquartz (6.2 pcf) to be about 0.10 BTU-in./hr-ft^2-°F at 550°F. The corresponding contact diameter for Dynaquartz was calculated to be 0.18 micron which seems reasonable for a partially sintered material and in light of the assumptions of this approach.

Wechsler and Glaser (Reference 1) also treated two [illegible]re simplified models. In the first model, the fibers were assumed to be stacked vertically only and separated by some distance. The major resistance to heat flow is in the contact region of the fiber rather than in the fibers. The following expression was derived:

$$\frac{(k_{app})_s}{k_s} = \frac{b^2(1-\delta)^2}{\pi R^2} \tag{13}$$

In this expression, the apparent solid-to-solid conductivity is proportional to the square of the ratio of contact diameter to fiber diameter. The result gives a much stronger influence due to contact area than Equations 9 and 11.

In the second simplified model, Wechsler and Glaser considered the solid-to-solid contact to be hemispherical instead of circular and derived the following equation:

$$\frac{(k_{app})_s}{k_s} = 1.97(1-\delta)^{1/3}\left[\frac{(1-\mu^2)\,C_c}{E}\right]^{1/3} \tag{14}$$

In this model, the apparent solid-to-solid conductivity is proportional to the ratio of the contact radius to the fiber radius.

In summary, the solid-to-solid contribution to effective thermal conductivity of fibrous materials such as Dynaquartz is a complex problem. Depending upon the physical model chosen for the solid-to-solid contact between fibers, the contribution can be a logarithmic, square function or linear function of the contact radius to fiber radius. In order to treat the problem quantitatively, mechanical properties such as the modulus of elasticity and Poisson's ratio of the fibrous matrix material must be known. In addition, other more pertinent physical characteristics such as contact areas, fraction of fibers crossing fiber mat planes at small angles, and load per contact must be determined or estimated. The apparent solid-to-solid conduction contribution in fibrous insulations such as Dynaquartz depends primarily on the contact area and the strength of the matrix material in fibrous form and is extremely difficult to evaluate quantitatively.

2. RADIATION

Radiation conduction becomes an important mechanism of heat transfer at temperatures beyond 1500°F (References 21 and 22). For fibrous materials, the mechanisms for radiation heat transfer have been considered both empirically and theoretically, both separately and simultaneously with the other processes in thermal conduction. In general, when considering the mechanism of radiation, the gross effect of interaction of the individual processes of absorption, scattering, reradiation, and transmission are treated by approximate models. For example, in considering the radiation contribution to effective thermal conductivity, Chen and Churchill (Reference 21) summarized the results of applying several of the classical models by the general equation

$$k_r = 4F\sigma D_f T^3 \tag{15}$$

where

σ = Stefan-Boltzmann constant

D_f = diameter of fiber

T = absolute temperature

and the quantity F, which represents the effect of geometric and optical properties of the system, is derived from various models. In all the analyses considering particles (References 16, 23, 24, 25, 26, and 27), the models predict that the radiation contribution increases with particle size and emissivity.

Strong, et al (Reference 14) interpret radiation heat transfer in terms of the diffusion of photons and an average mean free path, derive the same type of equation as Equation 15 in which the quantity F is defined by

$$F = \frac{1}{3\epsilon(1-\delta)} \tag{16}$$

where ϵ is the emissivity. Equation 16 gives a general increase of the radiation contribution with particle size which was correlated experimentally.

In another analysis of fibrous insulations, Verschoor and Greebler (Reference 18) derived an expression similar to Equation 15 by utilizing the general form for k_r, which led to the following expression for F:

$$F = \frac{0.785}{\alpha^2 (1-\delta)} \tag{17}$$

In Equation 17 $1/\alpha^2$ is an opacity factor obtained from infrared transmission data on the fibers.

Perhaps the most useful treatment of the radiation contribution to effective thermal conductivity in fibrous insulations is the two-flux model analysis. In this treatment of a fibrous insulation, transmission through the material is described by scattering, absorption, and reradiation mechanisms. In considering this analysis, a steady-state heat flow is assumed in one dimension. The material is considered to be homogeneous which infers that the smallest volume of the sample is considered as being representative of the whole material. This analysis was outlined by Schuster (Reference 28), used by Hamaker (References 29 through 32), and was extended by Chu and Churchill (Reference 33).

In these analyses an insulation was treated as an isotropic and continuous material and the heat transfer was described in terms of an integro-differential equation (sometimes referred to as the transport equation) and a differential energy balance with appropriate boundary conditions. The transport equation was treated only for a few restricted cases (References 29 through 32).

Under appropriate conditions the radiation can be considered in terms of a forward flux and a backward flux in one dimension as represented by Larkin (Reference 34) and Larkin and Churchill (Reference 35). A more general six-flux model (Reference 33) is applicable in the case of three-dimensional heat flow.

In the two-flux model, the flow of radiant energy is represented by two discrete fluxes, one in the forward direction and one in the backward direction as shown in Figure 1. The following equations (References 34 and 35) give the relations between the intensities of the fluxes:

$$\frac{dI_1(x)}{dx} = nBS_s I_1(x) + nS_s I_1(x) + nBS_s I_2(x) + nS_a \sigma T^4(x) \tag{18}$$

$$-\frac{dI_2(x)}{dx} = nBS_s I_2(x) + nS_s I_2(x) + nBS_s I_1(x) + nS_a \sigma T^4(x) \tag{19}$$

where

n = number of scatters per unit volume

B = fraction of scattered radiation scattered into the background hemisphere

S_s = scattering cross section per scatter

S_a = absorption cross section per scatter

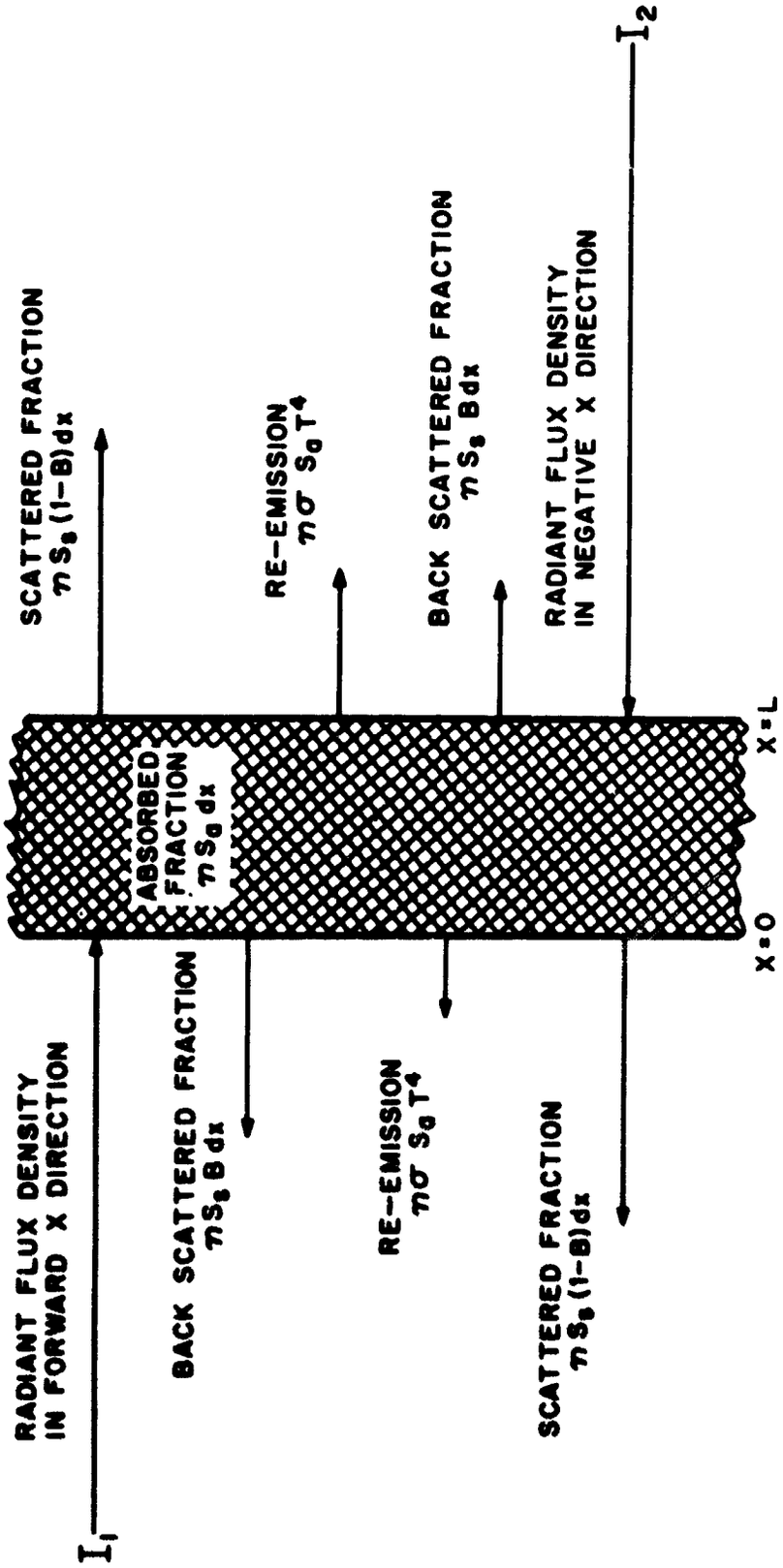

Figure 1. Schematic of Insulation Sample

$I_1(x)$ = radiant flux density in the forward direction

$I_2(x)$ = radiant flux density in the backward direction

Each term in Equation 18 represents the variation of the forward radiant flux density. As depicted in Figure 1, the following terms are expressions for changes in the flux density in the forward direction:

(a) $n B S_s I_1(x) dx$ - back scattering of forward flux which decreases in the forward direction;

(b) $n S_a I_1(x) dx$ - absorption of forward flux which decreases in the forward direction;

(c) $n B S_s I_2(x) dx$ - back scattering of backward flux which increases in the forward direction;

(d) $n S_a \sigma T^4(x) dx$ - reradiation which increases in the forward direction.

Equation 19 is similar to Equation 18 in describing the net change in the backward flux. The tacit assumption of the two-flux approach is that intercepted and reemitted radiation can be considered the same.

The differential energy balance is then applied, which is given by

$$Q = -k \frac{dT(x)}{dx} + I_1(x) - I_2(x) \tag{20}$$

The scattering and absorption cross sections per unit volume are defined as

$$N = nBS_s \tag{21}$$

and

$$P = nS_a \tag{22}$$

The interception cross section is the sum of the scattering and absorption cross sections

$$M = nBS_s + nS_a \tag{23}$$

Rewriting Equations 18 and 19 in terms of the cross sections gives

$$\frac{dI_1}{dx} = -MI_1 + NI_2 + P\sigma T^4 \tag{24}$$

and

$$-\frac{dI_2}{dx} = -MI_2 + NI_1 + P\sigma T^4 \tag{25}$$

In applying boundary conditions to Equations 24 and 25 for a particular insulation when the material does not absorb radiation, P = O, and assuming that k is constant, Larkin and Churchill (Reference 35) derived the following equation:

$$Q = \frac{k(T_0 - T_L)}{L} + \frac{\sigma(T_0^4 - T_L^4)}{\frac{1}{\epsilon_0} + \frac{1}{\epsilon_L} - 1 + NL} \tag{26}$$

where

T_0 is the temperature at x = o

T_L is the temperature at x = L

Equation 26 shows that there is a constant temperature gradient across the dimension of the insulation.

When radiation absorption in the insulation is not negligible, Equations 20, 24, and 25 can be reduced to a pair of equations in any two of the three variables, but such pairs are nonlinear. For boundary conditions where the net radiation flux is constant or when radiation is only a small contribution to the total heat transfer the result is a constant temperature gradient. These conditions were applied by Larkin and Churchill (Reference 35) who obtained solutions for heat transfer in an absorbing and scattering insulation bounded by opaque surfaces. Wechsler and Glaser (Reference 1) considered the same case and by neglecting conduction derived the following equation for heat transfer in an absorbing and scattering medium bounded by opaque surfaces of emissivity ϵ_0:

$$Q = \frac{2 J^2 \sigma(T_0^4 - T_L^4)\epsilon_0}{\epsilon_0(P + 2N)L + 4 - 2\epsilon_0} \tag{27}$$

Comparing this result with Equation 26 shows the equations are quite similar. Both equations indicate the fourth power of the temperature is linear with distance if the first term of Equation 26 is negligible.

A similar approach to the solution of the two-flux model equations for nonabsorbing materials bounded by opaque surfaces was used by Chen and Churchill (Reference 21). However, instead of using a linear function for the distance temperature relation, it was assumed that for small temperature differences, that the differences in T^4 could be approximated by the first two terms of a Taylor series expansion about some mean temperature, T_m. The solution to the equations is complicated but for locations sufficiently far from the boundaries of an optically thick fibrous mat, the following equation for radiant contribution to effective thermal conductivity was obtained:

$$k_r = \frac{8\sigma T_m^3}{P + 2N} \tag{28}$$

When P and N are defined by Equations 21 and 22, the value of F for use in Equation 15, for the general case would be

$$F = \frac{2}{P + 2N} \tag{29}$$

Including an index of refraction different from one in the two-flux model, requires that the factor F be modified by the index of refraction squared, J^2, where J represents the index of refraction.

A further analysis of the problem of radiant heat transfer coupled with conduction was made by Viskanta (Reference 36). He obtained exact solutions to the problem by numerical integration. The temperature distribution in an absorbing and scattering medium was found to be a strong function of the optical thickness and the ratio of energy transfer by solid conduction to radiation conduction. The effect of radiation without reabsorption is to increase the net heat transfer if the heat transfer is considered due to conduction alone. Due to different temperature dependencies of k_r and k_s, however, the net result is a reduction of the temperature gradient.

In summary, the two-flux model allows for the treatment of the radiation contribution to the effective thermal conductivity of fibrous insulations by means of transmission experiments. Increasing absorption and scattering cross sections of a fibrous insulation material will decrease the radiation contribution to effective thermal conductivity. A smaller fiber diameter and lower emissivity or highly reflecting fiber surfaces would tend to decrease the radiant energy transmission through a fibrous material. These effects should be manifested in the absorption and scattering cross sections. In view of the numerous assumptions involved in the two-flux model analysis, and the experimental problems involved in measuring transmission through highly scattering materials, only qualitative agreement between the theory and experiment can be expected.

SECTION III

EXPERIMENTAL

The experimental portions of this investigation were undertaken to

(a) evaluate the various contributions to total or effective thermal conductivity of fibrous insulations;

(b) measure the effective thermal conductivity of fibrous silica under various environmental conditions;

(c) correlate the results of the experiments performed with existing theoretical models for fibrous insulations.

To evaluate the radiation contribution to effective thermal conductivity, the following radiation transmission experiments were performed:

(a) Spectral normal transmission measurements

(b) Total normal transmission measurements

Spectral normal transmission measurements were required to obtain the spectral absorption and scattering cross sections as a function of wavelength and temperature. In this experiment, the sample is heated and spectral transmission is determined. Hence the spectral distribution of the source is constant and changes in the absorption cross section are due to changes in the sample as a result of heating. There is no expected change in the scattering cross section since the geometry of the sample is expected to be constant. The measured spectral transmission and a properly weighted distribution function for the intensities of the emitted wavelengths of the source give the integrated optical transmission of a sample. The integrated transmission can then be used to calculate the absorption and scattering cross sections.

Total normal transmission measurements were carried out to obtain the total energy transmitted through a sample from a given source. The total transmission experiments were of two types: first, where sample and source temperatures were the same, and second, where the sample was at room temperature and the source of radiation was variable. In the first experiment, the absorption cross section is expected to change due to changes in the sample as a result of heating. In addition the absorption and scattering cross sections are expected to change due to variable source temperature and wavelength distribution. In the second experiment, only changes in the absorption and scattering cross sections are expected due to changes in the source temperature and wavelength distribution.

Each of the experiments outlined will yield values for the absorption and scattering cross sections and must be interpreted in terms of the variables of the experiments. Thus absorption and scattering cross sections can be compared with calculated backscattered flux from an electromagnetic theory evaluation of the scattering coefficient.

Effective thermal conductivity measurements were carried out by use of a guarded hot plate apparatus. By using various gases and pressure as a variable of this experiment it is possible to isolate the effect of the gas conduction contribution to total thermal conductivity. Furthermore, the solid conduction contribution can be estimated from low temperature thermal conductivity measurements in vacuum. A correlation between the effective thermal conductivity and the calculation of the relative contributions of the gas conductivity, solid conductivity, and radiation conductivity could then be performed.

1. SPECTRAL TRANSMISSION EXPERIMENTS

a. Description of Equipment

The spectral normal transmittance for Dynaquartz was obtained with the Beckman IR-6 single beam recording spectrophotometer. The optical path of this instrument is shown in Figure 2. The use of the special transmission furnace (see Figure 2) allows measurements from 20°C to about 1000°C. The spectral range of the instrument is from 1 to 15 microns using a rocksalt prism (apex angle of 66°) as the dispersive element. The source of radiation is a Nernst glower with the radiation chopped at 150 rpm. Since the chopper is located between the source and the transmission furnace, only that portion of the radiation passing from the source through the sample will appear as an AC signal at the detector.

The transmission furnace is resistance heated with Tophet "A" (80/20 nickel-chromium type alloy) heating elements. Chromel-alumel thermocouples were used to measure the temperatures inside the furnace and the EMF of the thermocouples was fed to a Minneapolis-Honeywell circular recorder controller (0°-1000°C) which controlled the temperature. The radiation after passing through a spectrometer was focussed on a thermocouple detector by means of a spherical condensing mirror and a 2-power KBr magnifying lens. The detector was a conventional wire type thermocouple with a two-ohm resistance and a sensitivity of about one volt per watt of radiation at the chopping frequency.

b. Spectral Transmission Data

The normal spectral transmission of Dynaquartz was measured at various thicknesses between 20° and 900°C. I_o was obtained by measuring the spectral output of the source with air only in the light path. The transmitted intensity, I, with the sample in place was obtained next. The ratio I/I_o, ie the transmission was then obtained by taking this ratio as a function of wavelength. One of the limits in obtaining accurate transmission by use of a single beam instrument is the reproducibility of the sample location. The curves obtained from the instrument at about 20°C are shown in Figure 3 for two thicknesses, 0.030 and 0.060 inch. Figure 4 is a curve obtained at 400°, 800°, and 900°C for a thickness of 0.045 inch. The highest transmission peak is at 7.3μ. Its intensity decreases with increasing sample temperature. The intensity is most intense at room temperature and least at 900°C. Figure 5 is a transmission curve obtained at the same temperatures as Figure 4 for a thickness of 0.030 inch. The transmitted intensity obtained at 400°C was reproducible after heating to 900°C and indicated no spectral variation. Hence, the decrease in the transmission is reversible and apparently the material fiber configuration was not altered enough to be detected by the spectrophotometer.

The transmission curves at 20°C were plotted on semilog graph paper and the data tabulated in Table II gives the calculated absorption and scattering cross sections versus wavelengths. These showed the same dependency on wavelength as the transmission curves. The same spectral transmission experiment was run on a Perkin-Elmer Model 12U single beam spectrophotometer, but for thicknesses of Dynaquartz ranging from 0.015 to 0.045 inch. The spectral transmission was plotted as noted above, and the calculated absorption and scattering cross sections are shown in Table III. The values obtained agree with the data from the IR-6 except that the absorption cross sections are apparently higher for the Beckman IR-6 measurements.

It should be noted that in the region from 6.9 to 7.6μ (see Figures 3, 4, and 5) several water bands are present which increase the uncertainty in the evaluation of the transmission. This, coupled with the noise level of the instrument electronics, gives an error of about ±5% in I_o and higher errors in I.

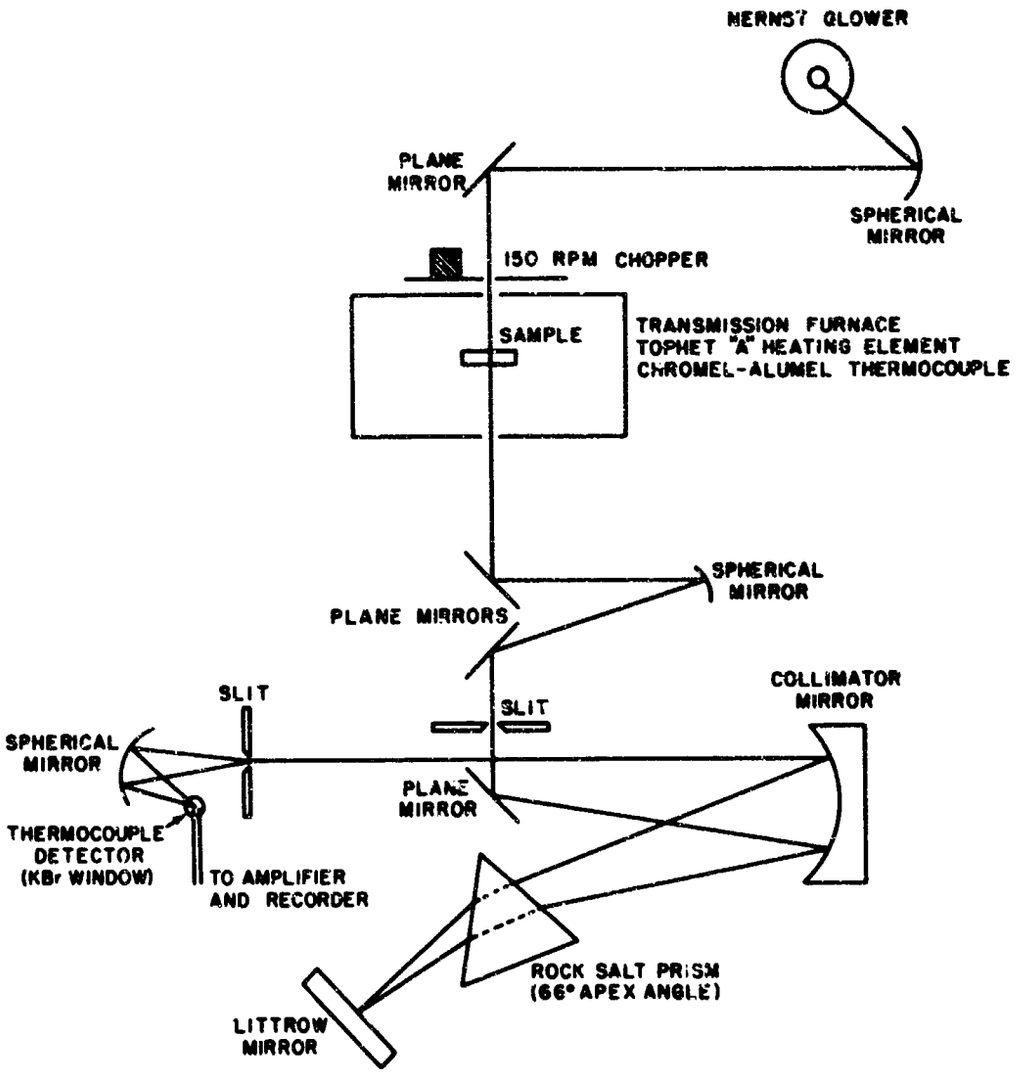

Figure 2. Optical Path of Beckman IR-6 Single Beam Recording Spectrophotometer

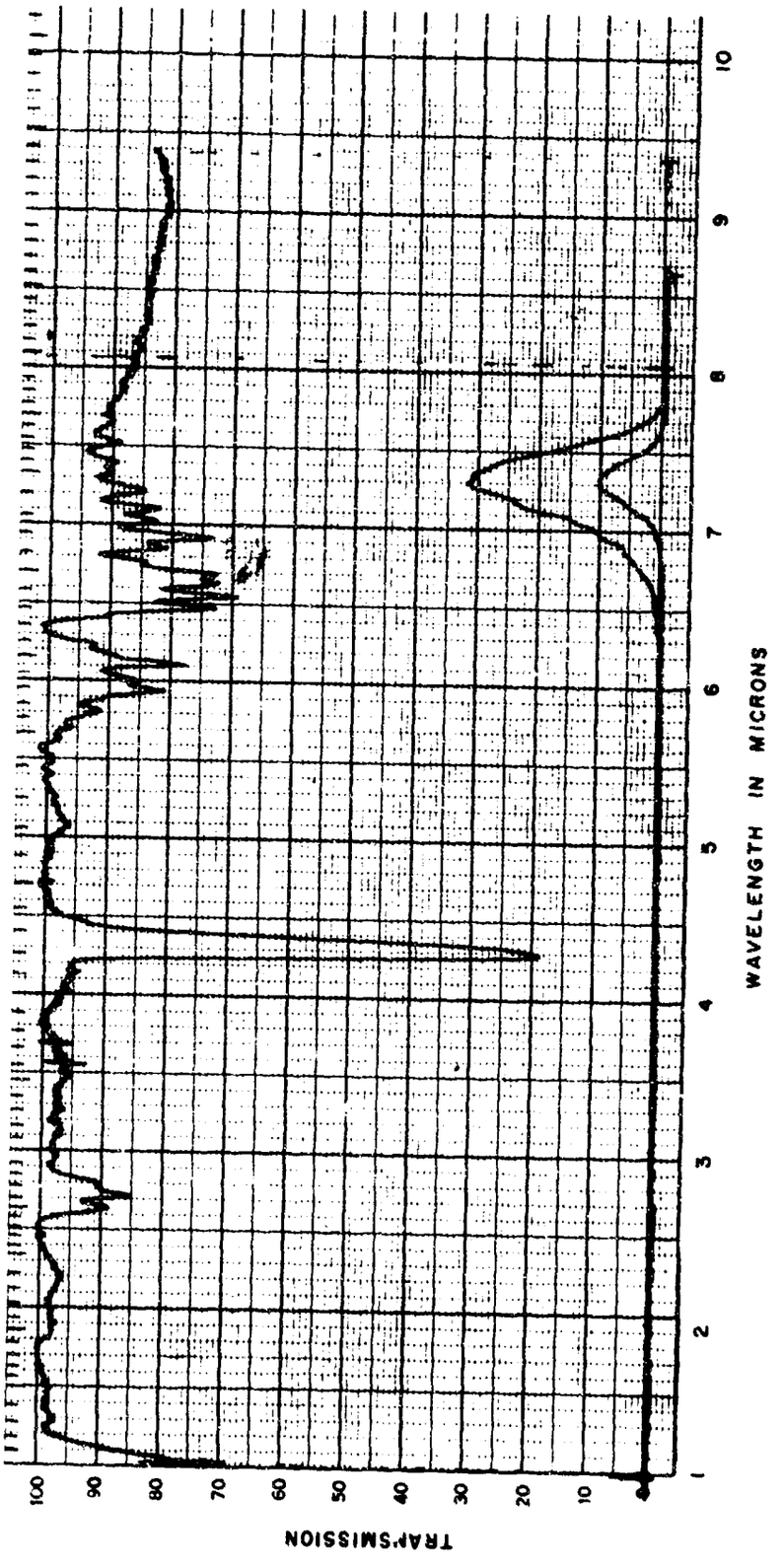

Figure 3. Spectral Transmission for Two Thicknesses of Dynaquartz

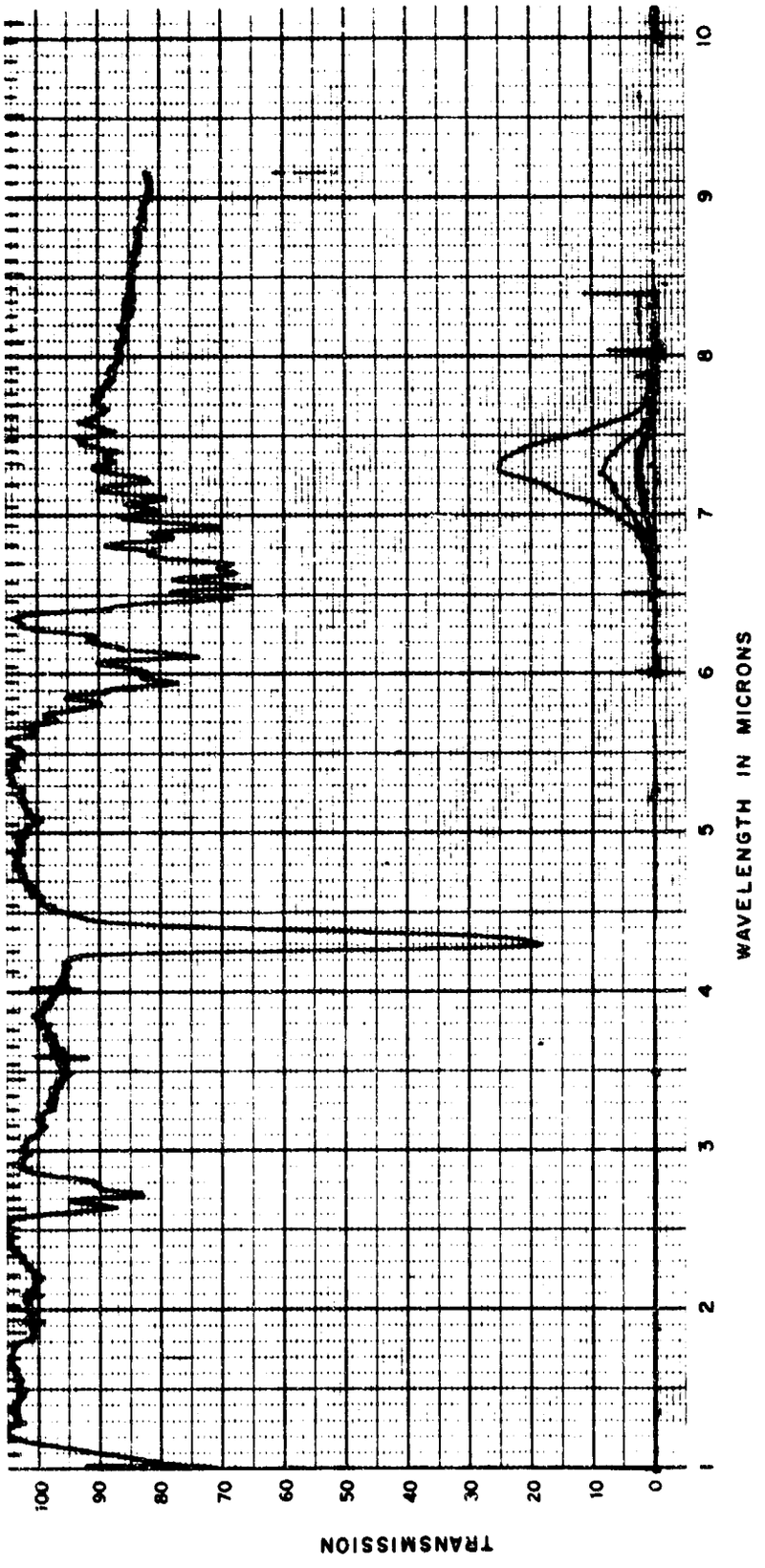

Figure 4. Spectral Transmission for 0.045 Inch Thickness of Dynaquartz at Elevated Temperatures

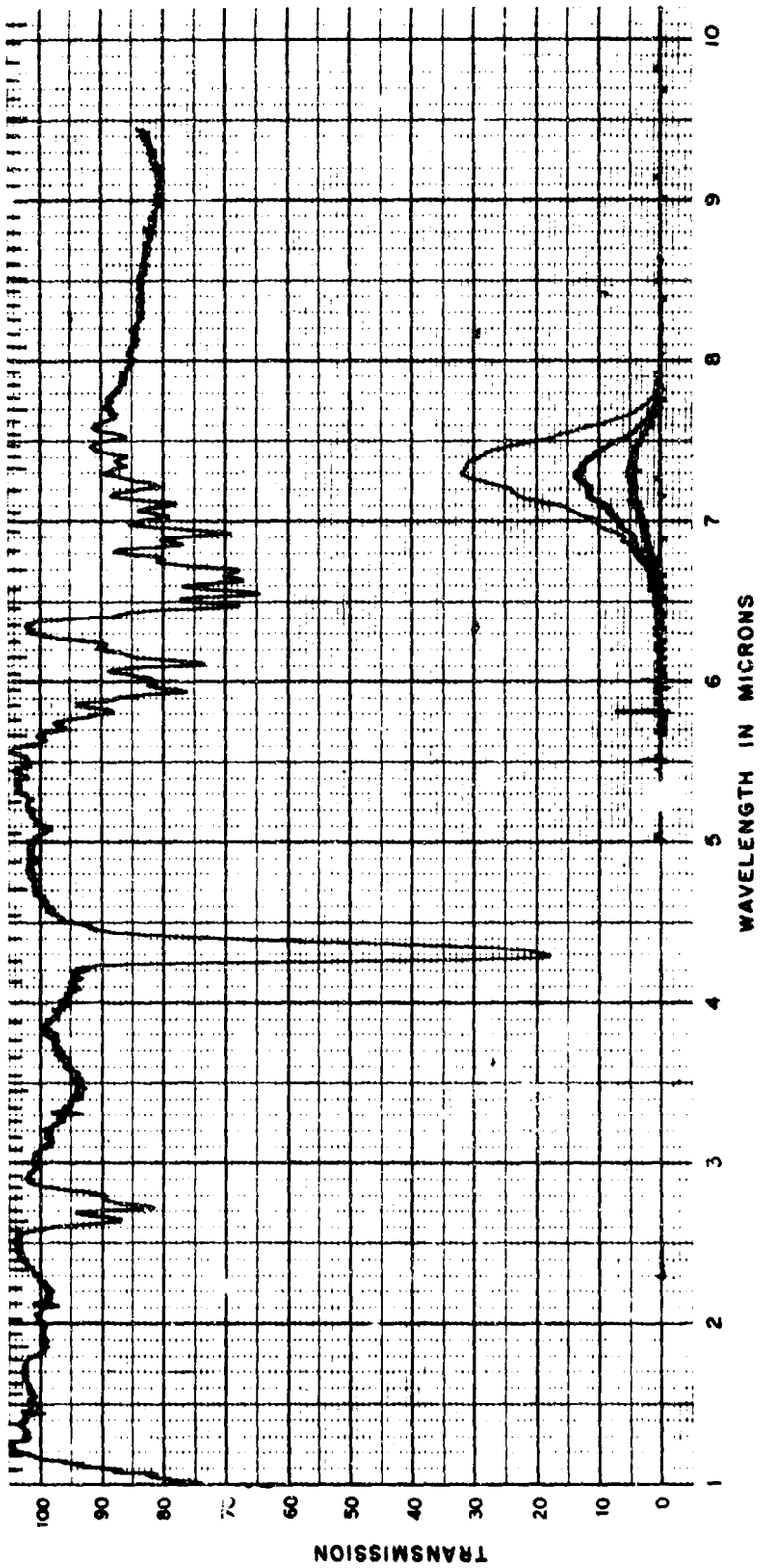

Figure 5. Spectral Transmission for 0.030 Inch Thickness of Dynaquartz at Elevated Temperatures

TABLE II

BECKMAN IR-6 ROOM TEMPERATURE TRANSMISSION DATA FOR DYNAQUARTZ (6.2 pcf) USING NERNST GLOWER

		L = 0.030"		L = 0.060"						
λ (μ)	I_o	I	tλ	I	tλ	slope (in^{-1})	Inter-cept	M (in^{-1})	N (in^{-1})	P (in^{-1})
6.9	79.4	7.0	8.81	2.8	3.52	30.53	.224	160	157.1	2.9
7.0	97.0	12.0	12.35	5.8	5.97	24.22	.26	162	160.2	1.84
7.1	92.0	19.0	20.65	11.0	11.95	18.2	.36	83	81	2
7.2	95.0	27.0	28.42	17.0	17.89	15.55	.54	42.1	39.1	3.0
7.3	102.5	35.6	34.73	23.5	20.88	17.35	.58	42.5	38.84	3.66
7.4	102.0	31.0	30.39	20.0	19.60	14.6	.456	49.4	47.2	2.2
7.5	104.2	20.0	19.19	11.0	10.95	18.53	.344	89.4	87.5	1.9
7.6	105	10.0	9.52	4.0	3.81	30.52	.224	160	157.1	2.9

TABLE III

PERKIN-ELMER 12U ROOM TEMPERATURE TRANSMISSION DATA FOR DYNAQUARTZ (6.2 pcf) USING FILAMENT GLOWER

Drum Rev.	λ (μ)	I_o	L = 0.015"		L = 0.046"		Slope (in^{-1})	Int	M (in^{-1})	N (in^{-1})	P (in^{-1})
			I	tλ	I	tλ					
14.6	7.6	62	7	11.29	1	1.61	65.0	.33	329	328.88	.12
14.8	7.35	70	25.5	35.7	9.5	13.6	31.1	.58	76.4	76.19	.21
14.9	7.25	75.8	30.2	39.8	13.5	17.8	25.95	.592	61.5	61.35	.15
15.0	7.16	73	26	35.6	10.5	14.4	29.2	.58	71.5	71.28	.22
15.2	6.9	90.6	16.5	18.2	4.0	4.41	45.7	.38	195	194.88	.12

The normal spectral transmission of Sapphire Wool for three thicknesses was measured at room temperature on the Beckman IR-6 (see Figure 6). Figure 6 shows the effect of increasing sample thickness. Curve 1 on Figure 6 is for 0.18 inch thick fused silica (Corning No. 7940).

The Sapphire Wool transmission curves peak at about 9.6 microns. Curves 2, 3, and 4 on Figure 6 are for 0.020, 0.045 and 0.090 inch thickness samples, respectively. The transmission curves for Sapphire Wool are much broader than those of Dynaquartz (see Figure 3) and therefore the radiation transmitted through the Sapphire Wool material would be higher even though at higher temperatures radiation is expected to shift more toward the lower wavelengths. Thus the radiation contribution to total thermal conductivity for Sapphire Wool should be higher than that of Dynaquartz (see Section III.5).

The normal spectral transmission of Dynaquartz, Sapphire Wool, and Dynaflex at room temperature was also measured on a Perkin-Elmer Model 621 grating spectrophotometer. The spectral range covered was from 2.5 to about 40 microns. The curves are approximately those shown previously except Dynaquartz has a secondary peak at about 16 microns and a somewhat higher peak at 18 microns; however, the largest peak is about 1/2 the peak height at 7.3 microns. These secondary peaks are not expected to alter the radiation attenuation characteristics of Dynaquartz.

Dynaflex transmission curves peaked at 7.7 microns building up gradually from 7.0 microns and dropping sharply past 7.7 microns to zero at 8.0 microns. Transmission through Dynaflex seems to be more efficient than through Dynaquartz and Sapphire Wool for comparable thickness samples.

c. Calculation of Integrated Transmission from Spectral Transmission Data

The calculation of integrated transmission of the radiation from a spectral source such as a black body from spectral transmission data requires the use of some averaging procedure since the spectral distribution function from black body radiation is not uniform as a function of wavelength. One method of averaging most commonly in use is to apply Planck's law as a distribution function which is written as

$$\sigma T^4 = \int_0^\infty g(\lambda, T)\,d\lambda = \int_0^\infty \frac{C_1 \lambda^{-5}\,d\lambda}{e^{C_2/\lambda T} - 1} \qquad (30)$$

where

g = the distribution function

λ = the wavelength

T = the absolute temperature

$C_1 = 3.74\,(10^{-5})$ erg-cm^2/sec

$C_2 = 1.439$ cm-°K

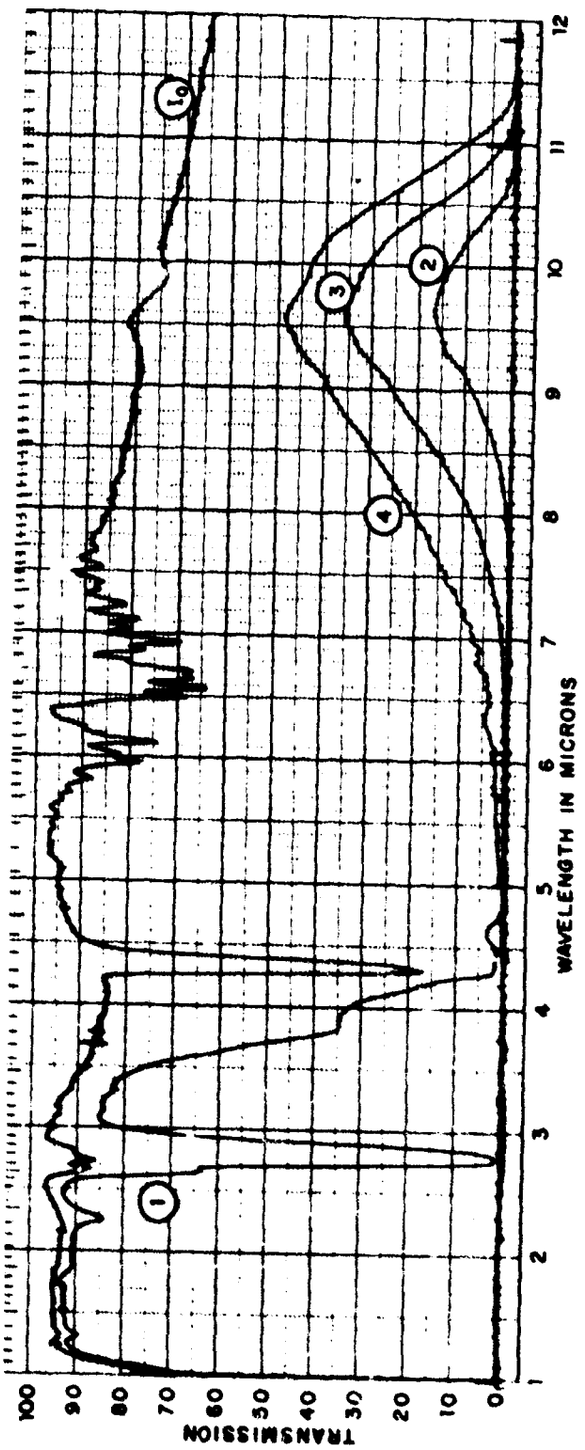

Figure 6. Spectral Transmission for Three Thicknesses of Sapphire Wool

and the integrated transmission using Planck's weighting function is

$$H = \frac{\int_0^\infty T(\lambda)\, g(\lambda,T)\, d\lambda}{\int_0^\infty g(\lambda,T)\, d\lambda} \qquad (31)$$

Using this procedure gives each wavelength a weight in proportion to the energy it carries. The total energy transmitted was calculated from spectral transmission measurements using the data from Figures 3, 4, and 5. By plotting the black body radiation curve at the temperature of the experiment and the product of the transmission and the intensity value at the wavelength considered, the total transmission can be calculated by graphical integration of the two curves. The black body radiation curve was calculated on a relative basis using the values tabulated in Reference 37 for λT. The values for total transmission using the spectral transmission data are summarized in Table IV.

2. TOTAL TRANSMISSION EXPERIMENTS

a. Description of Equipment

The values of total transmission obtained from the experiments described below are of two forms, where: (1) the sample and source temperatures are the same; and (2) the source temperature is different from the sample temperature. The second series of experiments was carried out with the sample at 20°C.

The experimental apparatus for the total transmission with the sample at 20°C and source at elevated temperatures is shown schematically in Figure 7.

The total transmission measurements were made with a Reeder Model RP 3W thermocouple detector which is shown schematically in Figure 30, Appendix I. The thermocouple sensitivity was determined to be linear, ie, the signal voltage was directly proportional to the radiant power impinging on the detector (see Appendix I). The angular response of the detector was not determined; however, care was taken to insure that the detector was normal to the black body. As pointed out by Larkin (Reference 34), actual comparisons of transmissions measured by a cosine detector and an actual detector showed that there was no appreciable error introduced by using an actual detector for highly scattered energy. The black body was that of a Hohlraum geometry which was available from the Beckman IR-6 spectrophotometer emissivity attachment. The radiation was chopped at 13 cycles per second. The signal from the detector was amplified by a Perkin-Elmer Model 121 amplifier similar to the one in use on several spectrophotometers. The signal was read directly from a Keithley Model 149 Milli-Microvoltmeter. The signals were read directly from a dial and maximum, minimum, and average readings were taken after the signal appeared steady, usually 20 minutes or so. The total normal transmission data were corrected for dark current in each case. No correction was made for absorption of the CaF_2 window of the detector. The gain on the amplifier was changed to give readings for I_o and the dark current was measured each time the gain was changed and rebalanced.

Attempts were made to obtain transmission samples 0.015 to 0.060 inch thick by slicing a thick piece of Dynaquartz with a razor blade. Difficulties were encountered in trying to cut the material uniformly and also in measuring the thickness. As the material was sliced, fibers parallel to the cutting plane would shear the rest of the sample. Several samples were destroyed in this manner. The thicknesses of the samples were measured with micrometer

TABLE IV

VALUES FOR INTEGRATED TRANSMISSION CALCULATED FROM SPECTRAL TRANSMISSION DATA ON DYNAQUARTZ (6.2 pcf)

Sample at Room Temperature = 20°C(293°K)

Thickness (inches)	Transmission
0.030	0.0101
0.040	0.0070
0.045	0.0057
0.070	0.0022

Sample at 400°C(673°K)

0.030	0.0078
0.040	0.0055
0.045	0.00464

Sample at 800°C(1073°K)

0.030	0.00196
0.040	0.00150
0.045	0.00140

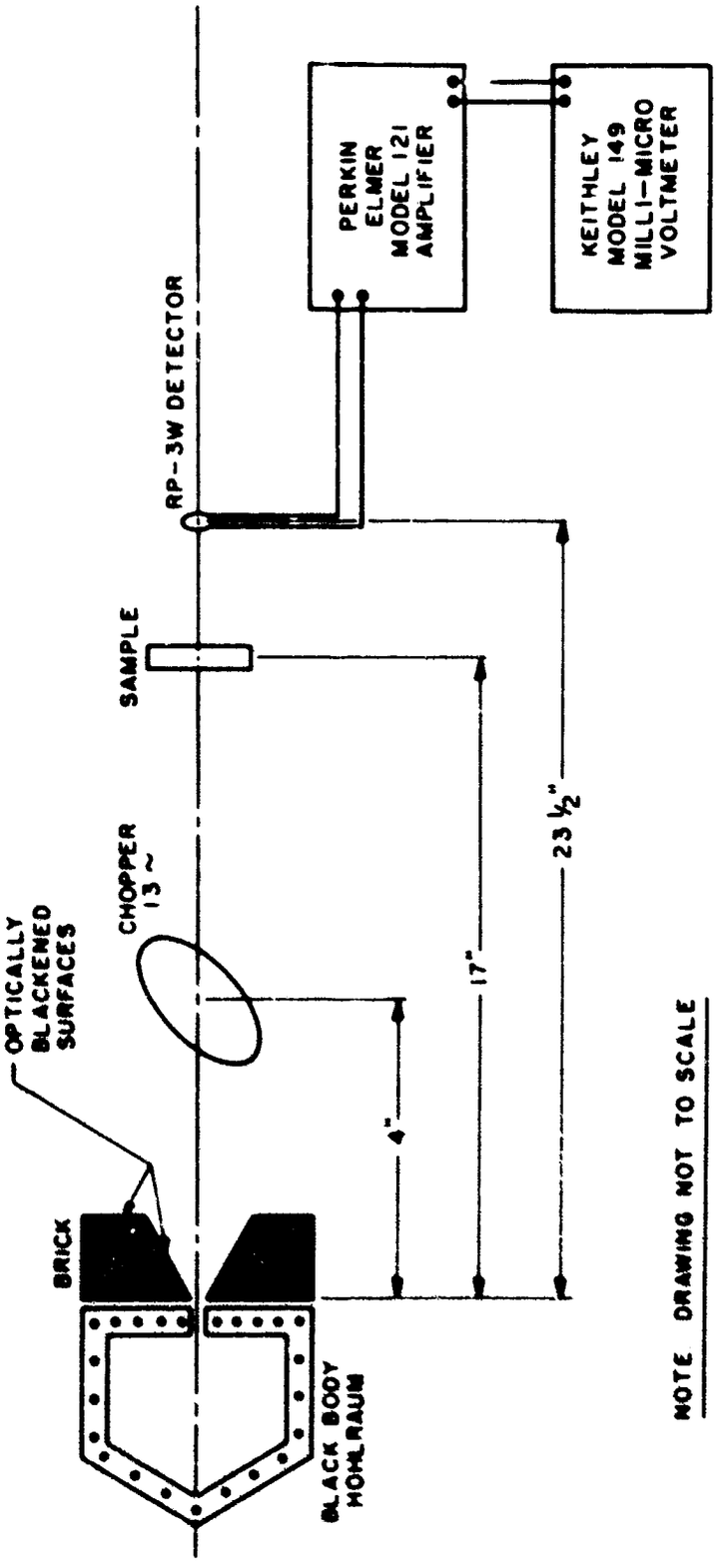

Figure 7. Schematic Diagram of Experimental Apparatus for Total Transmission at 20°C Sample Temperature

calipers; some samples were broken upon closing the calipers. The Dynaquartz samples compressed easily so that actual thicknesses found are approximate. Samples were cut from 6.2 pcf material, the same density at which the thermal conductivity was measured.

The total transmission data are tabulated in Table V for the sample at room temperature and the source temperature as variable. The transmission experiments, where the sample was shown schematically in Figures 8 and 9, were carried out with the transmission furnace in use on the Beckman IR-6 spectrophotometer. The same electrical circuit was used for temperature and readout. The total transmission data for variable source and sample temperature are tabulated in Table VI.

b. Calculation of Optical Scattering and Absorption Cross Sections

In applying the two-flux model to transmission experiments, Equations 24 and 25 are rewritten for the case where reradiation is small compared to the incident and transmitted flux. The equations are

$$\frac{dI_1}{dx} = -MI_1 + NI_2 \tag{32}$$

and

$$-\frac{dI_2}{dx} = -MI_2 + NI_1 \tag{33}$$

where all quantities have been defined in the theory previously. Applying the appropriate boundary conditions

$$\text{at } x = 0 \quad I_1 = 1 \tag{34}$$

and

$$\text{at } x = L \quad I_2 = 0 \tag{35}$$

the transmission can be expressed as (Reference 34)

$$I_1(L) = \frac{1}{\cosh(M^2-N^2)^{1/2}L + \frac{M}{(M^2-N^2)^{1/2}}\sinh(M^2-N^2)^{1/2}L} \tag{36}$$

For the case where $(M^2 - N^2)^{1/2} > 5$, Equation 36 can be reduced to

$$I_1(L) = \frac{2(M^2-N^2)^{1/2}}{(M^2-N^2)^{1/2}+M}\, e^{-L(M^2-N^2)^{1/2}} \tag{37}$$

Hence by plotting the transmission versus thickness on semilog paper, the values for the absorption and scattering cross sections can be determined from the slope and intercept (see Table VII).

The assumption involved in using this approach is that the material is optically thick and a plot of the logarithm of the thickness should be linear. However, for very small thicknesses, the approximation equation does not apply and the logarithmic plot must curve, since for zero thickness the transmission must be 100%.

In order to check the validity of the optically thick assumption, even for a limited spectral range, the reflectivity was measured on a Beckman DK-2 spectrophotometer whose wavelength

TABLE V

TOTAL TRANSMISSION DATA ON DYNAQUARTZ (6.2 pcf)
(Sample at Room Temperature)

Thermocouple Detector: Reeder 8657 w/CaF_2 window Model RP3W; Perkin-Elmer Model 121, 13 cps Amplifier tuned to chopper frequency; Keithley Model 149 Milli-Microvoltmeter

Source Temperature	I_o with no sample	I for t=0.040"	trans-mission	I_o with no sample	I for t=0.070"	trans-mission
400°C	1.4 mv	45μv(av)	.0231	1.4 mv	30μv(av)	.01226
		40μv(min)	.0195		20μv(min)	.0050
		60μv(max)	.0339		40μv(max)	.0195
600°C	2.9 mv	150μv(av)	.0474	2.9 mv	130μv(av)	.0405
		130μv(min)	.0405		120μv(min)	.0371
		170μv(max)	.0544		140μv(max)	.0440
800°C	5.3 mv	100μv(av)	.0133	6.4 mv	90μv(av)	.00942
		80μv(min)	.0095		80μv(min)	.00784
		120μv(max)	.0171		100μv(max)	.0110
900°C	.23 mv	6μv(av)	.0175	.28 mv	5μv(av)	.0108
		4μv(min)	.0088		4μv(min)	.0072
		8μv(max)	.0263		6μv(max)	.0144

Gain at 10.55 gives 1μv test signal = 10 mv; dark current 10-15μv, Average value 13μv for 400°C and 600°C runs.

Gain at 10.50 gives 1μv test signal = 5.2 mv; dark current 20-40μv, Average value 30μv for 800°C run.

Gain at 2.60 gives 1μv test signal = 10 mv; dark current 1-3μv, Average value 2μv for 900°C run.

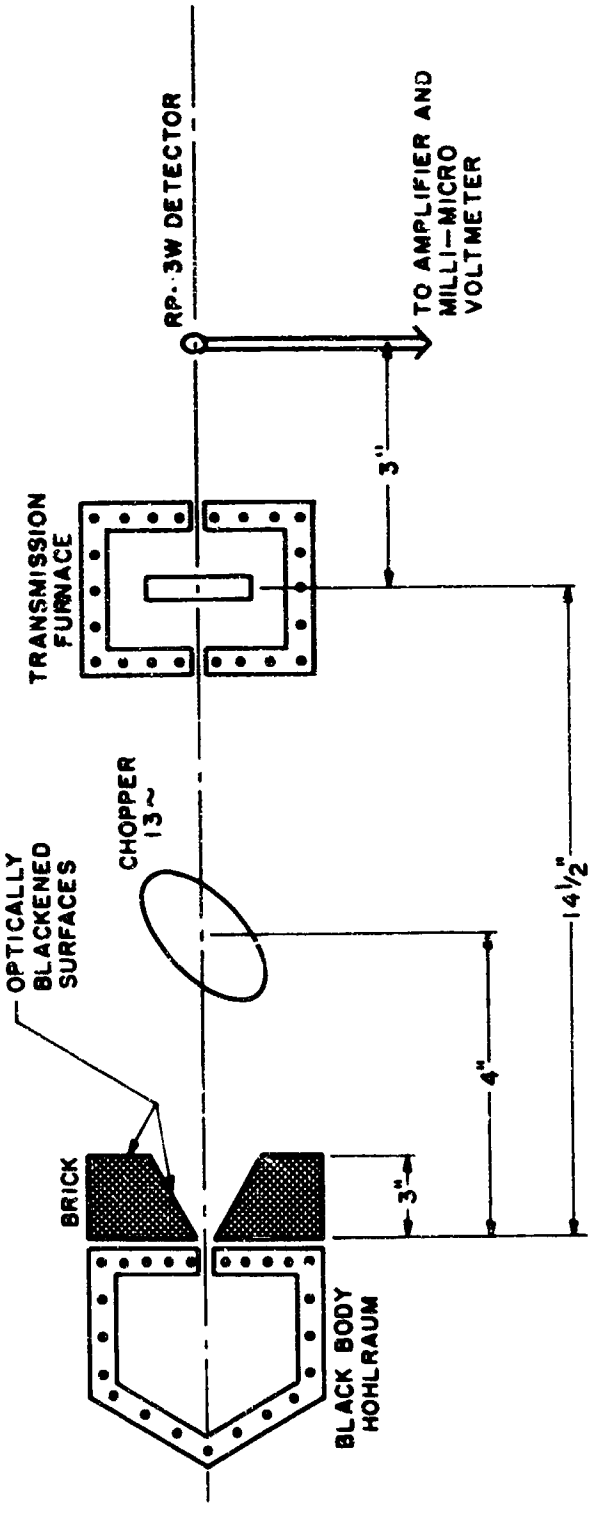

NOTE: DRAWING NOT TO SCALE

Figure 8. Schematic Diagram of Experimental Apparatus for Total Transmission at 400° and 600° Sample Temperatures

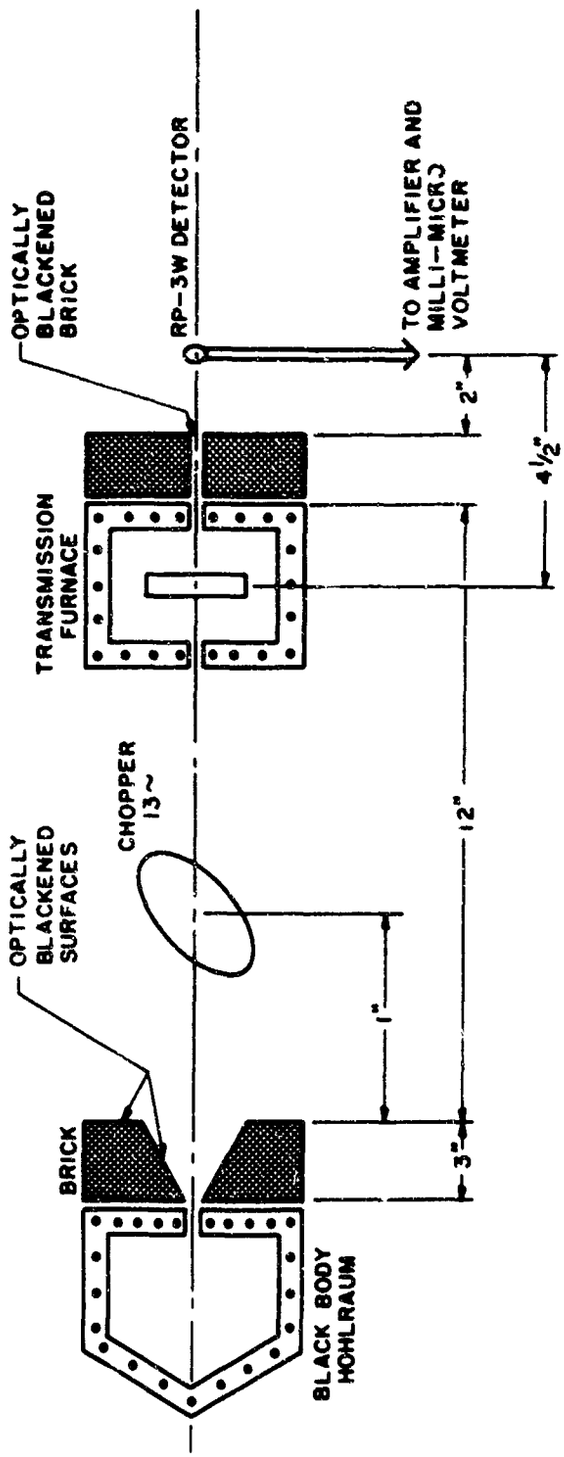

NOTE: DRAWING NOT TO SCALE

Figure 9. Schematic Diagram of Experimental Apparatus for Total Transmission at 700° and 800°C Sample Temperatures

TABLE VI

TOTAL TRANSMISSION DATA ON DYNAQUARTZ (6.2 pcf)

(SAMPLE AND SOURCE TEMPERATURE SAME)

Thermocouple Detector: Reeder 8657 w/CaF_2 window Model RP3W; Perkin-Elmer Model 121, 13 cps Amplifier tuned to chopper frequency; Keithley Model 149 Milli-Microvoltmeter

Source and Sample Temperature	I_o with no sample	I for t=.040"	trans-mission	I_o with no sample	I for t=.070"	trans-mission
400°C	1.4 mv	45μv(av)	.0231	1.4 mv	30μv(av)	.01226
		40μv(min)	.0195		20μv(min)	.0050
		60μv(max)	.0339		40μv(max)	.0195
600°C	2.9 mv	150μv(av)	.0474	2.9 mv	130μv(av)	.0405
		130μv(min)	.0405		120μv(min)	.0371
		170μv(max)	.0544		140μv(max)	.0440
800°C	5.3 mv	100μv(av)	.0133	6.4 mv	90μv(av)	.00942
		80μv(min)	.0095		80μv(min)	.00784
		120μv(max)	.0171		100μv(max)	.0110
900°C	.23 mv	6μv(av)	.0175	.28 mv	5μv(av)	.0108
		4μv(min)	.0088		4μv(min)	.0072
		8μv(max)	.0263		6μv(max)	.0144

Gain at 10.55 gives 1μv test signal = 10 mv; dark current 10-15 μv, Average value 13μv for 400°C and 600°C runs.

Gain at 10.50 gives 1μv test signal = 5.2 mv; dark current 20-40μv, Average value 30μv for 800°C run.

Gain at 2.60 gives 1μv test signal = 10 mv; dark current 1-3μv, Average value 2μv for 900°C run.

TABLE VII

CALCULATED CROSS SECTIONS FROM MEASURED
TOTAL TRANSMISSION OF DYNAQUARTZ (6.2 pcf)
(Sample and Source were heated independently)

Sample and Source Temp (°C)	Slope ($in.^{-1}$)	Intercept	M($in.^{-1}$)	N($in.^{-1}$)	P($in.^{-1}$)
400	21.028	0.0640	636.09687	636.0809	0.0265
600	5.2466	0.0585	174.060	174.031	0.0290
800	11.523	0.01540	1484.9675	1484.9636	0.0039

CALCULATED CROSS SECTIONS FROM MEASURED
TOTAL TRANSMISSION OF DYNAQUARTZ (6.2 pcf)
(Sample at Room Temperature)

Source Temp (°C)	Slope ($in.^{-1}$)	Intercept	M($in.^{-1}$)	N($in.^{-1}$)	P($in.^{-1}$)
400	27.233	0.00132	41,220.1940	41,220.1936	0.0004
600	30.266	0.00236	25,618.8850	25,618.8844	0.0006
800	69.5616	0.380	296.55	296.43	0.12

range is from 0.80 to 2.5 microns. Over the range from 2.5 to about 1.4 microns, the Dynaquartz appeared to have a higher reflectance value than $MgCO_3$, the standard. Beyond 1.4 microns to 0.8 micron, the reflection was about 85 to 86% of the standard. Both the total reflection and diffuse reflection were measured and it was found that all of the radiation was diffusely reflected, as would be expected with a material of this type, ie, fibrous layers of reflecting silica. The reflection in the spectral region from 0.38 to 0.70 micron was also examined on a GE spectrophotometer and was found to be about 98 to 99% diffuse. Thus Dynaquartz diffuses radiation in a few layers of fibers and can be considered semitransparent only for very small thicknesses of material.

3. CALCULATION OF RADIATION CROSS SECTION FROM ELECTROMAGNETIC THEORY

If the fibrous insulation is considered to be a random matrix of infinite cylinders whose axes are in parallel planes and the direction of heat flow to be perpendicular to the fibers it is possible to calculate the radiation attenuation parameters of fibrous materials such as Dynaquartz. Assuming that scattering and absorption occur in fibers, Larkin (Reference 34) derived the following equation for scattering cross section:

$$N = \left[\frac{4 B K_s}{\pi D_f}\right]\left[\frac{\rho - \rho_g}{\rho_s - \rho_g}\right] \tag{38}$$

where

$$K_s = 1/\alpha\left[|A_0|^2 + |P_0|^2 + 2\sum_{n=1}^{\infty}|A_n|^2 + |P_n|^2\right] \tag{39}$$

and

$$\alpha = \frac{\pi D_f}{\lambda} \tag{40}$$

where α is the cylinder circumference measured in wavelengths.

The values of A_n and P_n are a function of the index of refraction and the first Bessel function and first Hankel function whose arguments are a function of α and J. Larkin calculated the scattering coefficient, K_s, and the fraction of backscattered energy, B, for various indexes of refraction for monochromatic radiation. The most appropriate index of refraction for Dynaquartz is J = 1.5 (References 38 and 39), the value for fused silica. The method used for calculating average values for BK_s is similar to that used for calculating the transmission, ie, to use the Planck's law as a weighting function, so that

$$BK_s = \frac{\int_0^{\infty} BK_s(\lambda)\, g(\lambda,T)\, d\lambda}{\int_0^{\infty} g(\lambda,T)\, d\lambda} \tag{41}$$

where $g(\lambda,T)$ the weighting function, is the Planck law as defined previously. This procedure gives each wavelength a weight in proportion to the energy it carries. The values calculated

for the backscattering cross sections are tabulated in Table VIII using a fiber diameter of 1.3μ, an index of refraction of 1.5, a bulk density of Dynaquartz as 6.2 pcf and the specific gravity of the fiber material as 2.17 (see Appendix II). The procedure used was to take increments of λ, calculate values for α by use of Equation 40 and determine the value for the scattering parameter, BK_s (λ) by use of Figure 6 in Reference 34 for J = 1.5. Then by graphical integration as indicated in Equation 41, the value for BK_s was determined and used in Equation 38 to calculate N, the scattering cross section.

The absorption cross section as derived by Larkin (Reference 34) in terms of the insulation properties is

$$P = \left[\frac{4K_a}{\pi D_f}\right]\left[\frac{\rho - \rho_g}{\rho_s \rho_g}\right] \tag{42}$$

where K_a is the ratio of the absorption cross section to the geometrical cross section. For large fibers, K_a is equal to the absorptivity of the material. For very small fibers

$$K_a = \frac{a^3 \pi^2}{16} J_r J_i \left[1 + 2 \log 1.12/a\right] \tag{43}$$

where J_r is the real part of the complex refractive index and J_i the imaginary part. However, for nonconducting dielectric materials J_i is zero and J_r is the square root of the dielectric constant. Therefore, the absorption was ignored since the scattering cross section is at least two orders of magnitude greater than the absorption cross section (Reference 9) for Dynaquartz.

TABLE VIII

CALCULATED VALUES OF BACKSCATTERED ENERGY
AND SCATTERING CROSS SECTIONS FOR DYNAQUARTZ (6.2 pcf)

Temperature	BKs	N(in^{-1})
400°C	0.0847	95.25
600°C	0.1038	116.73
800°C	0.1183	133.04
900°C	0.1262	141.92
1200°C	0.1654	186.01
1600°C	0.1600	179.94

4. DISCUSSION OF RADIATION TRANSMISSION EXPERIMENTS

The spectral transmission experiments were run on a Beckman IR-6 spectrophotometer in the spectral range of 1 to 15 microns. It is in this wavelength range where high temperature radiation properties are important. Spectral transmission data are valuable in the case of transparent or translucent materials since one obtains the spectral characteristics of the absorption coefficients. For Dynaquartz or other fibrous insulation materials, however, the absorption coefficients in the wavelength region of interest are small and scattering is the dominant phenomena or mechanism for reduction of transmission. Temperature variations in the spectra of the transmitted radiation were examined to see if any changes occurred in the scattering coefficient. No such variations were found up to 900°C.

A comparison between the spectral transmission data and total transmission data is very difficult to make for the following reasons:

(a) the samples used were not the same in each of these measurements;

(b) the thicknesses of the samples are difficult to reproduce;

(c) the inherent scatter in the spectral transmission data is at least 5%;

(d) the noise level of the amplifier and detector for the total transmission measurements was high and some signals were about the same as the noise level;

(e) the total transmission detector was not completely isolated so that fluctuations in the room temperature affected the signal;

(f) the position of the detector was varied slightly for each measurement;

(g) no correction was made for the spectral absorption of CaF_2 window used on the detector.

Average readings were taken along with minimum and maximum values for the detector signals in the total transmission experiment. Nevertheless, the measured total transmission values were higher than the calculated values using spectral data (see Table IX). Values for the integrated transmission using spectral data, shown in Appendix III, were calculated by numerical integration indicated in Table IX. The variation in the absorption cross section is significant although the magnitude of the absorption cross section is small, compared to the scattering cross section.

However, in the present experiments, sample and source radiation differed; changes in the absorption cross sections with temperature affected the measured transmitted flux from the source. Corresponding changes in scattering cross section must be much smaller since the variations in transmission are reversible up to 900°C, thus indicating no gross change in fiber orientation. Furthermore, the scattering cross section is only dependent on the refractive index for the incident radiation. These factors do not change appreciably in the above experiments so that much smaller variation of the scattering cross section was measured than that of the absorption cross section.

It was observed during the total transmission experiments that the scattering cross section decreased as the source temperature increased (thus changing the spectral distribution of the radiation) while the sample was kept at room temperature. The data are tabulated in Table X along with those of Wechsler and Glaser (Reference 1) for higher temperatures and show qualitative agreement. The values for the scattering cross sections obtained from electromagnetic theory considerations are about one half the experimental values shown in Table X.

TABLE IX

CALCULATED CROSS SECTIONS FROM INTEGRATED TOTAL TRANSMISSION OF DYNAQUARTZ (6.2 pcf) USING SPECTRAL TRANSMISSION DATA

Sample Temp (°C)	Slope ($in.^{-1}$)	Intercept	N($in.^{-1}$)	P($in.^{-1}$)
20	40.4	0.0320	2488.5	$8.2(10^{-3})$
400	34.5	0.0220	3102.4	$5.5(10^{-3})$
800	28.9	0.003	15185.8	$9.0(10^{-4})$

TABLE X

COMPARISON OF CALCULATED CROSS SECTIONS OF DYNAQUARTZ (6.2 pcf) FOR VARIOUS SOURCE TEMPERATURES

Source Temperature	Scattering Cross Section ($in.^{-1}$)	Absorption Cross Section ($in.^{-1}$)
400°C (752°F)	$41\ (10^3)$	$4.0(10^{-4})$
600°C (1112°F)	$25\ (10^3)$	$6.0(10^{-4})$
800°C (1472°F)	$3.0(10^2)$	$1.2(10^{-1})$
1200°C (2192°F)*	$2\ (10^2)$	$1.2(10^{-1})$
1600°C (2912)*	$1.6(10^2)$	$2.8(10^{-1})$

*Values obtained from Reference 1.

It may, therefore, be inferred that at least qualitative agreement between measured and calculated scattering cross sections at elevated temperatures was obtained. The same general trend was indicated by the spectral transmission experiments.

All the transmission data are subject to large variations due to the instabilities of the apparatus used, sample inhomogeneities, and the theoretical limitations of applying the approximations to the Hamaker two-flux model. Therefore, only general trends in the cross sections have been indicated. The results, however, seem to be representative for the samples tested. The data indicate that there are difficulties involved in making total normal transmission measurements for highly scattering materials and that care must be taken in acquiring radiation cross sections. In attempting to correlate spectral with total transmission measurements, perhaps the largest experimental variables are those associated with (a) obtaining the intensity of radiant flux from the same solid angle, and (b) reflection of radiant flux at the front surface of the sample. Reflection at the front surface is not taken into account for the spectral transmission measurements.

In summarizing the radiation attenuation measurements it is obvious that problems in performing these experiments are numerous and accurate values for the scattering and absorption cross sections are difficult to obtain. Qualitative agreement between the calculated and measured values of the scattering cross section with source temperature of 800°C was obtained. In fibrous insulating materials, such as Dynaquartz, with small fiber diameters, it is apparent that scattering is the main mechanism of radiation attenuation.

5. THERMAL CONDUCTIVITY EXPERIMENTS

a. Description of Equipment

The thermal conductivity instrument used for these measurements is a Dynatech T 3000 model. The instrument (Figure 10) was designed to test a wide variety of materials ranging in conductance from 1.0 to 1000 BTU/hr-ft^2-°F. A complete description of the apparatus is contained in a report by Sparrell et al (Reference 40), and only what is germane to the measurement of low "k" materials is discussed here.

The test stack is shown diagrammatically in Figure 11. Radial heat losses around the test stack are minimized by using a 2-inch thickness of fine grain alumina powder (14-20 mesh). The alumina powder is held in place with a stainless steel wire enclosure lined with microquartz insulation, as shown in Figure 12.

The main and guard heater assembly (Figure 13) is a square flat plate, 12 x 12 x 3/4 inches. The main heater is surrounded by eight other heaters which guard the sides and corners. Each heater is 4 x 4 x 3/4 inches and is wound with platinum-40% rhodium resistance wire around a grooved alumina block which, in turn, is filled with alumina slip. Two samples, one on either side of the heater assembly, were used in the stack during the experiments. This experimental arrangement is in accordance with ASTM Specification C-177-63 (Reference 41). The heat fluxes through the sample are found by the use of ratio elements whose thermal conductivity must be linear with temperature. The sample size was 12 x 12 inches square with a thickness of 1/2 inch. The metered area was the central 16 square inches.

Since the room temperature compressive strength of the fibrous silica tested was approximately 11.1 psf (Reference 11), the sample and ratio elements were modified to support the excessive loads applied to the samples. The weight, roughly 100 pounds, resting on the top sample was supported by 40 zirconia pins each 1/4 x 1/4 x 1/2 inch, which were uniformly distributed throughout the guard area. Five pins were placed in each of the eight guard areas. The bottom sample is similar except that five additional pins are also inserted into the metered

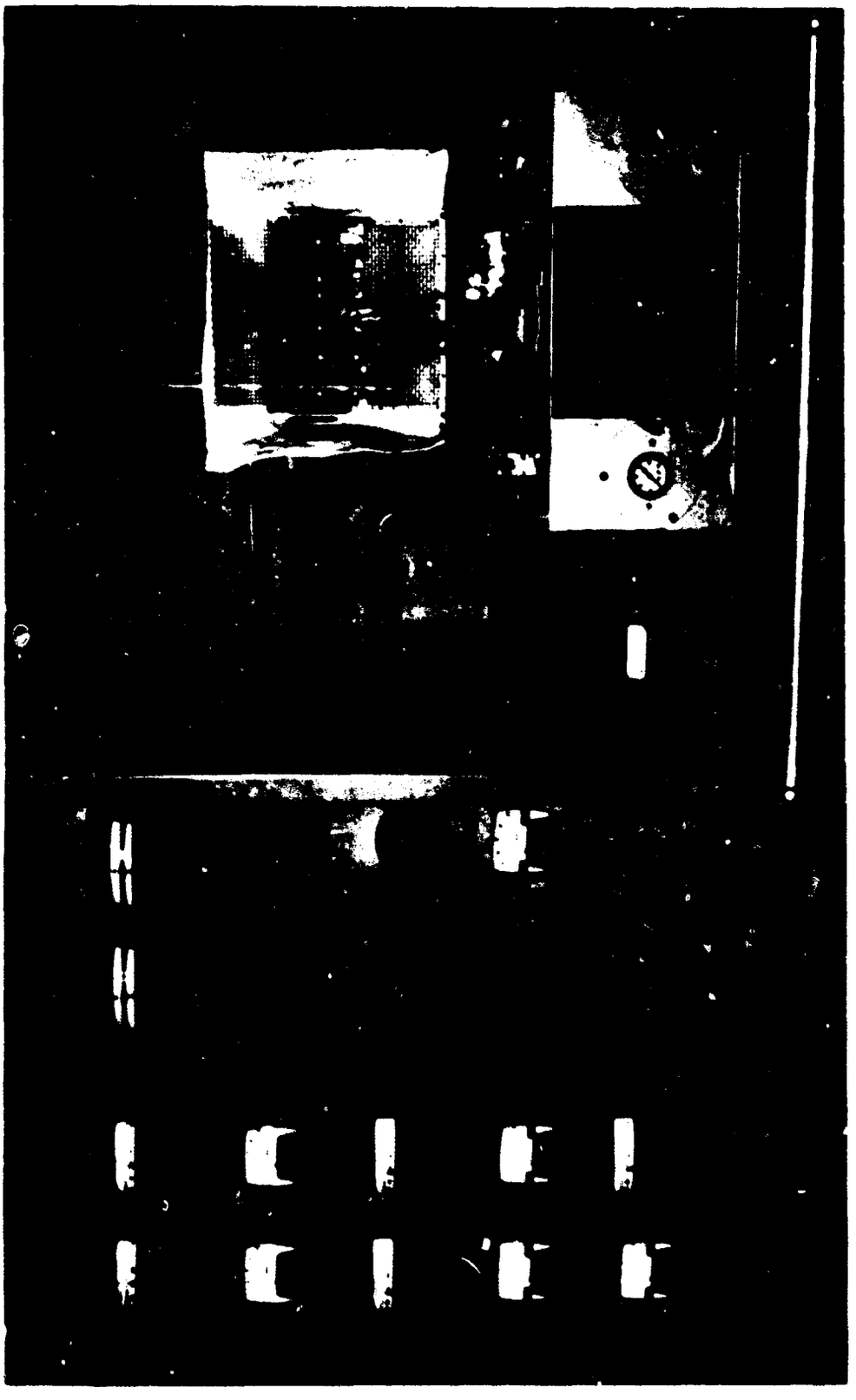

Figure 10. Overall View of Elevated Temperature Thermal Conductivity Apparatus

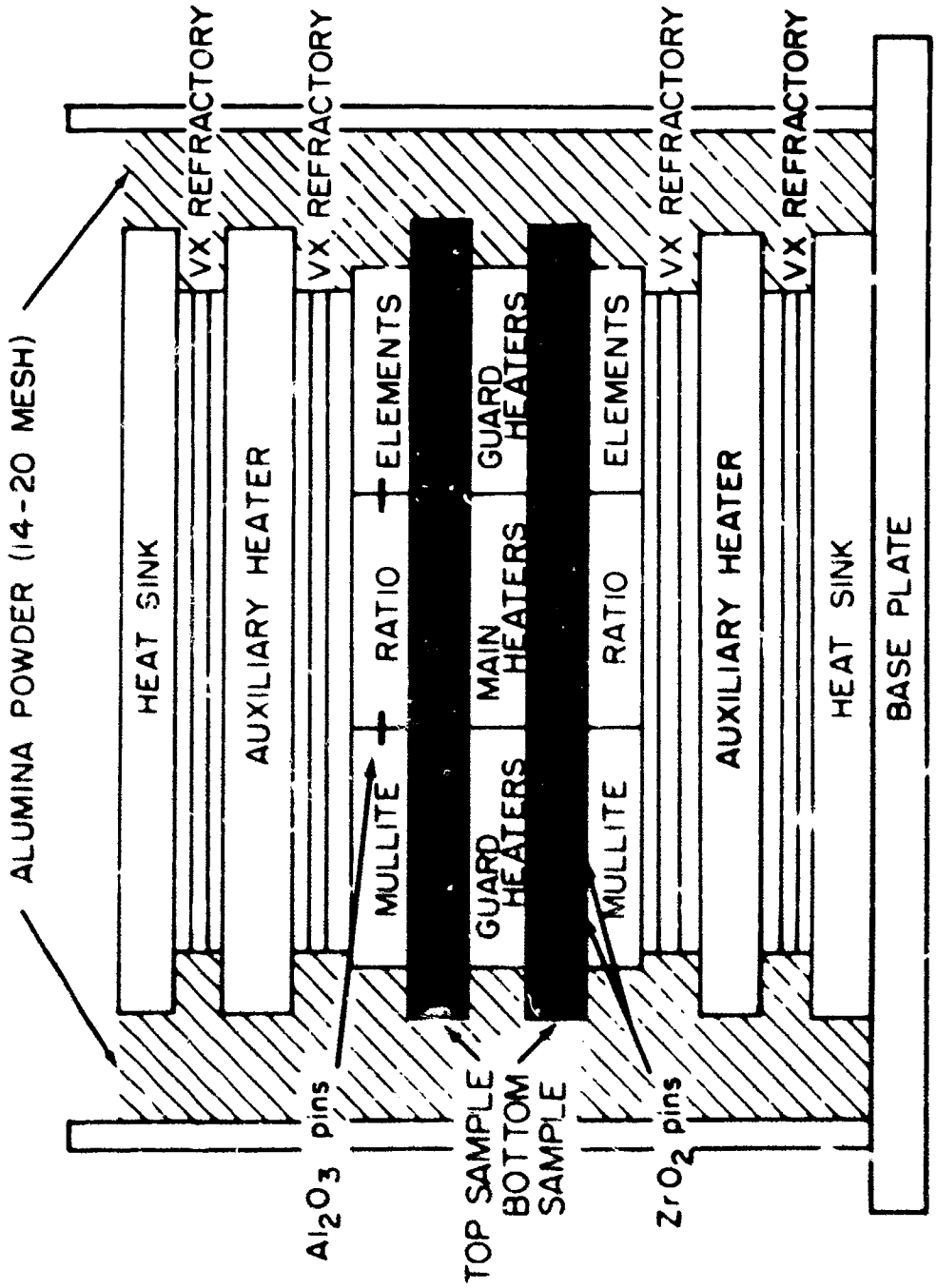

Figure 11. Schematic Diagram of Test Stack

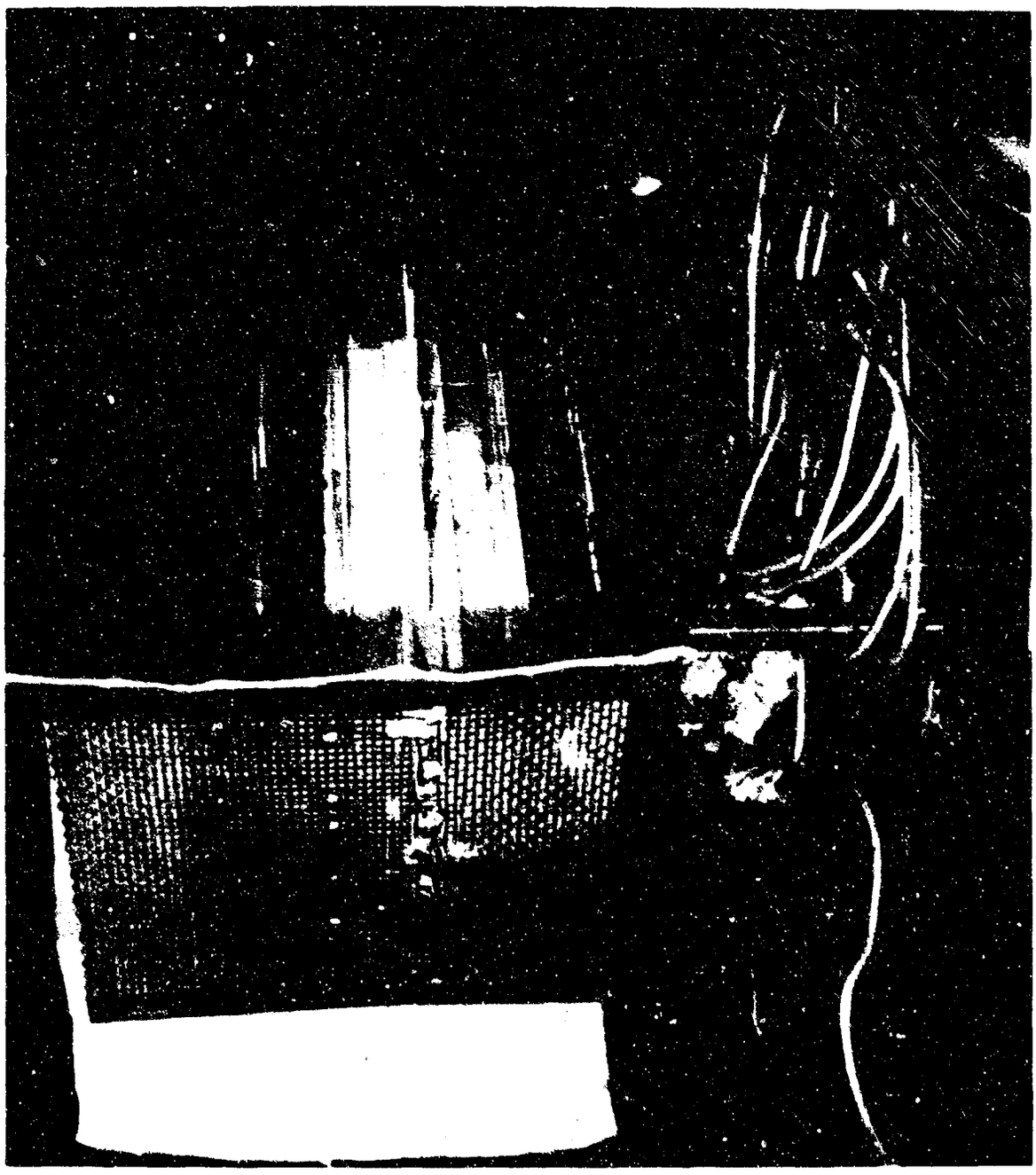

Figure 12. Overall View of Test Stack

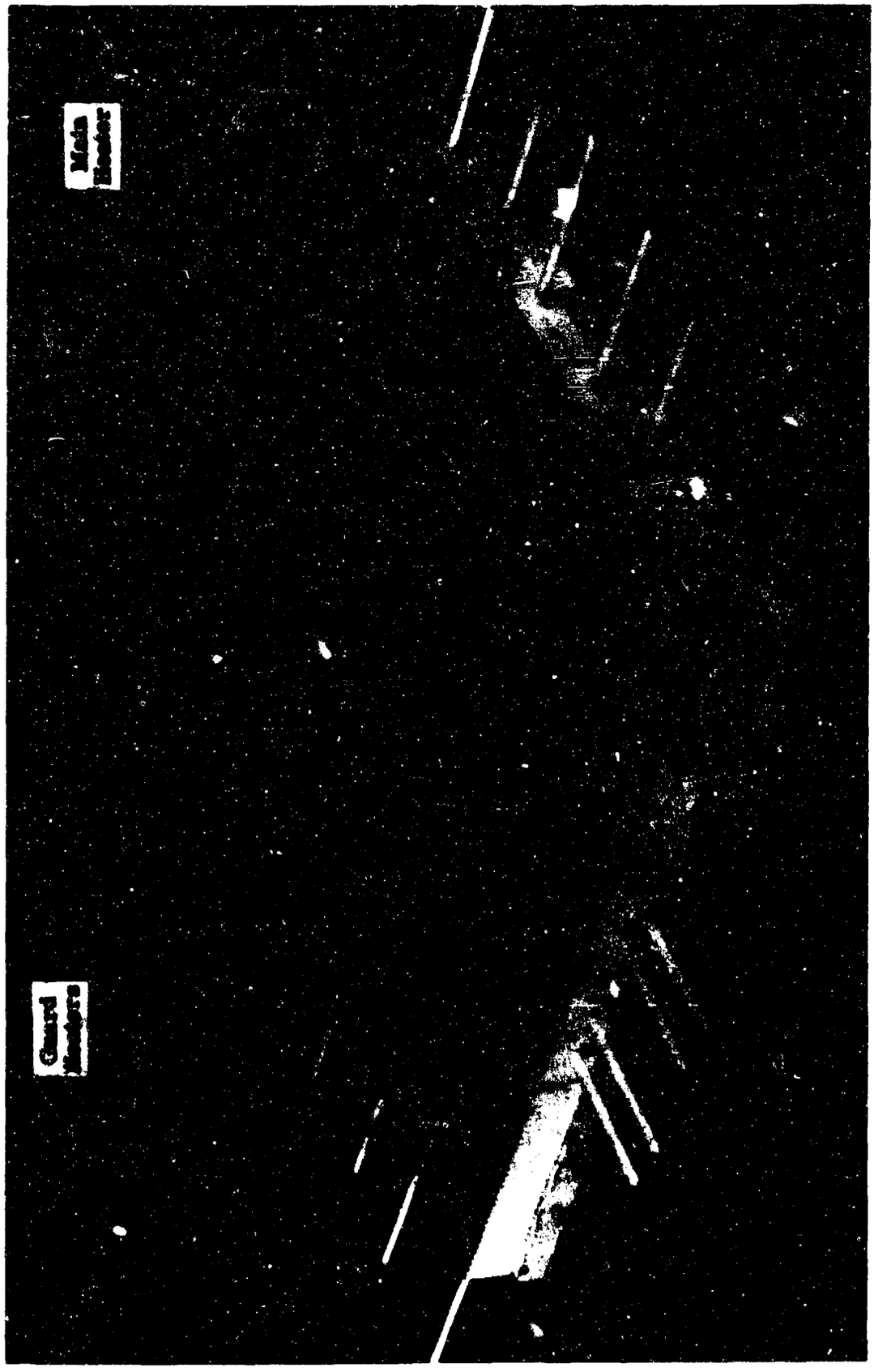

Figure 13. Main and Guard Heater Configuration

area (see Figure 14). This was necessary since the heater assembly is directly above the bottom sample and no provision to transfer the weight above the sample from the metered area to the guard area could be devised without altering the main heater.

Zirconia was chosen as the supporting material in these experiments because it has one of the lowest thermal conductivities (at 2200°F, 5.6 BTU-in./hr-ft^2-°F) (References 42 and 43) of any of the commercially available refractories. Zirconia also has a low volatility and chemical reactivity and a reasonable compressive strength (25,000 psi at 2600°F) (Reference 44). The zirconia used was calcia stabilized with a density of approximately 260 pcf. Since the chemical composition and density were very close to that of Jones (Reference 43), his data was used for the thermal conductivity. The chemical composition was determined quantitatively and is given in Table XI.

The ratio elements are porous mullite whose thermal conductivity varies linearly with temperature ensuring equal average values for the conductivity with varying temperature differentials across their thicknesses. Each ratio element consists of nine 4 x 4 inch blocks which are arranged in a manner identical to the heater assembly. In order to eliminate the use of zirconia pins in the metered area of the top specimen, the central ratio element was supported by four 1/4 inch alumina rods each one inch long and inserted midway between the unsupported central blocks and each of the four zirconia supported side blocks. Thermocouples were placed on the hot and cold surfaces of each central ratio element, and the ratio of the temperature differences was used to determine the heat flux through each mullite ratio element.

A single proportional controller with a null balance amplifier provides the automatic balance between the main and guard heaters. The power and control circuits are schematically drawn in Figure 15. The sensor for the proportional controller is a differential thermocouple placed on the surface of the test sample. One junction is placed on the main heater while the other junction is placed on the guard side heater. Theoretically, a zero signal indicates a balanced condition with both junctions at the same temperature. The controller visually indicates the degree of balance. In practice, the main and guard heaters are monitored manually until a rough temperature balance is attained. Since an actual zero or null balance could not be maintained for any reasonable length of time during an experimental run, the controller was set to balance around the signal from the differential couple.

The circuit of the top auxiliary heater is identical with the main heater circuit. The bottom auxiliary heater is automatically controlled by a Wheelco proportional controller. The control sensor for this circuit consists of four platinum vs platinum-10% rhodium thermocouples flush mounted on the surfaces of the two mullite ratio elements. This signal is subtracted from the sum of the outputs of the two thermocouples on the other ratio element. Equal average temperatures for both ratio elements result in a null condition. Any unbalance is indicated by a net signal, its polarity indicating the direction of unbalance.

Temperatures were monitored in the test stack with platinum vs platinum-10% rhodium thermocouples with a reference junction at 32°F. For the vacuum and argon experiments chromel-alumel thermocouples were used on the cold face of the samples. The physical arrangement of the equipment made it necessary to use two types of thermocouples when the test stack was covered with the vacuum bell jar. Thermocouples were placed as shown in Figures 16 and 17 on the hot and cold faces of the main, corner, and side heaters. The thermocouple beads were spot welded to a one inch diameter platinum disc, 0.001 inch in thickness in order to average the temperature over as large an area as possible (see Figure 18). Compensated lead wires are used from the thermocouple jacks, located at the base plate, and the thermocouple leads protruding from the test stack. All temperatures are read manually with a Rubicon potentiometer.

Figure 14. Bottom Dynaquartz Sample With Zirconia Pins

TABLE XI

CHEMICAL ANALYSIS OF ZIRCONIA

Element	Amount Present (parts per million)	
Si	5000	
Al	500	
Fe	200	
Ti	200	
Mg	1	percent of Total
Ca	5	
Zr	principal	

The auxiliary heaters shown in Figure 11 provide a means of establishing small temperature differences (200° - 500°F) across the specimens even at high temperatures, which is extremely important when measuring low "k" materials. With the auxiliary heaters, the power supplied to the main heater can be kept relatively small, even up to a sample mean temperature of 2500°F. In the tests performed, the temperature differences across the sample at mean temperatures of 500° to 1500°F were usually less than 300°F; whereas, at the high sample mean temperatures from 1500° to 2500°F they were about 400°F.

The power to the top auxiliary heater is set manually and the bottom heater is controlled automatically to maintain equal average temperatures of the ratio elements. The auxiliary heaters were designed to yield a maximum power dissipation of 15,000 BTU/hr-ft^2 and their maximum operating temperature is 2200°F. The auxiliary heaters use a Kanthal DA ribbon cast in Alundum cement especially developed to match the thermal expansion coefficient of the Kanthal. The casting is contained in an Inconel sheet metal box of about the same dimensions as the heater assembly. Wesgo VX super-refractory insulation was placed on both sides of the auxiliary heaters to minimize the amount of thermal energy dissipated by the water cooled, copper heat sinks. For the heat fluxes encountered in these experiments, three layers of 1/8 inch refractory were required. Maximum power dissipation of 15,000 BTU/hr-ft^2 can be met by a 17°F temperature rise at a water flow rate of four gpm. The VX refractory was chosen on the basis of its low thermal conductivity and expansion coefficient and high strength under compressive loads (Reference 40).

b. Thermal Conductivity Measurements

Although the basic procedure for the guarded hot plate experiment is outlined in ASTM C-177-63 (Reference 41), the construction of the apparatus and the temperature range covered caused major problems which necessitated operation of equipment in a slightly different manner. For the lower temperature runs, up to about 1200°F, the ASTM standard could be followed without too much deviation if the time required to reach steady state was longer than eight hours. The long period required to reach steady state is indicative of the high thermal inertia of the apparatus.

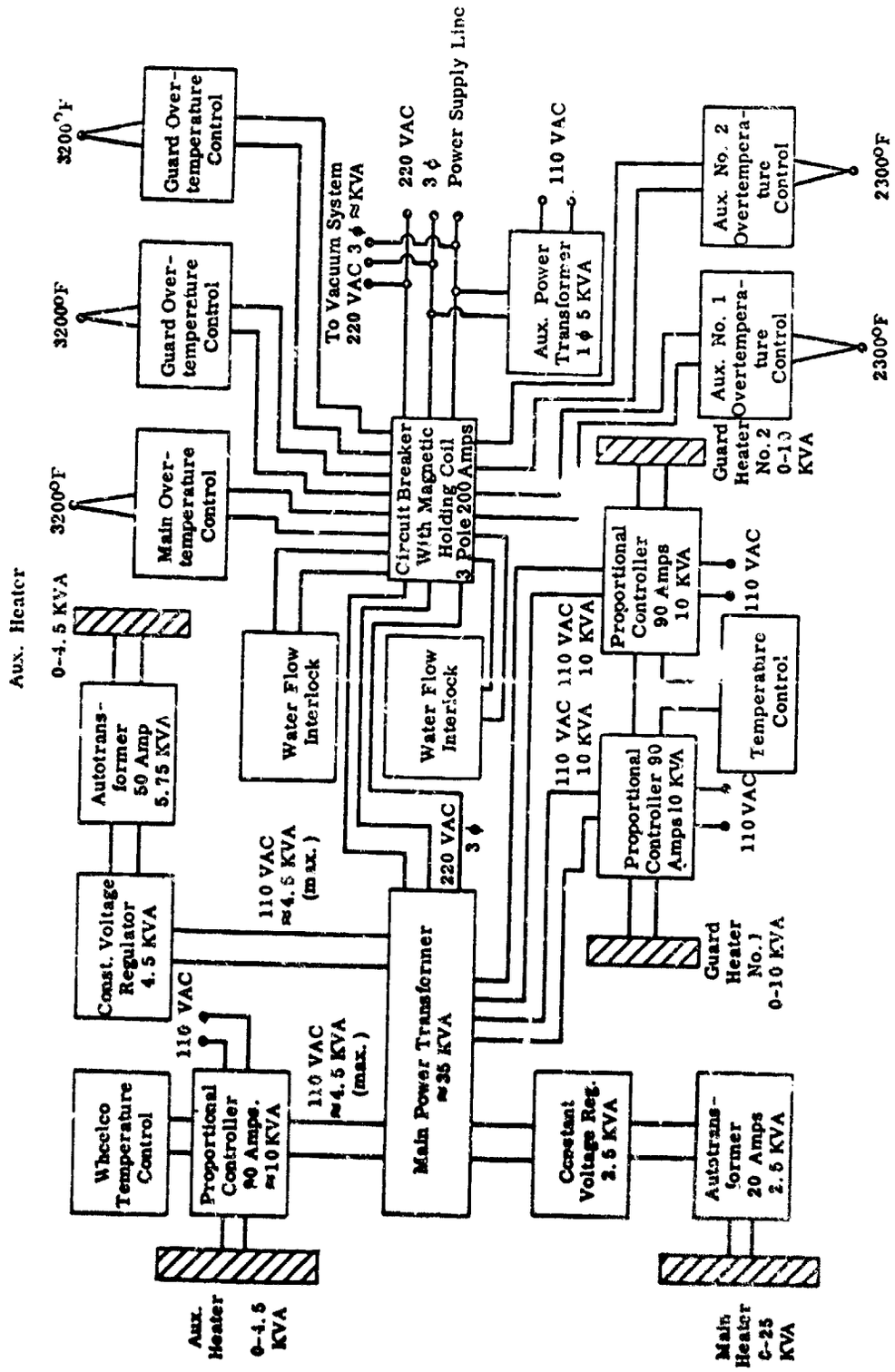

Figure 15. Power and Control Circuits for Elevated Temperature Thermal Conductivity Apparatus (Reference 40)

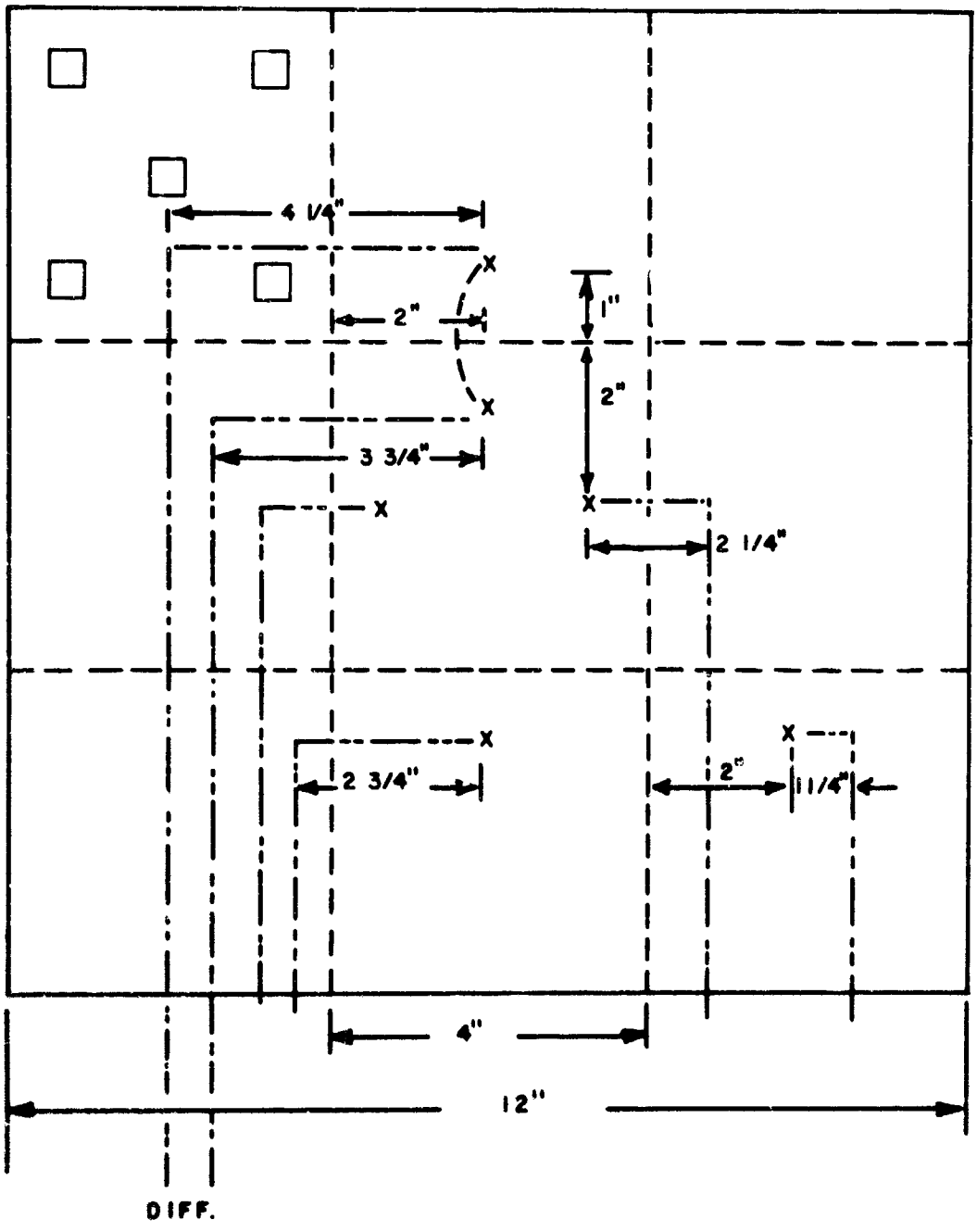

Figure 16. Schematic Diagram of Hot Face Thermocouple Placement

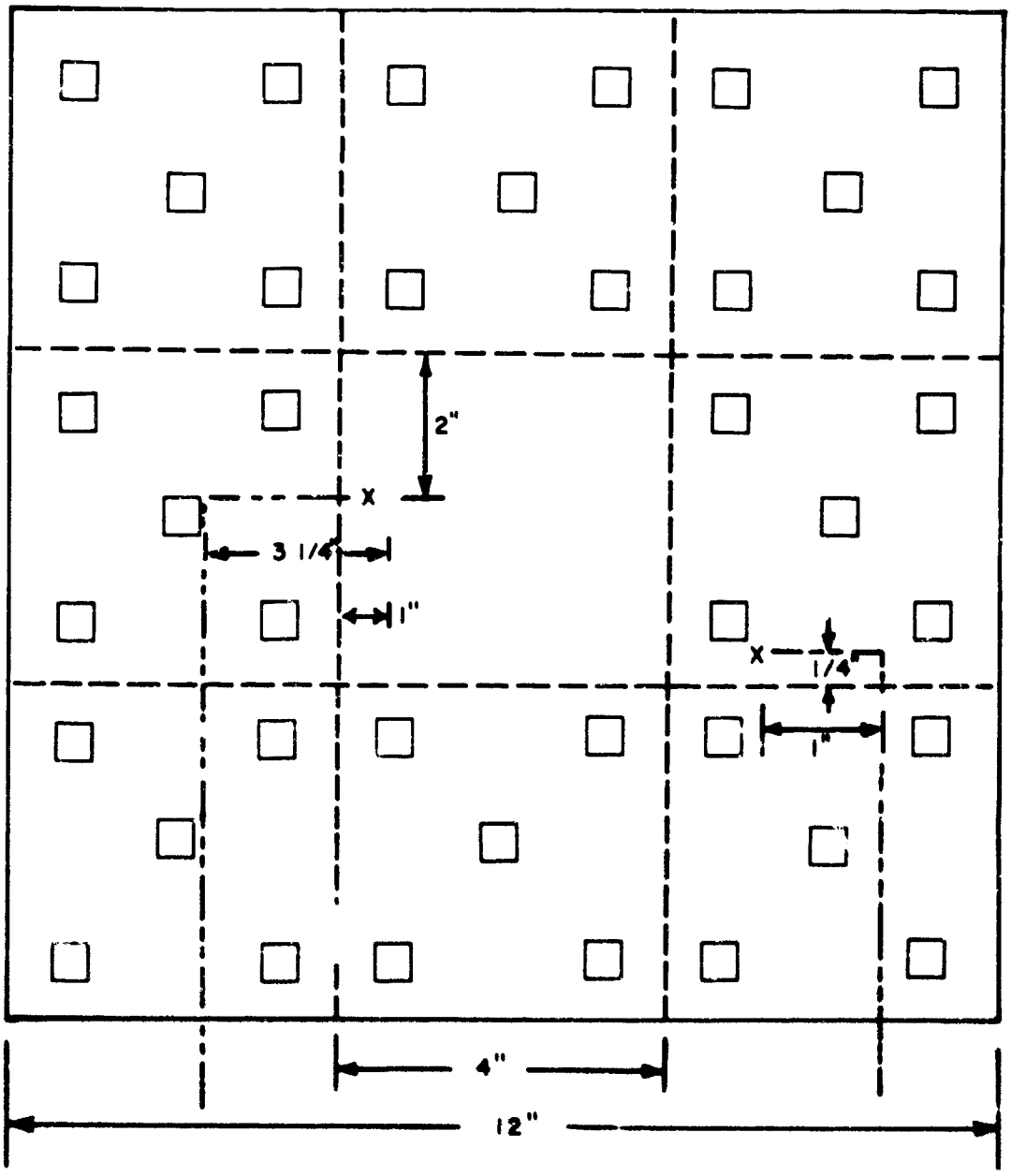

Figure 17. Schematic Diagram of Cold Face Thermocouple Placement

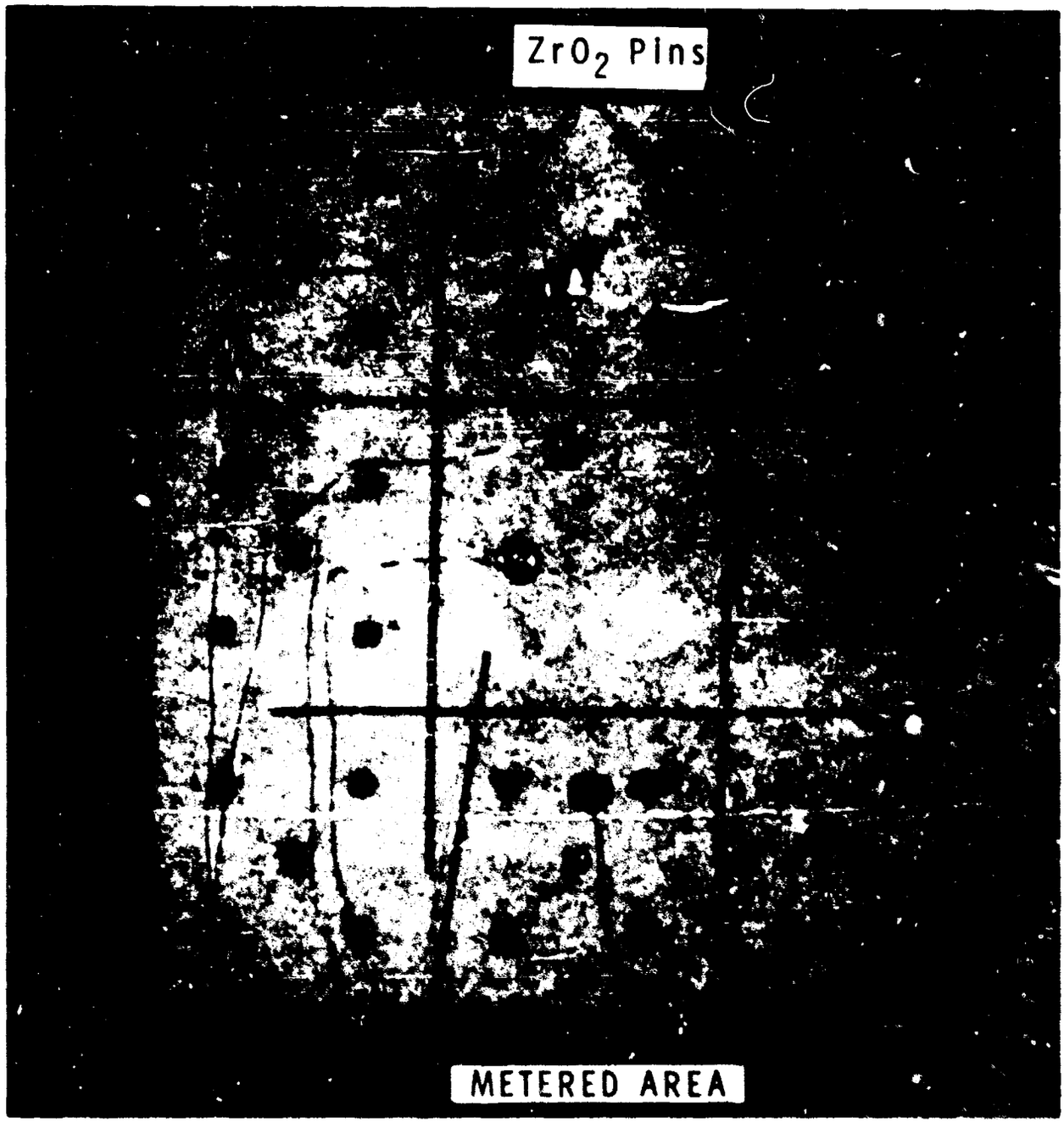

Figure 18. Top Dynaquartz Sample and Thermocouple Placement with Differential, Main, and Guard Thermocouples

Two main variances from the standard ASTM procedure were necessary for measurements made above 1200°F mean temperature. First, it was not usually possible during a 5-hour test observation to maintain a temperature difference between the main and guard heaters of 0.75% or less of the temperature differential across the thickness of the specimen. The average specimen temperature difference obtained was roughly 400°F, so that 0.75% would be 3°F. The heater imbalance varied between 5° and 20°F. Second, the thermal conductivity of the specimen did not usually remain within a 1% variance over a five-hour period after steady-state conditions were obtained (usually eight hours). Thermal conductivity values which varied less than 5% were considered very good and those that varied by 10% were considered to be comparable in magnitude to the average experimental error in the measurements. To ensure good control and accurate measurements, new thermocouples were used for each new sample tested. The maximum error estimated for these measurements is ±15% and the average experimental error is estimated to be about ±10% (see Appendix IV for error analysis). Only those data which were obtained at steady state and at a 5% imbalance between guard side and main heater of the temperature difference across the specimen were retained as good data. All other data were taken at regular intervals but were not considered for further analysis once one of the previous two conditions was not satisfied.

Thermocouple placement for hot and cold face temperature determinations are shown schematically in Figures 16 and 17. Figure 18 shows the outline of the heaters and arrangement of the zirconia supporting pins. Figure 18 also shows the physical arrangement of the thermocouples as used in the experimental test setup. The thermal conductivity of Dynaquartz (6.2 pcf) was determined in air, argon, and vacuum.

(1) Thermal Conductivity Measurements in Air

Several experimental runs were made in order to obtain good data for Dynaquartz in air. Three separate experiments were necessary since

(a) the sample cracked during the first run and all the data had to be disregarded (although tabulated in Appendix V);

(b) there was considerable difficulty in achieving a desirable heat flow ratio between bottom and top specimens at the higher temperatures and there was extreme scatter in the data for the second run.

Two experiments were carried out using Dynaquartz in the top and bottom specimens; the top sample however had no zirconia pins in the measuring section (these data are designated by run 1 and run 2 in Appendix V). In the third experiment, two different samples were used, Dynaquartz as the top specimen and sapphire wool as the bottom specimen, both with zirconia pins in the metered area. A correction was applied to obtain the thermal conductivity for no zirconia pins. The placement of the thermocouples is shown in Figures 16 and 17 for hot and cold surfaces respectively.

The magnitude of the correction applied to the bottom sample (for Run 2) to compensate for the conduction through the zirconia pins is shown in Figure 19 along with the top sample conductivity. The top curve is the data obtained for the bottom sample with zirconia pins in the metered area for Run 2. The middle curve has been corrected for the effect of the pins. In general, the correction is about 4 to 5% (see Appendix VI for tabulated results and calculations). The bottom curve represents the top sample data for the same run; it was obtained by fitting a least square polynomial equation of the third degree for the top sample data. The equation is

$$k_{eff} = -0.2905 + 0.7709\,(10^{-3})\,T - 0.1543\,(10^{-6})\,T^2 + 0.0365\,(10^{-9})\,T^3 \qquad (44)$$

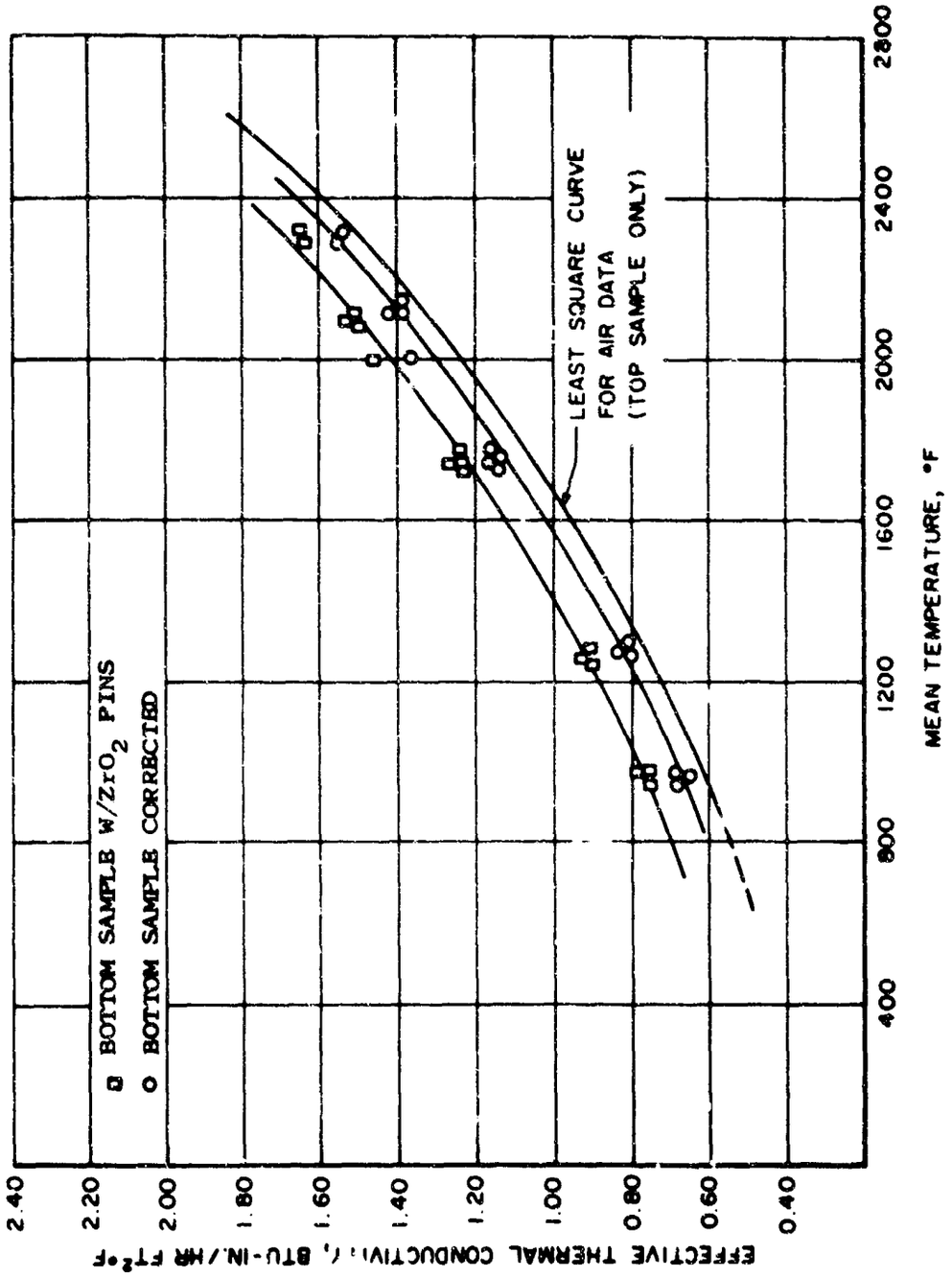

Figure 19. Effective Thermal Conductivity of Dynaquartz (6.2 pcf) in Air Correcting for Zirconia Pins

where T is in °R. The maximum deviation from the equation is 0.0612 for the data point at 2159°F mean temperature. The root mean square deviation was 0.0228.

As shown in Figure 19, the correction applied does not exactly match the data obtained on the top sample; however the correction is reasonable and within the experimental scatter of the data on the top specimen. Therefore, the corrections as applied to the run for Dynaquartz-Sapphire Wool experiment for Dynaquartz are justified. Since no other measurements were made for Dynaquartz in air, further analysis of the data for steady-state and low temperature imbalance conditions could only be made on these measurements.

Further analysis of the measured data was necessary since good thermal conductivity measurements are predicated on attainment of steady state and little or no lateral heat transfer across the specimen faces. Hence, the data obtained in air were carefully examined and only those data which fulfilled both conditions were further reduced. All the data are shown in Appendix V and the retained data are indicated by an asterisk. The corrections as applied to the specimens are tabulated in Appendix VI.

(2) Thermal Conductivity Measurements in Vacuum

The thermal conductivity of Dynaquartz was determined in vacuum from about 450° to 2000°F mean temperatures. Due to the shortage of compensated plug-in connectors for the platinum-10% rhodium thermocouples in the base plate of the apparatus, chromel-alumel thermocouples were used on the cold face of the samples. Hence, an upper temperature limit on the cold face was about 2200°F. The same was true for the argon experiments.

All the experiments carried out in this investigation were on 6.2 pcf Dynaquartz. The bottom sample utilized zirconia pins in the guard and main heater area; the top sample had zirconia pins in the guard areas only. The data are tabulated in Appendix V. Corrections applied to the bottom sample to compensate for the conduction of the zirconia pins are shown in Figure 20 along with the top sample conductivity. The top curve represents the data obtained from the bottom sample with zirconia pins in the metered area. The middle curve depicts the data obtained from the top sample without zirconia pins in the metered area. The bottom sample data corrected for zirconia pins in the metered area (bottom curve) shows the magnitude of the applied correction.

As can be seen from Figure 20, the experimentally measured thermal conductivity values for both top and bottom samples were in good agreement below 1000°F. From 1000° to 2000°F, the difference in the measured conductivities was appreciable. The correction became progressively better beyond 1000°F until at about 1500°F the measured data on the sample without pins were in good agreement with the corrected data for the sample with pins in the metered area. An average correction of about 20% was required above 1000°F. At the lower temperatures the correction was closer to 30%.

For the thermal conductivity measurements in vacuum, the values obtained were for specimen temperature differences of roughly between 200° and 350°F. The imbalance between the center and guard heaters was usually within 5% of the specimen temperature differences. Only the data which were at steady state and low temperature imbalance across the face of the specimens were retained for further analysis. All the data are shown in Appendix V; the retained data are indicated by an asterisk. The corrections as applied to the bottom specimens are tabulated in Appendix VI.

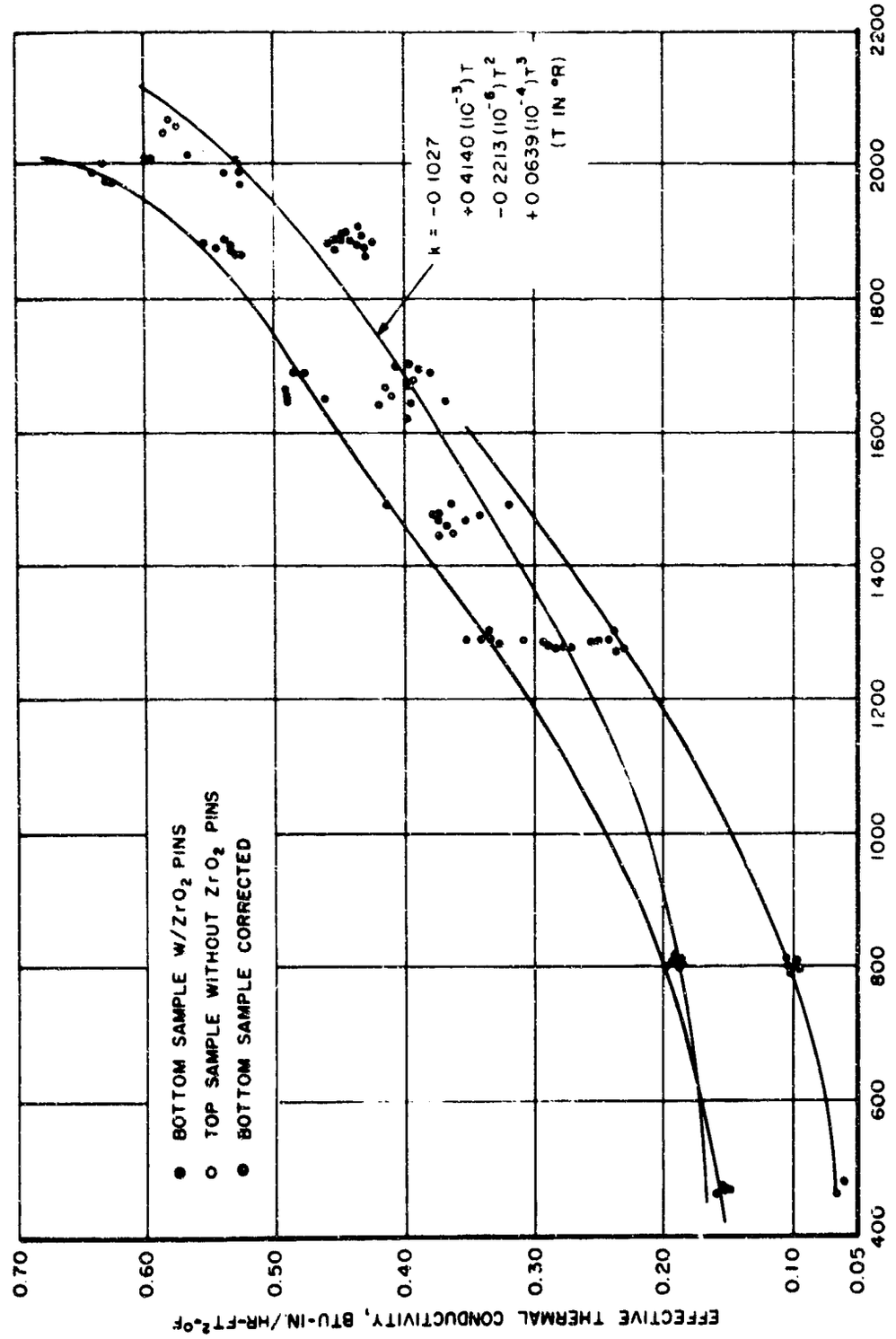

Figure 20. Effective Thermal Conductivity of Dynaquartz (6.2 pcf) in Vacuum Correcting for Zirconia Pins

The experimental data points for the top sample were fitted to a least squares polynomial equation of the third degree and the equation obtained was

$$K_{eff} = -0.1027 + 0.4140(10^{-3})T - 0.2213(10^{-6})T^2 + 0.0639(10^{-9})T^3 \quad (45)$$

where T is in °R

The maximum deviation from the equation is 0.0529 for the data point obtained at 1914°F mean temperature. The root mean square deviation is 0.0223.

The consistency of the experimental results obtained in air and in vacuum can be checked if a correction for the conductivity of air is applied to the measurements made in air. If the conductivity of air multiplied by the void volume is subtracted from the conductivity of Dynaquartz obtained in an air environment for the second run, the result is within the scatter of data obtained in vacuum. This is not true for the first experimental run in air, and hence lends further evidence that the values obtained in air for the first experimental run were in error since the sample cracked during the experiment.

3) Thermal Conductivity Measurements in Argon

The thermal conductivity of Dynaquartz (6.2 pcf) was determined in an argon environment from about 275° to 1950°F mean temperatures. The measurements made in argon followed the experimental run in vacuum. When the apparatus was cooled to room temperature after the vacuum experiment, 99.9% pure argon was purged into the bell jar surrounding the test stack. After two purges, the bell jar was pressurized to one atmosphere of argon. For reasons previously enumerated, chromel-alumel thermocouples were used on the cold faces of the specimens. Experimental setup and sample arrangement were the same as for the vacuum measurements.

The data for the argon environmental experiment are tabulated in Appendix V. Corrections applied to the bottom sample to compensate for the conduction of the zirconia pins are shown in Figure 21 along with the top sample conductivity. The curves shown in Figure 21 show the scatter of the experimental data. The upper curve represents the effective thermal conductivity of the sample supported by the zirconia pins in the metered area, whereas the bottom curve represents the data obtained for Dynaquartz alone (no zirconia in metered area). The curve for the correction of the zirconia pins was not drawn due to the scatter in the data. In general, the correction applied to the bottom sample assuming one dimensional heat conduction was about 15%. (See Appendix VI.)

For the thermal conductivity measurements in argon, the values obtained were for specimen temperature differences of between 150° and 400°F. The imbalance between the center and guard heaters was usually within 5% of the specimen temperature differences. Only the data which were at steady state and low temperature imbalance across the face of the specimens were retained for further analysis. All the data are shown in Appendix V; the retained data are indicated by an asterisk. The corrections as applied to the bottom specimens are tabulated in Appendix VI. The experimental data points for the top sample were fitted to a least squares polynomial equation of the third degree and the equation obtained was

$$K_{eff} = 1337 + 1.088(10^{-3})T - 0.7141(10^{-6})T^2 + 0.2011(10^{-9})T^3 \quad (46)$$

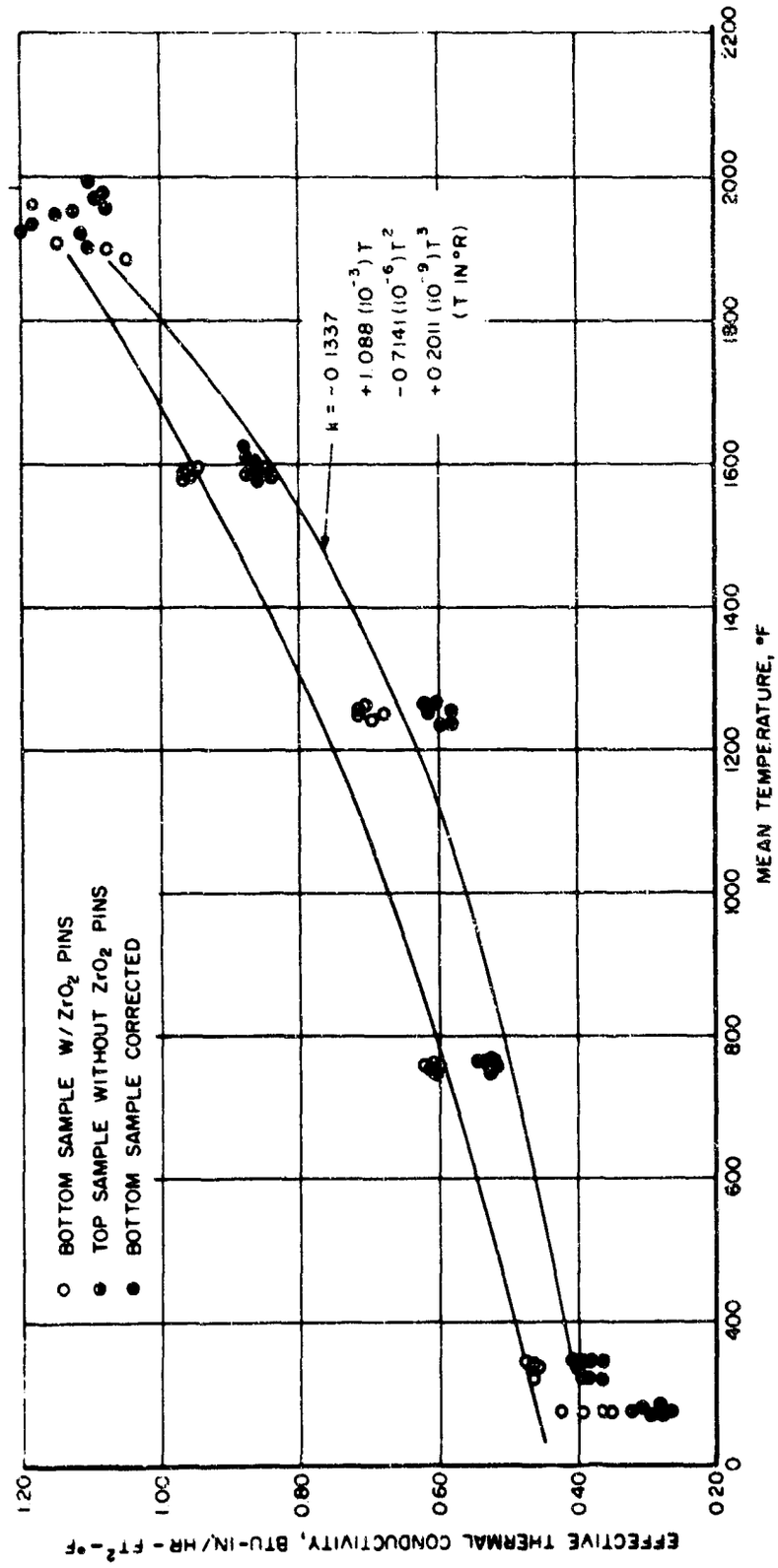

Figure 21. Effective Thermal Conductivity of Dynaquartz (6.2 pcf) in Argon (1 atm) Correcting for Zirconia Pins

where T is in °R.

The maximum deviation from the equation is 0.113 for the data point obtained at 1979°F mean temperature. The root mean square deviation is 0.044.

The self consistency of the experimental results obtained in argon and in vacuum may be checked in a manner similar to that done for the air environment. The extreme scatter in the experimental points in argon makes a comparison difficult; however, the values obtained in argon are qualitatively consistent with the vacuum data. The results are not in as good agreement as the second run in the air environment where self consistency was determined, but much better than the first experimental run in air where self consistency was not verified.

(4) Summary of Thermal Conductivity Measurements on Dynaquartz

The thermal conductivity of Dynaquartz (6.2 pcf) was determined in air from 400° to 2400°F mean temperature, in argon (1 atm) from 150° to 2000°F mean temperature, and in vacuum from 200° to 2000°F mean temperature. The major causes for experimental errors are due to unsteady-state conditions in the apparatus and imbalance between the main and guard heaters. The experimental data, shown in Figures 19, 20, and 21, were carefully examined for conformance with 5% imbalance condition and attainment of steady state. Hence, the experimental data for all runs carried out in this investigation were carefully reexamined and the best data points were determined. Close adherence of experimental conditions to a 5% imbalance between guard side and main heaters of the temperature difference across the specimen and attainment of steady state were necessary until data were retained. All the data are tabulated in Appendix V; the retained data are indicated by an asterisk. The experimental measurements represented in Figure 22 show the best available data for all the measurements carried out in the guarded hot plate apparatus.

The data shown in Figure 22 are tabulated in Tables XII, XIII, and XIV. In addition to the thermal conductivity and mean temperature, the temperature difference and imbalance between the side guard heater and main heater are also tabulated. As shown in Figure 22, the thermal conductivity in air varies from 0.6 to roughly 2.0 BTU-in./hr-ft^2-°F and in argon from 0.3 to 1.5 over the temperature range from 400° to 2000°F mean temperatures. The general shape of the two curves is about the same. In vacuum, however, the curve is flatter than anticipated and does not show the expected change in slope above 1500°F mean temperature. The least square curves used in Figure 22 are for the first and last terms of a third degree polynomial equation fitted to the data in Tables XII, XIII, and XIV. These curves have a higher average and rms error than the ones with four constants but they are still within the experimental error of the measurements. There is no physical significance to the equations fitted with four constants since that is only a mathematical technique for averaging the data. The two-term least square equations are better for interpretation of the radiative contribution of effective or total thermal conductivity and are therefore the preferred ones, although both types are shown in Tables XII, XIII, and XIV. It should be noted that two points in Table XII and three points in Table XIII have a larger than 5% temperature imbalance between main and guard heater. These points were retained because they were considered to be steady-state data while still retaining a tolerable temperature imbalance.

c. Comparison of Thermal Conductivity Data

In comparing the experimental results obtained in the guarded hot plate apparatus and that of others, it should be pointed out that different techniques are used and a wide variety of test methods can be chosen. The guarded hot plate is perhaps the most widely accepted thermal conductivity measurement technique below 1000°F mean temperature. It is the purpose of this investigation to extend the guarded hot plate measurements of fibrous insulations beyond 1000°F to as close to the operating temperature of a fibrous insulation as possible.

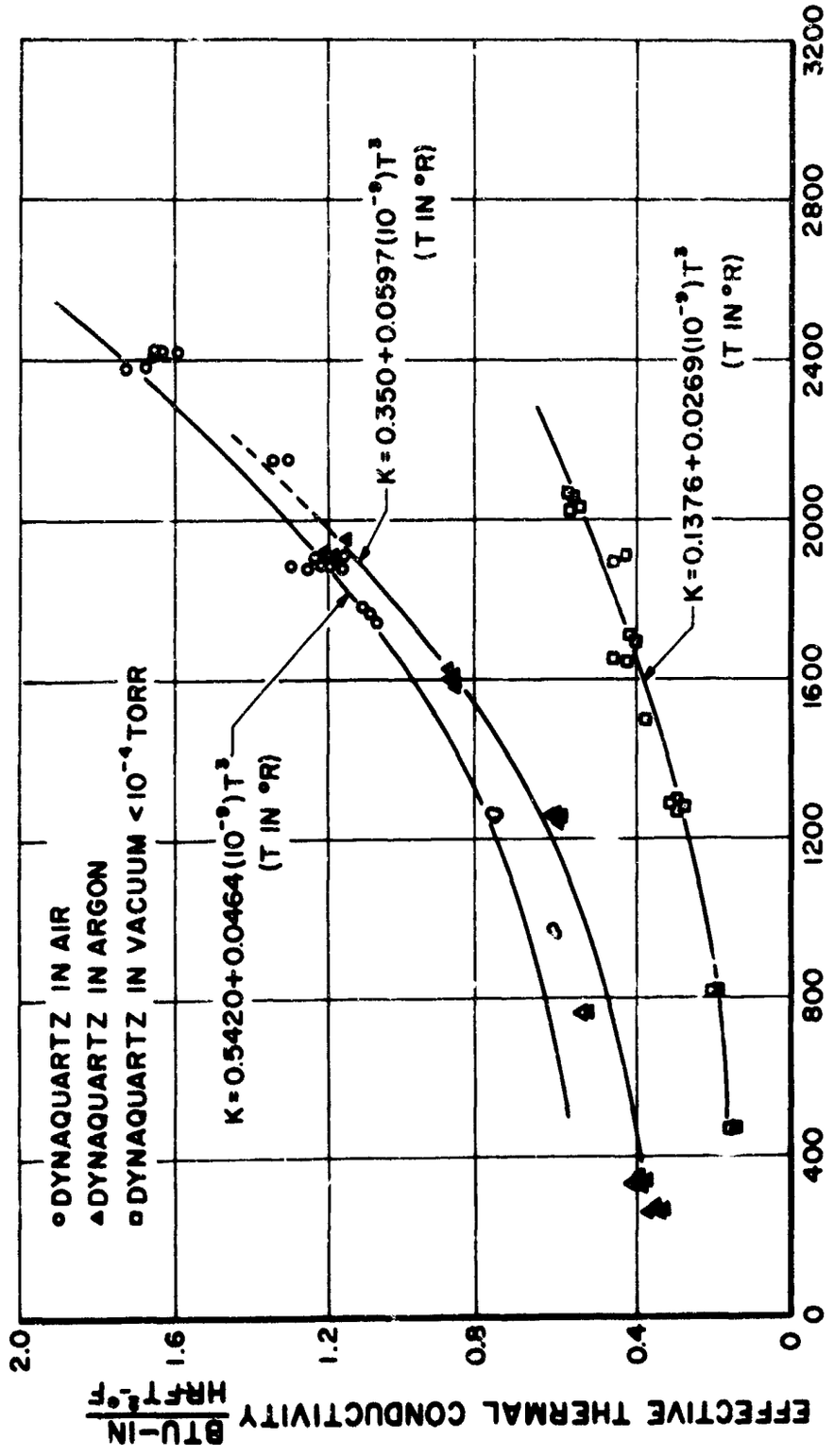

Figure 22. Effective Thermal Conductivity of Dynaquartz (6.2 pcf) in Air, Argon, and Vacuum at Elevated Temperatures

TABLE XII

THERMAL CONDUCTIVITY OF DYNAQUARTZ (6.2 pcf)
IN AIR, COMPOSITE DATA

k $\frac{\text{BTU-in.}}{\text{hr-ft}^2\text{-°F}}$	T(°F)Mean	ΔT(°F)	Imbalance (°F)
0.606	961.9	409.1	4.0
0.614	973.9	406.9	7.3
0.614	975.3	409.5	6.9
0.760	1259.8	451.9	6.7
0.752	1262.5	454.9	8.1
0.750	1266.2	455.9	7.8
0.764	1256.3	466.6	9.9
1.074	1749.0	425.1	7.5
1.083	1770.9	419.9	4.9
1.101	1787.0	411.8	9.0
1.195	1878.8	378.3	8.7
1.160	1879.6	388.7	2.7
1.250	1883.0	365.2	8.0
1.210	1884.2	376.4	14.4
1.298	1887.1	361.7	7.3
1.255	1887.1	373.0	13.3
1.222	1905.0	373.0	16.0
1.151	1911.6	393.9	-0-
1.292	2150.1	363.7	18.0
1.258	2159.1	362.7	10.3
1.298	2155.7	347.0	16.0
1.338	2148.2	343.9	17.4
1.724	2388.0	373.3	15.8
1.622	2407.9	360.8	15.7
1.657	2406.5	353.6	18.3
1.627	2421.8	350.3	7.6
1.564	2421.3	362.7	10.7
1.639	2426.3	355.3	5.0
1.596	2426.5	364.3	12.3

Least square equation is:

$$k = -1.068 + 1.911(10^{-3})T - 0.7025(10^{-6})T^2 + 0.1261(10^{-9})T^3$$

Emax = 0.1347 at 2388°F mean temp
ERMS = 0.0561

$$k = 0.5420 + 0.0464(10^{-9})T^3$$

Emax = 0.155 at 1887.1°F mean temp
ERMS = 0.067

TABLE XIII

THERMAL CONDUCTIVITY OF DYNAQUARTZ (6.2 pcf)
IN ARGON (1 atm)

k $\frac{\text{BTU-in.}}{\text{hr-ft}^2\text{-}^\circ\text{F}}$	T(°F)Mean	ΔT(°F)	Imbalance (°F)
0.347	271.3	156.0	1.2
0.341	273.4	158.9	0.9
0.321	277.3	162.0	1.7
0.372	267.0	145.5	1.0
0.340	277.6	159.6	1.2
0.394	344.7	192.9	10.4
0.401	338.0	192.1	11.1
0.385	318.8	179.1	11.4
0.528	767.4	370.9	15.6
0.531	765.3	372.6	15.0
0.530	767.3	369.9	15.9
0.532	766.6	369.3	16.2
0.608	1245.5	444.8	7.4
0.611	1257.6	444.6	10.8
0.612	1257.5	431.9	5.5
0.615	1256.0	429.1	4.1
0.612	1259.7	433.3	5.2
0.610	1259.4	431.7	4.7
0.605	1258.2	430.4	5.6
0.880	1625.2	364.2	10.0
0.873	1610.2	383.9	11.1
0.869	1603.4	388.6	10.9
0.857	1597.4	393.3	12.1
0.876	1588.1	386.6	0.8
1.200	1913.2	331.2	4.5
1.155	1945.9	351.8	4.5
1.205	1918.6	334.3	12.1
1.182	1931.4	339.7	10.9

Least square equation is:

$$k = -0.4776 + 1.927(10^{-3})T - 1.334(10^{-6})T^2 + 0.3439(10^{-9})T^3$$

T in °R
Emax 0.068 at 1945.9°F mean temp
ERMS 0.027

$$k = 0.350 + 0.0598(10^{-9})T^3$$

Emax 0.0712 at 766.6°F mean temp
ERMS 0.0412

TABLE XIV

THERMAL CONDUCTIVITY OF DYNAQUARTZ (6.2 pcf)
IN VACUUM ($<10^{-4}$ torr)

k $\frac{\text{BTU-in.}}{\text{hr-ft}^2\text{-°F}}$	T(°F)Mean	ΔT(°F)	Imbalance (°F)
0.154	467.5	216.1	1.4
0.150	470.7	222.3	2.0
0.189	809.0	356.9	7.9
0.187	808.9	358.6	9.5
0.187	809.9	360.2	8.2
0.186	810.2	360.1	9.8
0.187	810.2	360.1	7.5
0.308	1295.1	316.7	1.2
0.292	1293.4	336.8	1.3
0.287	1287.3	340.5	0.2
0.273	1285.8	345.4	1.9
0.278	1282.8	350.5	2.1
0.281	1281.1	351.6	3.6
0.363	1500.1	335.9	11.1
0.418	1646.9	333.6	10.6
0.457	1660.0	333.8	10.1
0.392	1688.4	342.3	15.0
0.407	1706.5	331.4	6.4
0.395	1709.8	333.5	5.8
0.435	1913.8	333.6	4.5
0.449	1899.5	343.5	15.0
0.575	2063.0	345.8	9.9
0.561	2055.0	334.1	2.9
0.581	2071.8	318.0	9.9
0.583	2017.0	322.3	9.1
0.555	2027.7	340.9	8.1

Least square equation is:

$$k = 0.0873 + 0.04879(10^{-3})T - 4.492(10^{-9})T^2 + 0.0239(10^{-9})T^3$$

T in °R Emax = 0.063 at 1913.8°F mean temp
ERMS = 0.0225

$$k = 0.1376 + 0.0289(10^{-9})T^3$$

Emax = 0.063 at 1913.8°F mean temp
ERMS = 0.023

Besides the variations due to different apparatus used for thermal conductivity measurements, an expected difference in the sample density of Dynaquartz can be as high as 10% (Reference 9).

(1) Dynaquartz in Air

A comparison of most of the available thermal conductivity measurements on 6.2 pcf Dynaquartz is shown in Figure 23. The scatter in most of the data is high at mean temperatures close to or in excess of 2000°F. As can be expected from such a plot, the comparison is quite good in some instances and quite poor in others. The data obtained in this investigation are in qualitative agreement with most of the results shown in Figure 23 and are tabulated in Table XII. In reviewing the methods used by the various investigators, no data was previously obtained on a guarded hot plate. Literature data obtained from several sources with different type apparatus are also shown in Figure 23. Data presented by Ryan, et al (Reference 5) were obtained by two different investigators using different types of apparatus. The data points obtained by Plunkett and recorded in Reference 45 are for Dynaquartz of 4.6 pcf density. The curve drawn through the points represents a least square fit of all data points for the material with 6.2 pcf density except those obtained by Hurley and Traiger (Reference 4). These data were excluded because sample degradation was reported. The least square polynomial equation obtained using the guarded hot plate measurements (data of Table XII), and the data from References 5 and 9 was:

$$k = 0.6071 - 0.5323(10^{-3})T + 0.4589(10^{-6})T^2 - 0.0529(10^{-9})T^3 \quad (47)$$

where T is in °R. The maximum deviation from the equation is 0.153 at 2159°F data point using the guarded hot plate measurement. The root mean square deviation is 0.0583.

By neglecting the T and T^2 terms in the least squares polynomial equation, larger errors are introduced; however the curve obtained can be treated from a theoretical standpoint. The least square equation which is plotted in Figure 23 is of this type and has the following form:

$$k = 0.5299 + 0.04832(10^{-9})T^3 \quad (48)$$

where T is in °R. The maximum deviation from the equation is 0.188 at 1951°F data point using the guarded hot plate measurement. The root mean square deviation is 0.075.

Examination of Figure 23 shows that although the data are somewhat scattered, the variation is relatively independent of the test method or measurement technique. There is as much variation between different samples measured on the same apparatus as there is among several types of apparatus. Further, samples of Dynaquartz were obtained by various investigators at different times; no attempt was made to obtain identical samples. The present data, and that reported in the literature, generally fall within ±15% of the least square curve. This is in agreement with the estimated experimental accuracy of the guarded hot plate apparatus (see Appendix IV). There seems to be little difference in the thermal conductivity of the 4.6 and 6.2 pcf Dynaquartz. The least square curve shows the strong dependence of thermal conductivity on temperature as shown in Figure 23. This dependence is indicative of the importance of thermal radiation and is discussed in more detail in the next section.

(2) Dynaquartz in Vacuum

A comparison of the thermal conductivity values obtained in vacuum with other investigators is shown in Figure 24. The top curve represents the data of Wechsler and Kritz (Reference 38) using a radial heat flow apparatus evacuated to 1×10^{-5} torr.

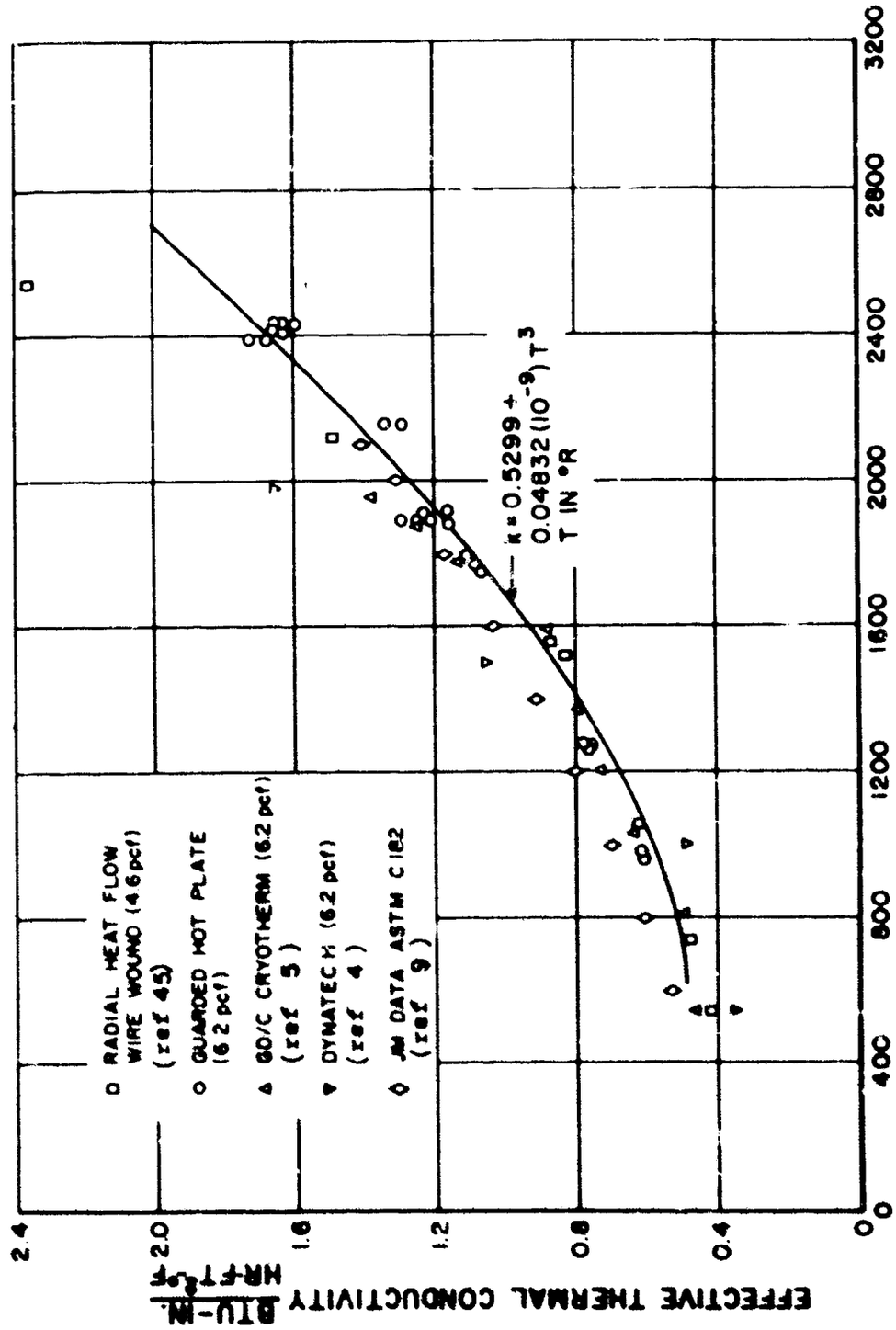

Figure 23. Comparison of Effective Thermal Conductivity of Dynaquartz in Air

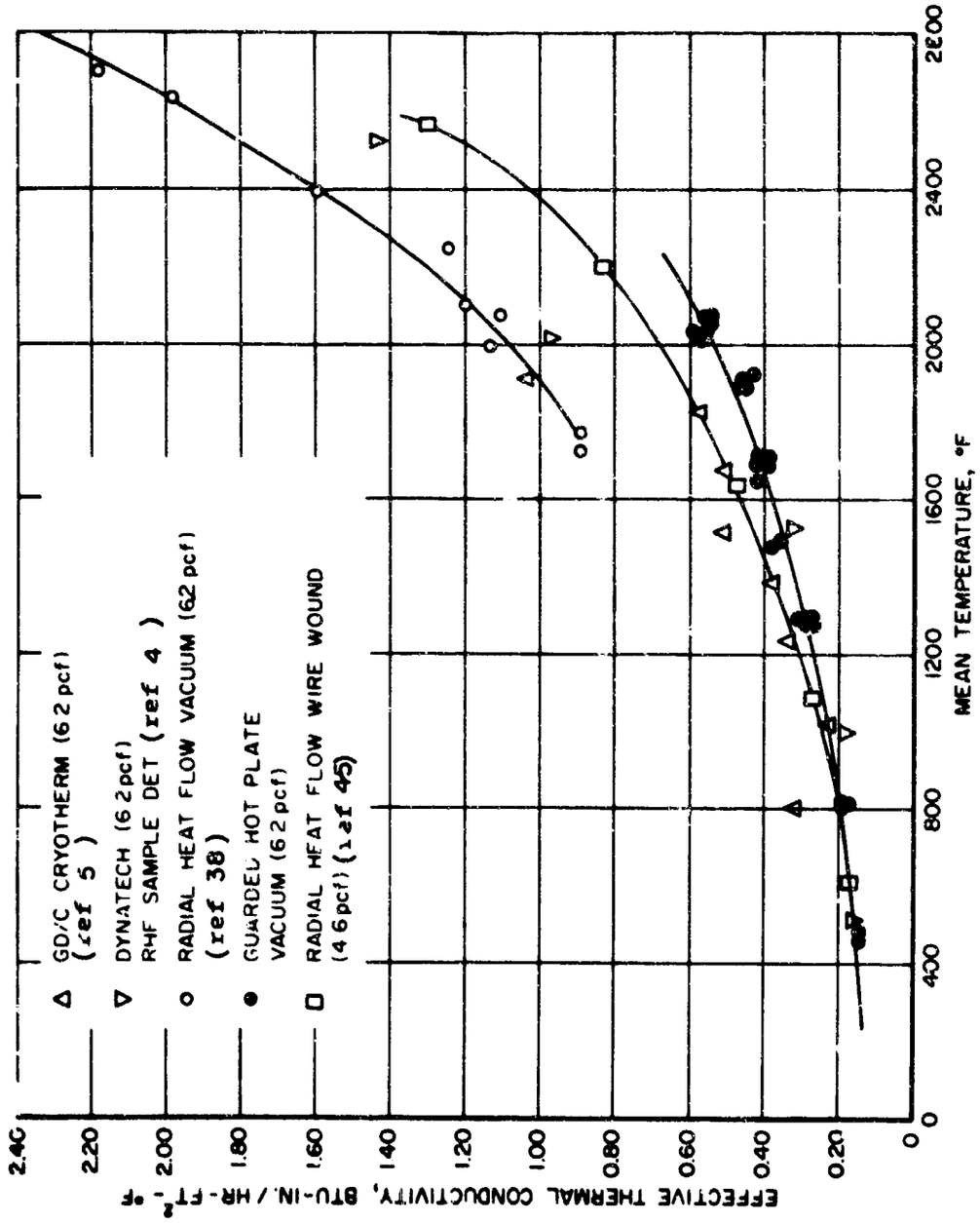

Figure 24. Comparison of Effective Thermal Conductivity of Dynaquartz in Vacuum

In comparing the experimental results of the two measurement techniques, two important features may be noted. First, the thermal conductivity in vacuum is significantly lower than in air. At 1000° and 2000°F, the thermal conductivities of evacuated Dynaquartz are approximately 1/3 and 1/2 that of the unevacuated material. Second, there is a significant difference between the data obtained in the guarded hot plate and radial heat flow apparatus. The data obtained in the guarded hot plate are in fair agreement with literature data (obtained in both one-dimensional apparatus and radial apparatus) at low temperatures, but shows lower conductivity values at higher temperatures. The conductivity values obtained in the radial heat flow apparatus (with outward heat flow) are higher than most of the literature data over the entire temperature range studied. These discrepancies may be caused by four factors:

(1) The contact resistance between the sample and the boundary walls in the hot plate apparatus is probably greater than in the radial heat flow apparatus--this would result in lower thermal conductivity values for the data obtained in the hot plate.

(2) The samples used in the radial flow apparatus were "turned" from a block of material. This could result in anisotropy of fiber orientation and a greater conductivity for the radial sample.

(3) The average temperature gradients were larger in the guarded hot plate than in the radial flow apparatus. Temperature gradients in the guarded hot plate measurements were between 662° and 692°F per inch, whereas in the radial heat flow measurements (Reference 38) the temperature gradients were between 278° and 551°F per inch. Because radiation is a principal mechanism in evacuated insulations, the difference in temperature gradients would lead to a difference in effective thermal conductivities.

(4) Imbalance between the main and guard heater in the case of the guarded hot plate affected measurements because radiation interchange between the heaters is possible at the higher temperatures. Based on these factors, there should be greater variation in thermal conductivity data obtained in vacuum than in air.

d. Discussion of Thermal Conductivity of Dynaquartz

Heat transfer in an insulation material may be examined in terms of the relative contributions of gas conduction, solid conduction, convection, and thermal radiation. In a fibrous insulation, convection heat transfer may usually be neglected because the empty spaces in the material are too small for the establishment of convection currents. The effective thermal conductivity of a fibrous material may be written (Reference 1) directly by applying Equation 1:

$$k_{eff} = (k_{app})_s + \delta k_{gas} + k_r \qquad (49)$$

where

$(k_{app})_s$ = the solid conduction contribution to the effective thermal conductivity.

k_{gas} = the gaseous conduction contribution to the effective thermal conductivity.

k_r = the radiative contribution to the effective thermal conductivity.

δ = the void volume of 6.2 pcf fibrous Dynaquartz, 0.954 (see Appendix II).

The experimental data for Dynaquartz was used to evaluate these contributions and determine their importance.

At low temperatures, in evacuated insulations, the principal contribution to the effective thermal conductivity should be solid conduction, ie, conduction across fiber contacts. By extrapolating the effective thermal conductivity data of Dynaquartz in vacuum to 400°F, where radiation is small, the value obtained for the solid conduction contribution is approximately 0.1 BTU-in./hr-ft^2-°F. This value seems quite reasonable when compared with thermal conductivity measurements of Dynaquartz made in vacuum at cryogenic temperatures, -310° to -125°F mean temperatures (Reference 46). The thermal conductivity of quartz decreases with temperature in the temperature region below 1000°F (Reference 47). However, the effective contact area between fibers becomes larger as the temperature is raised because of the decreasing strength of the fibers. These two effects tend to cancel each other so that the solid conduction contribution is not expected to vary much with temperature.

The gas contribution to thermal conductivity may be obtained from literature values of the conductivity of air (Reference 17) the bulk density of the insulation, and the fiber density (see Appendix II).

Two approaches were used to determine the radiation contribution to effective thermal conductivity. First, by assuming that the radiative contribution to thermal conductivity has the following form:

$$k_r = A_3 T^{\gamma} \tag{50}$$

where A_3 is an empirical constant determined by experiment and γ, the power of the absolute temperature. At high temperatures, if we assume that radiation is the principal mechanism of heat transfer, the value of γ may be obtained as the slope of the curve from a plot of logarithm of effective thermal conductivity versus logarithm of absolute temperature. Figure 25 is such a plot showing data for Dynaquartz. In most cases, a straight line may be drawn through the experimental points at high temperatures. The values of the slope, obtained for vacuum measurements where radiation is the most important heat transfer mechanism, vary between 2.5 and 3.18. The slope obtained from air data is lower because gas conduction is a significant contribution.

From theoretical considerations, the radiation contribution to thermal conductivity is given by

$$k_r = \frac{8 \sigma J^2 T^3}{P + 2N} \tag{51}$$

where

σ = Stefan-Boltzmann constant

J = index of refraction, dimensionless

T = mean sample temperature (absolute)

P = absorption cross section, inch^{-1}

N = scattering cross section, inch^{-1}

The temperature exponent obtained in theory is 3, provided the absorption and scattering cross sections are independent of temperature. The experimental data shown in Figure 25 agree qualitatively with this value. The proportionality constant $(P+2N)^{-1}$ may be obtained from curve fitting of the vacuum data at high temperatures or by separate measurements of

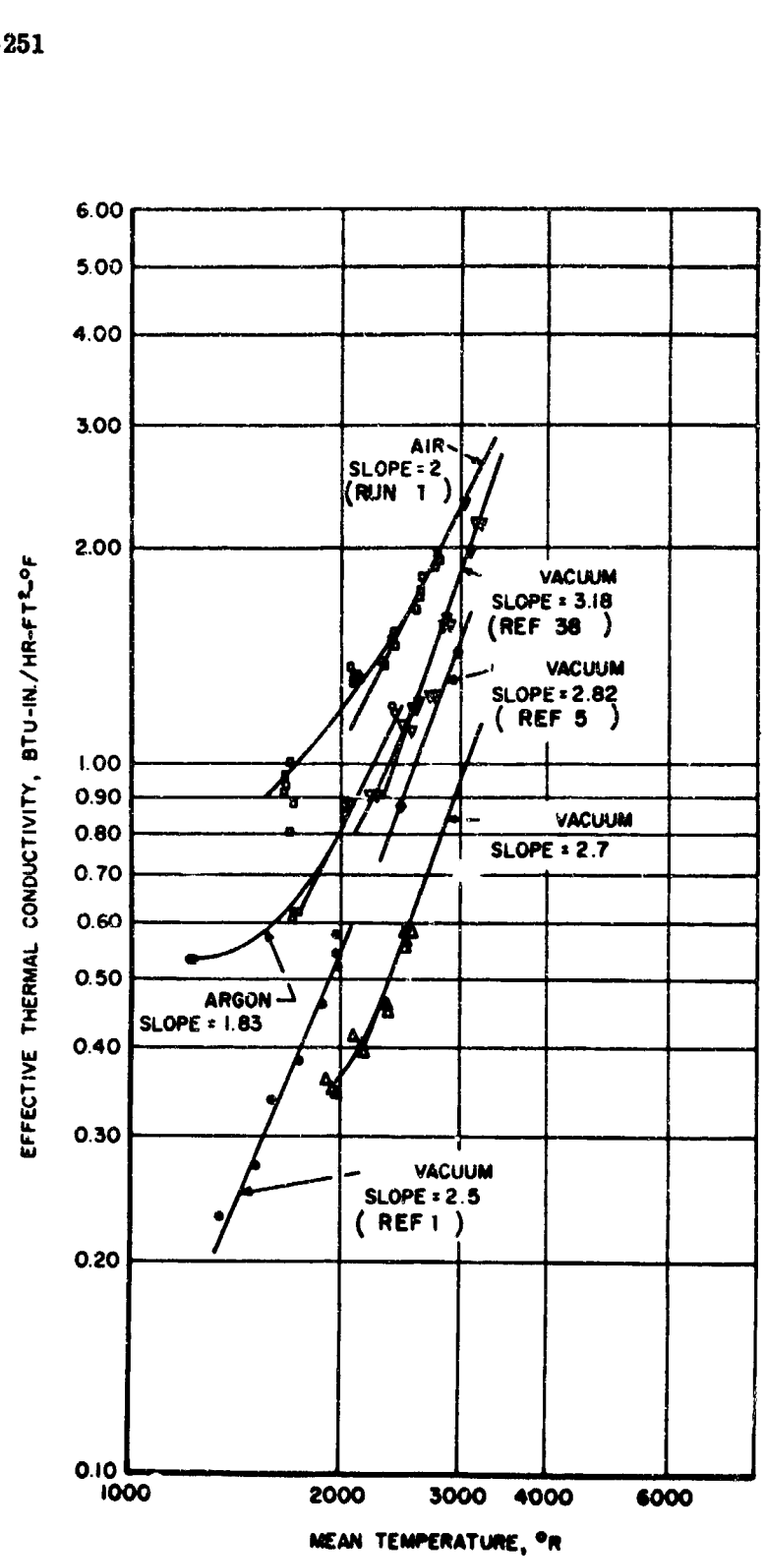

Figure 25. Logarithmic Plot of Effective Thermal Conductivity Versus Temperature for Dynaquartz

the absorption and scattering cross sections. Curve fitting of the vacuum data indicates that the value of P + 2N should be approximately 600 $in.^{-1}$. Experimental measurements of the absorption and scattering cross sections (Reference 1) indicate that the absorption cross section is negligible compared to the scattering cross section and that the scattering cross sections vary from about 300 $in.^{-1}$ at 1500°F to about 160 $in.^{-1}$ at 3000°F. The most appropriate value of the scattering cross section seems to be 300 $in.^{-1}$ in the temperature region where radiation heat transfer becomes significant (References 21 and 22).

Based on the foregoing discussion, the effective thermal conductivity of Dynaquartz is shown in Figure 26. As can be seen, the dominant mode of heat transfer is radiation at high temperatures. A direct comparison between the thermal conductivity measurements and the reconstructed curve shows that the least squares polynomial equation of the third degree is in good agreement with the theoretical approach using superposition. This indicates that the total heat transfer in fibrous insulation materials may be predicted on the basis of relatively few measurements. The chemical and physical stability, however, can only be determined from exposure to the high temperature environment. The solid conduction contribution must be estimated from low temperature measurements under conditions in which it is the principal mechanism. The gas conduction contribution may be readily evaluated from published data (Reference 17). Experiments to determine the absorption and scattering cross sections are required to estimate the radiation contribution.

e. Thermal Conductivity of Sapphire Wool

The thermal conductivity of Sapphire Wool was determined in air. Measurements were made only on a sample which contained zirconia pins in the metered area. The correction for pin conduction was 4.5% below 1000°F and 1.0% above. The thermal conductivity values obtained were for specimen ΔT's of roughly 250°F. The imbalance between the guard and main heaters was higher than that in the Dynaquartz runs, being as high as, and sometimes greater than, 10% of the specimen ΔT's. However, since the specimen ΔT's were lower in this experiment, the magnitude of the ratio of imbalance to specimen ΔT's was approximately the same as for the other Dynaquartz runs. The experimental error is estimated to be about ±15%. The thermal conductivity data for Sapphire Wool are tabulated in Table XV along with the temperature difference across the sample and imbalance. The thermal conductivity curve shown in Figure 27 is for the sample which consisted of four laminations of 1/8 inch thickness each forming the required 1/2 inch thick sample.

f. Thermal Conductivity of Dynaflex

The thermal conductivity of Dynaflex was determined in air using two different sample densities (8-10 pcf and 8.2 pcf) from about 450° to 2350°F mean temperatures; in vacuum from about 575° to 1950°F mean temperatures; and in helium environment from about 400° to 850°F mean temperatures for 8 to 10 pcf density. The data are tabulated in Tables XVI and XVII for air, Table XVIII for vacuum, and Table XIX for helium environment. The data are plotted for air in Figure 28. The experimental data were carefully examined for conformance with 5% imbalance condition and attainment of steady state. Better control of the imbalance condition was more possible in some runs than in others, and in some cases a larger imbalance data point was retained as indicated in Tables XVI through XIX.

Since Dynaflex is still a comparatively new material, and its overall density cannot be controlled, two sample densities were used in performing the thermal conductivity measurements in air. The data shown in Figure 28 are not in agreement with the data obtained from the manufacturer using an ASTM C-182 method. Apparent discrepancies may be the result of the different techniques used, differences in test apparatus, differences in sample thicknesses, and the variability of sample density.

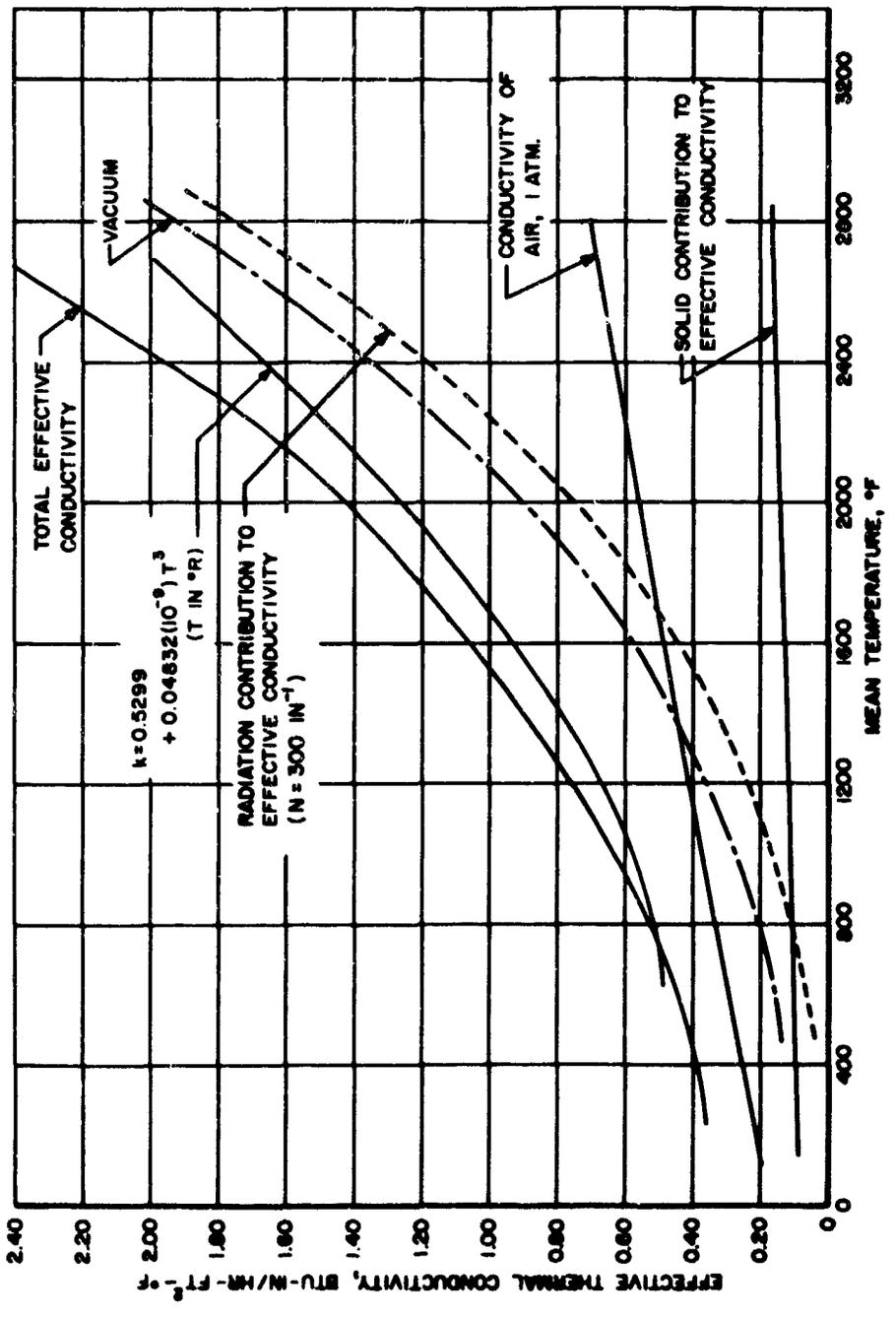

Figure 26. Effective Thermal Conductivity of Dynaquartz by Superposition

TABLE XV

THERMAL CONDUCTIVITY OF SAPPHIRE WOOL (1 pcf)
IN AIR (1 atm)

$k[\frac{BTU\text{-}in.}{hr\text{-}ft^2\text{-}^\circ F}]$	T($^\circ$F)mean	ΔT($^\circ$F)	Imbalance($^\circ$F)
0.747	422.3	136.6	5.0
0.713	442.8	142.4	4.7
0.706	427.8	143.6	14.0
0.670	438.8	150.3	14.7
1.800	933.0	218.0	22.4
1.757	996.1	228.3	33.0
1.750	1004.0	224.0	37.6
1.696	1007.3	236.0	48.0
2.962	1487.0	276.0	23.0
2.915	1502.8	280.3	41.0
4.390	1882.9	265.3	12.6
4.419	1887.1	264.3	3.7
4.482	1890.3	257.3	13.1
4.312	1899.6	270.0	31.6
4.329	1902.1	269.7	14.0
4.406	1907.2	271.6	30.8
4.471	1911.7	250.6	16.0
4.340	1925.8	268.3	8.8
6.857	2385.1	260.9	42.3
6.634	2400.2	269.5	61.7
6.758	2408.5	241.0	5.2
6.532	2419.1	249.1	19.9
6.394	2428.1	234.3	15.3
6.494	2438.0	230.0	16.0
6.274	2439.3	238.7	28.7
6.372	2448.1	234.3	18.3

Least square equation is:

$$k = 0.8743 - 1.197(10^{-3})T + 1.336(10^{-6})T^2 - 0.0831(10^{-9})T^3$$

$E_{max} = 0.049$ at 2385°F

$E_{RMS} = 0.016$

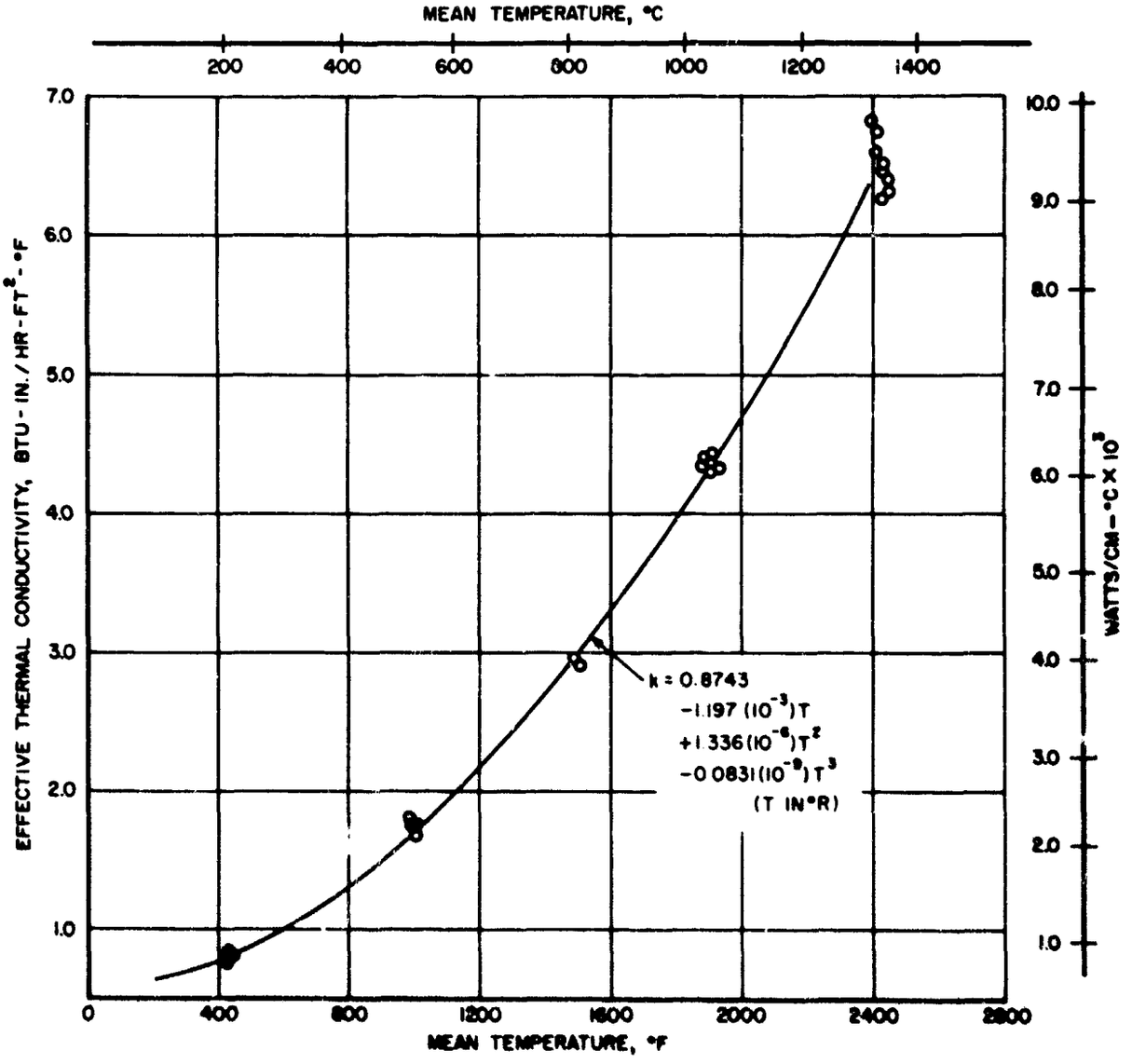

Figure 27. Thermal Conductivity of Sapphire Wool (1 pcf) in Air Corrected for Zirconia Pins

TABLE XVI

THERMAL CONDUCTIVITY OF DYNAFLEX (8-10 pcf) IN AIR

$k\left[\frac{BTU\text{-}in.}{hr\text{-}ft^2\text{-}^\circ F}\right]$	T($^\circ$F)mean	ΔT($^\circ$F)	Imbalance ($^\circ$F)
0.307	459.0	231.4	0.9
0.295	452.6	246.8	3.7
0.315	420.9	232.7	6.3
0.297	421.6	244.4	1.6
0.237	484.2	303.9	14.6
0.315	594.3	342.3	2.5
0.347	540.4	308.9	5.9
0.389	505.5	286.0	0.5
0.394	494.7	283.4	5.0
0.450	847.5	359.9	4.9
0.461	869.8	364.5	2.5
0.495	883.1	363.5	5.2
0.755	1316.7	405.2	0.2
0.831	1300.9	368.8	6.0
1.181	1768.2	250.2	5.5
1.159	1741.3	248.5	7.6
1.157	1734.7	250.4	3.8
1.136	1731.9	256.9	0.6
1.382	1987.2	271.8	3.8
1.394	1944.9	262.4	9.0
1.326	1955.2	275.1	3.1
1.295	1961.6	280.3	12.8
1.583	2220.8	287.5	6.8
1.845	2202.4	284	16.0
1.958	2195.9	286.5	0.5
1.984	2182.0	280.1	8.3

Least square equation is:

$$k = -0.377 + 1.182(10^{-3})T - 0.655(10^{-6})T^2 + 0.195(10^{-9})T^3$$

$E_{max} = 0.258$ at 2220°F

$E_{RMS} = 0.086$

TABLE XVII

THERMAL CONDUCTIVITY OF DYNAFLEX (8.2 pcf) IN AIR

$k\left[\frac{\text{BTU-in.}}{\text{hr-ft}^2\text{-}^\circ\text{F}}\right]$	T($^\circ$F)mean	ΔT($^\circ$F)	Imbalance($^\circ$F)
0.486	445.6	259.3	5.6
0.503	407.2	255.9	4.5
0.445	431.8	285.7	1.2
0.497	407.5	259.7	1.5
0.503	396.4	261.0	4.5
0.447	419.1	287.9	28.8
0.520	639.8	333.7	0.9
0.552	669.2	355.1	13.9
0.561	665.2	349.4	3.8
0.667	945.1	362.0	11.0
0.685	932.3	353.7	3.0
0.646	963.4	380.8	3.0
0.737	934.6	335.5	0.7
0.662	971.2	364.6	1.4
1.035	1193.9	316.0	2.1
1.035	1210.7	305.4	21.7
1.023	1221.6	320.5	14.1
1.122	1514.4	276.0	12.6
1.052	1601.3	286.3	2.6
1.857	2105.5	256.7	11.2
1.776	2163.3	269.6	43.6
1.880	2228.1	266.5	8.8
1.742	2209.7	259.7	3.1
2.536	2387.9	244.9	3.3
2.792	2386.8	222.9	13.4
2.593	2361.5	236.9	1.9
2.690	2374.8	226.5	10.5
2.472	2369.8	247.7	11.5

Least square equation is:

$$k = -1.534 + 3.940(10^{-3})T - 2.384(10^{-6})T^2 + 0.529(10^{-9})T^3$$

$E_{max} = 0.313$ at 2210°F

$E_{RMS} = 0.125$

TABLE XVIII

THERMAL CONDUCTIVITY OF DYNAFLEX (8-10 pcf)
IN VACUUM ($<10^{-4}$ torr)

$k\left[\frac{BTU\text{-}in.}{hr\text{-}ft^2\text{-}^\circ F}\right]$	T($^\circ$F)mean	ΔT($^\circ$F)	Imbalance($^\circ$F)
0.102	572.9	449.9	8.8
0.098	736.7	401.3	1.2
0.102	763.4	390.5	0.6
0.241	915.0	315.1	8.5
0.234	927.2	320.8	6.3
0.229	946.6	336.0	3.8
0.235	956.7	338.6	18.0
0.363	1212.3	294.6	3.1
0.372	1194.5	289.0	0
0.378	1187.5	293.2	10.8
0.428	1216.8	298.3	3.1
0.511	1614.2	282.0	7.4
0.527	1595.9	274.4	7.0
0.513	1611.2	298.5	9.0
0.475	1619.6	307.5	6.8
0.516	1606.6	267.4	5.3
0.563	1604.6	285.8	17.8
0.611	1736.3	180.9	0.3
0.587	1835.9	212.3	1.8
0.648	1870.3	222.1	1.8
0.748	1945.2	230.9	1.2
0.739	1980.1	227.2	6.2
0.822	1946.6	216.3	8.9
0.793	1951.1	227.0	5.2
0.800	1944.5	226.2	6.9

The thermal conductivity of Dynaflex in vacuum was measured, although the sample seemed to outgas profusely. Figure 29 shows the hot face of the top Dynaflex sample without pins in the measuring zone along with the cold face of the bottom sample where droplets of the vapor seemed to recrystallize. The data are tabulated in Table XVIII; however, a least square equation was not determined for the vacuum environment measurements.

The data obtained in helium environment was restricted to lower sample mean temperatures because of the power requirements on the heater assembly. Several matching data points for the helium runs were obtained, hence the data listed in Table XIX are representative data points only.

TABLE XIX

THERMAL CONDUCTIVITY OF DYNAFLEX (8-10 pcf)
IN HELIUM (1 atm)

$k\left[\frac{\text{BTU-in.}}{\text{hr-ft}^2\text{-}^\circ\text{F}}\right]$	T($^\circ$F)mean	ΔT($^\circ$F)	Imbalance($^\circ$F)
1.676	446.1	215.8	5.4
1.658	458.7	217.3	3.5
2.070	757.4	335.0	4.5
2.026	767.3	340.7	4.0
2.163	851.8	360.7	1.7
2.141	866.8	364.7	6.8
2.177	872.4	362.1	1.1
3.265	994.2	341.3	42.3*
3.634	1014.2	341.9	56.5*

*These data are questionable due to thermocouple discontinuities.

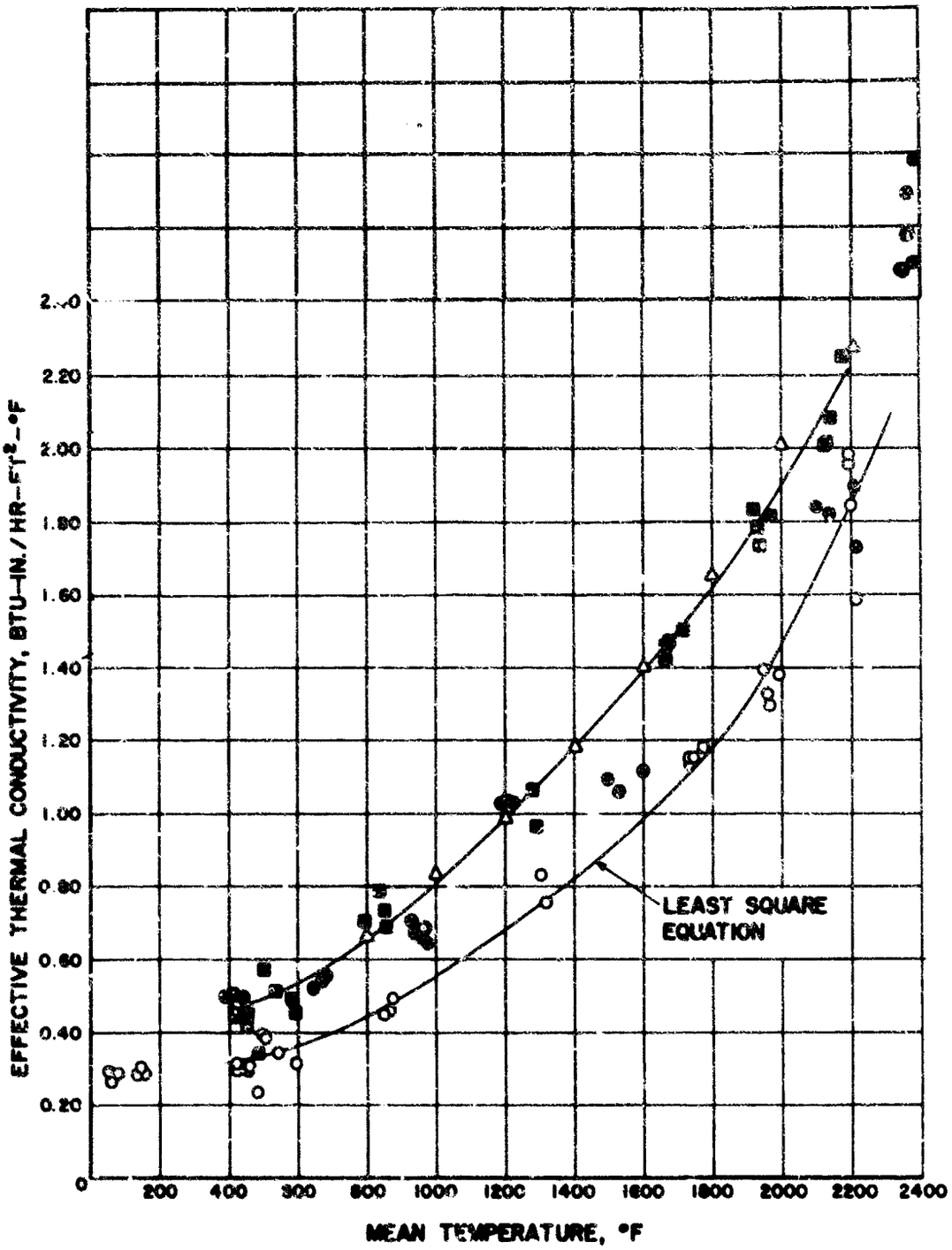

Figure 28. Effective Thermal Conductivity of Dynaflex (8-10 pcf) in Air

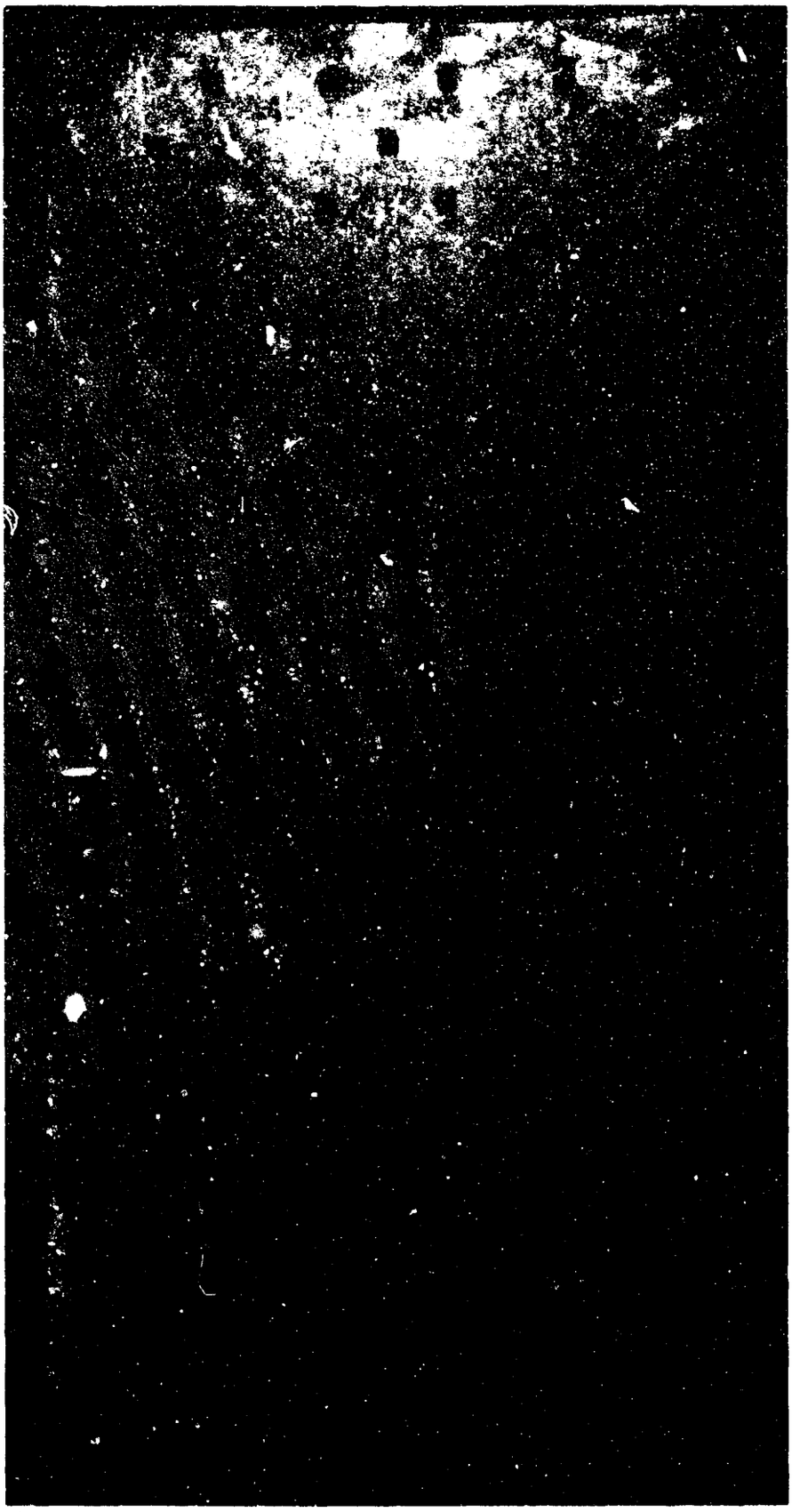

Figure 29. Dynaflex Samples (8-10 pcf) After Thermal Conductivity Measurements in Vacuum

SECTION IV

SUMMARY AND CONCLUSIONS

1. SUMMARY

An experimental investigation was undertaken to discern treatment of the mechanisms by which fibrous insulations attenuate the transfer of thermal energy. Dynaquartz, a 2750° heat stabilized silica material, was selected for this analysis. The analysis was conducted of the relative contributions of gaseous, solid, and radiative heat transport over the range from about 400° to 2500°F. In support of this analysis, the effective thermal conductivity of Dynaquartz was measured from room temperature to 2500°F mean temperature in an air environment. Additional conductance measurements were made from about 250° to 2000°F in an inert environment and in a vacuum.

Selected experimental data for Dynaquartz, Sapphire Wool, and Dynaflex were treated using a least square polynominal equation of the third degree to fit the measured values. Table XX is a summary table of the least square parameters determined.

Expressions were obtained for Dynaquartz using (1) all available thermal conductivity measurements on Dynaquartz (6.2 pcf) in air, and (2) the guarded hot plate measurements only. Both equations obtained for Dynaquartz are in good agreement with the theoretical analysis using the calculated scattering cross sections determined from total radiation transmission experiments.

Comparison of the data with those of other investigators shows good agreement for Dynaquartz where conduction is the dominant mode of heat transfer in the measurement apparatus. The data obtained for Dynaquartz on the guarded hot plate apparatus are consistent, in that the results obtained in air and those in vacuum can be correlated within experimental scatter.

The experimental data obtained in vacuum for Dynaquartz with the guarded hot plate and that obtained with a radial heat flow apparatus show significant deviations. Discrepancies in the data are qualitatively attributed to variations in the mechanisms of heat transfer to the sample, specimen temperature gradients, fiber orientation, contact resistance between the fibers and the heaters, and the imbalance in the guard and main heaters present in the guarded hot plate apparatus. In applying the effective thermal conductivity data for design purposes, the dominant mode of heat transfer may prove to have an important effect. Thermal conductivity results should therefore be carefully analyzed before applying them to a specific requirement.

The experimental conditions for the thermal conductivity measurements are summarized in Table XXI. Radiation transmission experiments were carried out in order to evaluate the relative contribution of radiation attenuation parameters. The most significant radiation attenuation mechanism in fibrous insulations is scattering. The absorption and scattering cross sections for Dynaquartz were determined at 800°C (1475°F) and found to be in qualitative agreement with the scattering cross sections calculated from the electromagnetic theory for infinite cylinders. Radiation attenuation properties can have a significant effect in the behavior of a fibrous insulation but are difficult to determine experimentally.

The interactions between solid-to-solid conduction, gaseous conduction, and radiation were separated for Dynaquartz in order to treat the total heat transfer as a sum of three independent contributions. This seems to be a justifiable approximation for Dynaquartz based on the consistency between experimental values and theoretical calculations, since most of the data obtained were for moderate temperature gradients where the effects of radiation on the temperature distribution can be neglected.

TABLE XX

LEAST SQUARE PARAMETERS OF THERMAL CONDUCTIVITY DATA

Sample	a	b (10^{-3})	c (10^{-6})	d (10^{-9})	Maximum Deviation °F	RMS Deviation
Dynaquartz (6.2 pcf) in Air						
A. guarded hot plate data	-1.068	1.911	-0.702	0.126	0.135@ 2388°	0.056
B. composite of all data	0.607	-0.532	0.459	-0.053	0.153@ 2159°	0.058
Dynaquartz (6.2 pcf) in Argon	-0.478	1.927	-1.334	0.344	0.068@ 1946°	0.027
Dynaquartz (6.2 pcf) in Vacuum	0.087	0.049	-0.005	0.024	0.063@ 1914°	0.022
Dynaflex (8-10 pcf) in Air	-0.377	1.182	-0.655	0.195	0.258@ 2220°	0.086
Dynaflex (8.2 pcf) in Air	-1.534	3.940	-2.384	0.529	0.313@ 2210°	0.125
Sapphire Wool (1.0) in Air	0.874	-1.197	1.336	0.083	0.049@ 2385°	0.016

a,b,c, and d are constants of the polynomial equations describing the best fit of the thermal conductivity data. The data were fitted to an equation of the following type:

$$k = a + b\,(10^{-3})\,T + c\,(10^{-6})\,T^2 + d\,(10^{-9})\,T^3$$

where k is in BTU-in./ft^2-hr-°F units and T is in °R.

TABLE XXI

EXPERIMENTAL CONDITIONS OF THERMAL CONDUCTIVITY MEASUREMENTS

Sample	Heater Imbalance (Guard Side vs Main)	Temperature Differential (°F) (Across Sample Thickness)	Mean Temperature Range (°F)
Dynaquartz (6.2 pcf) in Air	within 5% of sample ΔT	250 to 450	950 to 2450
Dynaquartz (6.2 pcf) in Argon	within 5% of sample ΔT	150 to 400	300 to 2000
Dynaquartz (6.2 pcf) in Vacuum	within 5% of sample ΔT	200 to 350	500 to 2000
Dynaflex (8-10 pcf) in Air	within 6% of sample ΔT	230 to 400	450 to 2220
Dynaflex (8.2 pcf) in Air	within 10% of sample ΔT	250 to 380	400 to 2385
Dynaflex (8-10 pcf) in Vacuum	within 7% of sample ΔT	180 to 450	575 to 2000
Dynaflex (8-10 pcf) in Helium	within 12% of sample ΔT	215 to 360	450 to 1000
Sapphire Wool (1.0 pcf) in Air	10 to 12% of sample ΔT	200 to 300	400 to 2450

2. CONCLUSIONS

Based upon the experimental measurements carried out during this investigation, the following conclusions can be made:

(1) Experimental measurements of the effective thermal conductivity of fibrous Dynaquartz, Dynaflex, and Sapphire Wool in air at temperatures up to 2500°F may be carried out in a one dimensional guarded hot plate apparatus with an expected accuracy of ±15%.

(2) Experimental measurements of the effective thermal conductivity of evacuated fibrous Dynaquartz and Dynaflex may be subjected to greater errors than measurements in air because of the influence of contact resistance and the large radiation contribution to heat transfer.

(3) At temperatures above 1500°F, radiation is the principal contribution to heat transfer in fibrous insulating materials. Gas conduction is the second largest contribution but it can be effectively reduced by evacuation of the fibrous insulation to moderate pressures. Solid conduction is of lesser importance in low density fibrous insulations.

(4) The effective thermal conductivity of Dynaquartz may be predicted from estimates of the solid conduction contribution, gas conductivity data, and estimates of the absorption and scattering cross sections of the insulation. Measurements of the absorption and scattering cross sections can be used to guide the choice of insulation components at high temperatures where radiation is the principal heat transfer mechanism.

(5) Because of the high contribution of radiation to effective thermal conductivity of fibrous insulations, temperature gradients in the insulation will not be linear under steady-state heat transfer conditions.

APPENDIX I

THERMOCOUPLE DETECTOR SENSITIVITY

A schematic diagram of the thermocouple detector used in the total transmission experiments is shown in Figure 30. The determination of thermocouple sensitivity was made by varying the distance between the source and detector. Figures 31 and 32 are plots of the detector readings versus distances and show a linear relationship. The tabulated values of the readings and best line by least square are shown in Table XXII.

To determine if the experimental arrangement follows Lambert's law and to test the validity of the black body assumptions, the thermocouple sensitivity was measured.

Assuming that black body radiation is isotropic, the radiant energy emanating from a black body is distributed with respect to angle by Lambert's law (Reference 48).

$$\frac{(E_{bb})_\theta}{A_h} = \frac{(E_{bb})}{\pi} \cos\theta = \frac{\sigma T^4}{\pi} \cos\theta$$

where

$(E_{bb})_\theta$ = energy of the black body emitted per unit time per unit solid angle in a direction θ from the normal

(E_{bb}) = energy of the black body emitted per unit time = σT^4

A_h = area of the black body emittor hole

σ = Stefan-Boltzmann constant

T = absolute temperature

if θ = 0° from normal cos θ = 1 and

$$(E_{bb})_n = \frac{\sigma T^4 A_h}{\pi}$$

$(E_{bb})_n$ = black body energy emitted normal to hole.

The response of the detector is given by:

$$R_d = K E_n(r) A_d$$

where

R_d = response of detector (μv)

$E_n(r)$ = energy incident on the detector normal to the source at some distance r from source (watts).

A_d = area of detector

K = coefficient of thermocouple sensitivity $\frac{\mu\text{volts}}{\mu\text{watts}}$

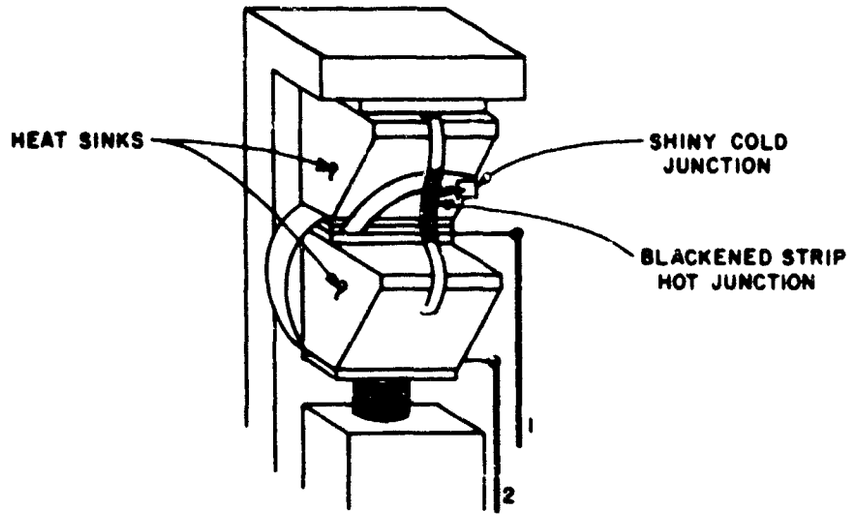

Figure 30. Schematic Diagram of Thermocouple Detector

Using the inverse square law, we know that the energy incident on a surface r distance away is given by assuming $(E_{bb})_n$ is now a point source (Reference 49).

$$E_n(r) = \frac{(E_{bb})_n}{r^2}$$

and

$$R_d = \frac{K(E_{bb})_n A_d}{r^2}$$

and finally

$$R_d = \frac{K\sigma T^4 A_h A_d}{\pi r^2}$$

If we plot $R_d^{-1/2}$ versus r, a straight line should result since all other terms are constant and determined and since

$$R_d r^2 = \frac{K\sigma T^4 A_h A_d}{\pi}$$

$$r = \left[\frac{K\sigma T^4 A_h A_d}{\pi}\right]^{1/2} R_d^{-1/2}$$

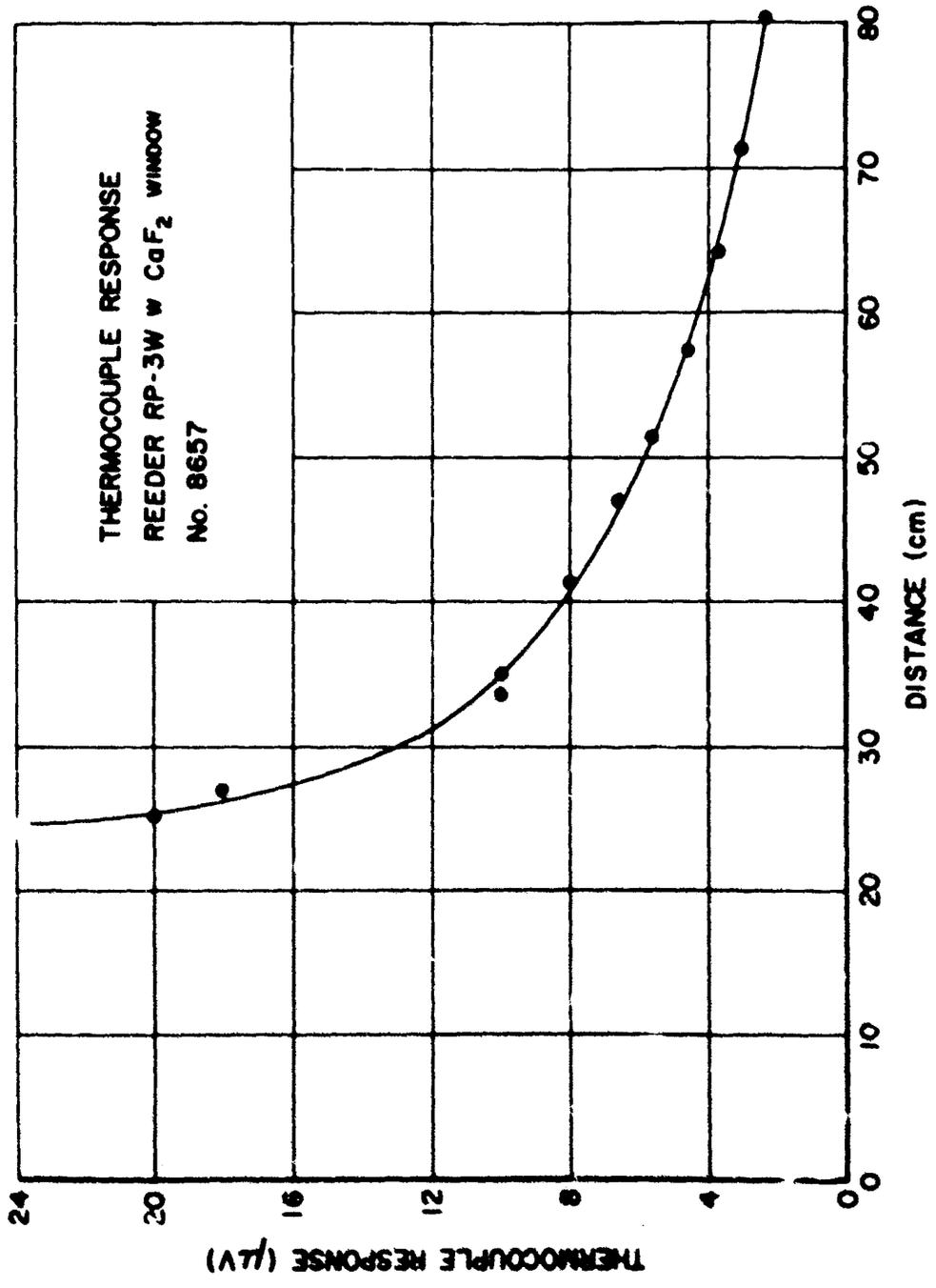

Figure 31. Thermocouple Response Versus Distance

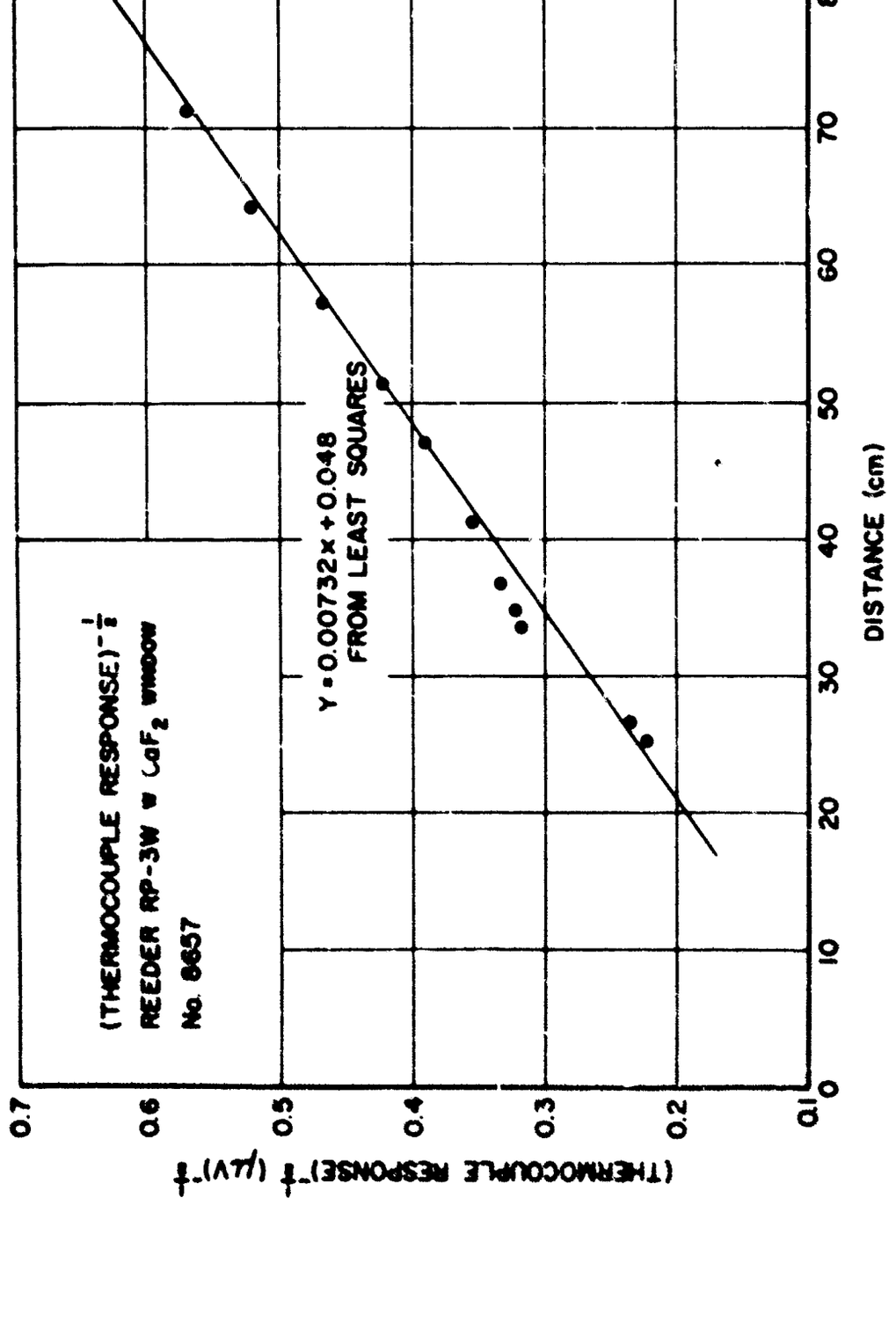

Figure 32. Linearity Plot of Thermocouple Detector

TABLE XXII

THERMOCOUPLE DETECTOR SENSITIVITY

Thermocouple: Reeder RP-3W with CaF_2 window No. 8657
Furnace temperature (found by optical pyrometer): 889 °C
Area of hole in black body 0.12011 cm^2
Dark current: 17μv (Dark current was never near signal which was in mv all the time.)
1μv test signal corresponded to 1 mv output. Gain set at 7.70.

Signal Reading mv	Thermocouple Response μv	$(Response)^{1/2}$ $(R)^{1/2}$	$(Response)^{-1/2}$ $1/(R)^{1/2}$	Distance from Front of Furnace (r) cm
20.0	20.0	4.48	0.223	25.40
18.0	18.0	4.24	0.236	26.90
10.0	10.0	3.16	0.317	33.90
9.8	9.8	3.13	0.320	34.90
9.0	9.0	3.00	0.333	36.90
8.0	8.0	2.83	0.353	41.40
6.6	6.6	2.57	0.389	47.10
5.6	5.6	2.37	0.422	51.40
4.6	4.6	2.14	0.467	57.40
3.7	3.7	1.92	0.521	64.40
3.1	3.1	1.76	0.569	71.40
2.4	2.4	1.55	0.645	80.40

Best straight line from least square equation: $R^{-1/2} = 0.00732(r) + 0.048$

and

$$R_g^{-1/2} = \left[\frac{\pi}{K\sigma T^4 A_h A_g}\right]^{1/2} r$$

$$m = \text{slope} = \frac{\Delta R_g^{-1/2}}{\Delta r} = \left[\frac{\pi}{K\sigma T^4 A_h A_g}\right]^{1/2} \mu v^{-1/2} cm^{-1}$$

and solving for K

$$K = \frac{\pi}{m^2 \sigma T^4 A_h A_g}$$

The values determined from experiment and manufacturer are

$m = 7.23(10^{-3})\ cm^{-1}\text{-}\mu v^{-1/2}$, least square fit to data

$T = 289°C$ from pyrometer sighted to black body hole

$\sigma T^4 = 10.25\ watt\text{-}cm^{-2}$

A_h = for No. 23 drill = $.12011\ cm^2$

$A_d = 4(10^{-3})cm^2$ detector is 2mm x 0.2mm

and

$$K = \frac{\pi}{[(7.23)(10^{-3})]^2 (10.25)(10^6)(.12011)(4)(10^{-3})} \quad \frac{\mu\ volt}{\mu\ watt}$$

$$K = \frac{\pi}{(53.5)(1.23)(4)(10^{-3})}$$

$$K = \frac{\pi}{0.2635} = 11.92\ \frac{\mu\ volt}{\mu\ watt}$$

The Reeder catalog indicates the sensitivity as 14 to 18 and at 13 cps there should be 75% of maximum DC response. Therefore the sensitivity as calculated is correct and assumptions for Lambert's law and black body are valid.

APPENDIX II

MATERIAL CHARACTERISTICS OF DYNAQUARTZ

The gross characteristics of Dynaquartz, fiber density, diameter, and void volume fraction, were determined and are indicated in this Appendix.

1. DETERMINATION OF FIBER DENSITY

To determine the fraction of void volume in Dynaquartz, the density or specific gravity of the fibers was determined. The specific gravity was determined by using a 10-ml volumetric flask, filling it up to the meniscus, inserting a known quantity of Dynaquartz into the flask, and measuring the volume change due to addition of the Dynaquartz.

	gm
Weight of flask + water filled to meniscus	23.2768
Weight of Dynaquartz and paper	0.8360
Weight of paper after inserting Dynaquartz	0.5760
Dynaquartz added	0.2600
Weight of flask + water + Dynaquartz	
-water to get back to meniscus	23.4165
	0.2600
	23.1565
Amount of water removed	23.2768
	23.1565
Amount of water lost	0.1203

$$\text{Specific Gravity} = \frac{0.2600 \text{ gm}}{0.1203 \text{ ml}} = 2.17 \text{ gm/cm}^3$$

The specific gravity of Corning 7940 fused silica is between 2.1 and 2.3, the average value being 2.2 (Reference 47).

2. DETERMINATION OF FIBER DIAMETER

Dynaquartz was examined under a microscope and an attempt was made to determine the average fiber diameter. To calibrate the microscope, a plate with 288 lines per millimeter was used and 13 lines corresponded to 100 scale divisions with a 20X eyepiece. Nine scale divisions corresponded to an average fiber diameter of about 4 microns. Fibers were examined at random, and the fibers measured were those which could be focused easily, and those which lay as close as possible in a perpendicular direction so that fiber diameters could be measured. As can be expected, parallax was a problem and the width of the lines on the eyepiece caused an error which was estimated to be about one scale division. The average fiber diameter of thirteen readings was 4.4 microns with the error of 0.5 microns. The readings ranged from 3.3 to 6 microns.

The fiber diameter is determined by the manufacturer by use of a Williams Freeness Test and an air permeability method (Reference 10).

The normal distribution of the fiber diameters is supposed to peak at 1.3 microns (Reference 9), although any random sample, when measured, may have some other fiber diameter as determined above.

3. DETERMINATION OF VOID VOLUME

The void volume is given by the following equation:

$$(1-\delta) = \frac{\rho - \rho_g}{\rho_s - \rho_g}$$

Using the values of

ρ = 6.2 pcf for Dynaquartz

ρ_g = 0.08 lb/ft^3 at one atmosphere

ρ_s = 2.17 (62.4) = 135.41

$(1-\delta)$ = 0.0452 and δ = 0.954

APPENDIX III

SPECTRAL TRANSMISSION AND INTEGRATED TRANSMISSION CALCULATIONS

The spectral transmission curves shown in Figures 3, 4, and 5 were used to calculate the integrated transmission inferred by Equation 31. The integration is done graphically for each temperature. The values for black body radiation are relative to the maximum (Reference 37) where tabulated numbers are given. The tabulated spectral transmission and graphically integrated transmission data are shown in Table XXIII.

TABLE XXIII

SPECTRAL AND INTEGRATED TRANSMISSION DATA ON DYNAQUARTZ (6.2 pcf)

Sample Thickness 0.044 inch
Sample Temperature = 300°K

$\lambda(\mu)$	I_o	I	Transmission	λT	$(E_{bb})_\lambda$ Relative	trans X $(E_{bb})_\lambda$
6.6	81.6	1.0	0.01225	.1934	.632	0.01774
6.7	75	2.0	0.0266	.1963	.655	0.01742
6.8	91.7	4.0	0.0436	.1992	.677	0.02952
6.9	82	6.0	0.0732	.2022	.699	0.05117
7.0	85.5	10.5	0.1228	.2051	.720	0.08842
7.1	82	16.0	0.1951	.2080	.741	0.14457
7.2	77	24.0	0.3116	.2109	.760	0.23682
7.3	92.1	31.6	0.3431	.2139	.779	0.26828
7.4	90	28.0	0.3111	.2168	.797	0.24795
7.5	90.6	18.2	0.2008	.2198	.815	0.16365
7.6	91	9.0	0.0989	.2227	.831	0.08218
7.7	90	2.6	0.0288	.2256	.847	0.02439

Integrated transmission by graphical integration: $\frac{163}{18,505} = 0.88\%$
(See equation 31)

NOTE: Values for λT are used to obtain relative values for $(E_{bb})_\lambda$ from Ref 37.

Sample Thickness 0.070 inch
Sample Temperature = 300°K

$\lambda(\mu)$	I_o	I	Transmission	λT	$(E_{bb})_\lambda$ Relative	trans X $(E_{bb})_\lambda$
6.6	81.6	0.1	0.0012	.1934	.632	0.00072
6.7	75	0.2	0.0026	.1963	.655	0.00170
6.8	91.7	0.4	0.0044	.1992	.677	0.00298
6.9	82	0.6	0.0073	.2022	.699	0.00510
7.0	85.5	1.0	0.0177	.2051	.720	0.00842
7.1	82	2.8	0.0341	.2080	.741	0.02526
7.2	77	6.5	0.0844	.2109	.760	0.06414
7.3	92.1	10.1	0.1096	.2139	.779	0.08538
7.4	90	8.1	0.0900	.2168	.797	0.07173
7.5	90.6	3.4	0.0375	.2198	.815	0.03056
7.6	91	0.8	0.0088	.2227	.831	0.00731
7.7	90	0.4	0.0044	.2256	.847	0.00373

Integrated transmission by graphical integration: $\frac{41}{18,505} = 0.22\%$
(See equation 31)

NOTE: Values for λT are used to obtain relative values for $(E_{bb})_\lambda$ from Ref 37.

TABLE XXIII(CONTD)

SPECTRAL AND INTEGRATED TRANSMISSION DATA ON DYNAQUARTZ (6.2 pcf)

Sample Thickness 0.044 inch
Sample Temperature 673°K

$\lambda(\mu)$	I_o	I	Transmission	λT	$(E_{bb})_\lambda$ Relative	trans X $(E_{bb})_\lambda$
6.6	71	1.0	0.0141	.4442	.686	0.00967
6.7	62.5	1.4	0.0224	.4509	.669	0.01499
6.8	80	2.4	0.0300	.4576	.653	0.01959
6.9	72	3.1	0.0430	.4644	.636	0.02735
7.0	75	5.1	0.0680	.4711	.620	0.04216
7.1	71	7.0	0.0986	.4778	.605	0.05965
7.2	76	9.1	0.1197	.4846	.589	0.07050
7.3	79	10.9	0.1379	.4913	.574	0.07915
7.4	76	8.8	0.1158	.4980	.559	0.06473
7.5	79	5.0	0.0633	.5048	.545	0.03450
7.6	80	2.3	0.0288	.5115	.530	0.01526
7.7	78.5	0.7	0.0089	.5182	.517	0.00460

Integrated transmission by graphical integration: $\frac{105}{16,168} = 0.65\%$
(See equation 31)

NOTE: Values for λT are used to obtain relative values for $(E_{bb})_\lambda$ from Ref 37.

Sample Thickness 0.044 inch
Sample Temperature 873°K

$\lambda(\mu)$	I_o	I	Transmission	λT	$(E_{bb})_\lambda$ Relative	trans X $(E_{bb})_\lambda$
6.6	71	0.8	0.0113	.5762	.411	0.00464
6.7	62.5	1.0	0.0160	.5849	.397	0.00635
6.8	80	1.8	0.0225	.5936	.383	0.00862
6.9	72	2.2	0.0305	.6024	.370	0.01128
7.0	75	3.6	0.0480	.6111	.358	0.01718
7.1	71	4.6	0.0650	.6198	.346	0.02249
7.2	76	5.8	0.0763	.6386	.334	0.02548
7.3	79	6.6	0.0835	.6373	.323	0.02697
7.4	76	5.4	0.0710	.6460	.312	0.02215
7.5	79	3.2	0.0400	.6548	.302	0.01208
7.6	80	1.5	0.0187	.6635	.292	0.00546
7.7	78.5	0.6	0.0076	.6722	.282	0.00214

Integrated transmission by graphical integration: $\frac{83}{24,756} = 0.34\%$
(See equation 31)

NOTE: Values for λT are used to obtain relative values for $(E_{bb})_\lambda$ from Ref 37.

TABLE XXIII (CONTD)

SPECTRAL AND INTEGRATED TRANSMISSION DATA ON DYNAQUARTZ (6.2 pcf)

Sample Thickness 0.044 inch
Sample Temperature 1073°K

λ(μ)	I_o	I	Transmission	λT	$(E_{bb})_\lambda$ Relative	trans X $(E_{bb})_\lambda$
6.6	71	0.6	0.0084	.7082	.246	0.000206
6.7	62.5	0.8	0.0128	.7184	.237	0.00303
6.8	80	1.2	0.0150	.7296	.227	0.00340
6.9	72	1.5	0.0208	.7404	.218	0.00453
7.0	75	2.0	0.0266	.6511	.210	0.00558
7.1	71	3.0	0.0416	.7618	.202	0.00840
7.2	76	3.8	0.0500	.7726	.194	0.00970
7.3	79	4.1	0.0519	.7833	.187	0.00970
7.4	76	3.8	0.0500	.1940	.180	0.0090
7.5	79	2.5	0.0316	.8048	.173	0.00546
7.6	80	1.1	0.0138	.8155	.167	0.00230
7.7	78.5	0.5	0.0064	.8262	.160	0.00102

Integrated transmission by graphical integration: $\frac{30}{20,324} = 0.15\%$
(See equation 31)
NOTE: Values for λT are used to obtain relative values for $(E_{bb})_\lambda$ from Ref 37.

Sample Thickness 0.030 inch
Sample Temperature 300°K

λ(μ)	I_o	I	Transmission	λT	$(E_{bb})_\lambda$ Relative	trans X $(E_{bb})_\lambda$
6.6	77	1.2	0.0156	.1934	.632	0.00986
6.7	70	2.0	0.0286	.1963	.655	0.01873
6.8	88	4.2	0.0477	.1992	.677	0.03229
6.9	76.5	6.0	0.0784	.2022	.699	0.05480
7.0	83	10.6	0.1277	.2051	.720	0.0919
7.1	80	16.1	0.02012	.2080	.741	0.1491
7.2	83.5	24.3	0.2910	.2109	.760	0.2212
7.3	90	32.0	0.3555	.2139	.779	0.2769
7.4	86	28.8	0.3348	.2168	.797	0.2668
7.5	89	20.0	0.2247	.2198	.815	0.1792
7.6	90.5	10.5	0.1160	.2227	.831	0.0964
7.7	88.7	3.3	0.0372	.2256	.847	0.01911

Integrated transmission by graphical integration: $\frac{187}{18,505} = 1.01\%$
(See equation 31)
NOTE: Values for λT are used to obtain relative values for $(E_{bb})_\lambda$ from Ref 37.

TABLE XXIII (CONTD)

SPECTRAL TRANSMISSION DATA ON DYNAQUARTZ (6.2 pcf)

Sample Thickness 0.030 inch
Sample Temperature 1073°K

$\lambda(\mu)$	I_o	I	Transmission	λT	$(E_{bb})_\lambda$ Relative	trans $\times$ $(E_{bb})_\lambda$
6.6	77	0.4	0.0052	.7082	.246	0.0013
6.7	70	0.9	0.0128	.7189	.237	0.0030
6.8	88	1.8	0.0204	.7296	.227	0.0046
6.9	76.5	2.2	0.0287	.7404	.218	0.0063
7.0	83	3.3	0.0397	.7511	.210	0.0083
7.1	80	4.0	0.0500	.7618	.202	0.0101
7.2	83.5	5.0	0.0598	.7726	.194	0.0116
7.3	90	5.2	0.0577	.7833	.187	0.0108
7.4	86	5.0	0.0581	.7940	.180	0.0105
7.5	89	3.2	0.0359	.8048	.173	0.0062
7.6	90.5	1.8	0.0198	.8155	.167	0.0033
7.7	88.7	0.7	0.0079	.8262	.160	0.0013

Integrated transmission by graphical integration: $\frac{40}{20,324} = 0.196\%$
(See equation 31)
NOTE: Values for λT are used to obtain relative values for $(E_{bb})_\lambda$ from Ref 37.

Sample Thickness 0.030 inch
Sample Temperature 673°K

$\lambda(\mu)$	I_o	I	Transmission	λT	$(E_{bb})_\lambda$ Relative	trans $\times$ $(E_{bb})_\lambda$
6.6	77	1.1	0.0143	.4442	.686	0.0098
6.7	70	1.9	0.0272	.4509	.669	0.0182
6.8	88	3.6	0.0409	.4576	.653	0.0267
6.9	76.5	4.5	0.0588	.4644	.636	0.0374
7.0	83	7.0	0.0843	.4711	.620	0.0523
7.1	80	8.9	0.1112	.4778	.605	0.0673
7.2	83.5	11.6	0.1389	.4846	.589	0.0818
7.3	90	13.8	0.1533	.4913	.574	0.0880
7.4	86	11.0	0.1279	.4980	.559	0.0715
7.5	89	7.0	0.0786	.5048	.545	0.0428
7.6	90.5	3.0	0.0331	.5115	.530	0.0175
7.7	88.7	0.8	0.0090	.5182	.517	0.0046

Integrated transmission by graphical integration: $\frac{126}{16,168} = 0.78\%$
(See equation 31)
NOTE: Values for λT are used to obtain relative values for $(E_{bb})_\lambda$ from Ref 37.

TABLE XXIII (CONT)

SPECTRAL TRANSMISSION DATA ON DYNAQUARTZ (6.2 pcf)

Sample Thickness 0.045 inch
Sample Temperature 300°K

λ(μ)	I_o	I	Transmission	λT	$(E_{bb})_\lambda$ Relative	trans I $(E_{bb})_\lambda$
6.6	78	0.1	0.0128	.1934	.632	0.0081
6.7	70	0.8	0.0114	.1963	.655	0.0074
6.8	88	1.9	0.0216	.1992	.677	0.0146
6.9	78	3.0	0.0385	.2022	.699	0.0269
7.0	84	6.0	0.0714	.2051	.720	0.0514
7.1	80.2	11.1	0.1384	.2080	.741	0.1025
7.2	85.1	18.1	0.2126	.2109	.760	0.1616
7.3	90.6	25.1	0.2110	.2139	.779	0.2158
7.4	88	22.1	0.2511	.2168	.797	0.2001
7.5	90.1	13.0	0.0442	.2198	.815	0.1752
7.6	92	5.4	0.0587	.2227	.831	0.0488
7.7	90	1.2	0.0133	.2256	.847	0.0113

Integrated transmission by graphical integration: $\frac{88}{18,505} = 0.475\%$
(See equation 31)
NOTE: Values for λT are used to obtain relative values for $(E_{bb})_\lambda$ from Ref 37.

Sample Thickness 0.045 inch
Sample Temperature 673°K

λ(μ)	I_o	I	Transmission	λT	$(E_{bb})_\lambda$ Relative	trans I $(E_{bb})_\lambda$
6.6	78	0	0	.4442	.686	0
6.7	70	0.6	0.0086	.4509	.669	0.0057
6.8	88	1.5	0.0170	.4576	.653	0.0111
6.9	78	1.9	0.0243	.4644	.636	0.0154
7.0	84	3.4	0.0405	.4711	.620	0.0251
7.1	80.2	5.1	0.0636	.4778	.605	0.0385
7.2	85.1	6.9	0.0811	.4846	.589	0.0477
7.3	90.6	8.0	0.0883	.4913	.574	0.0507
7.4	88	6.1	0.0693	.4980	.559	0.0387
7.5	90.1	3.0	0.0332	.5048	.545	0.0181
7.6	92	1.0	0.0109	.5115	.530	0.0058
7.7	90	0	0	.5182	.517	0

Integrated transmission by graphical integration: $\frac{75}{16,168} = 0.46\%$
(See equation 31)
NOTE: Values for λT are used to obtain relative values for $(E_{bb})_\lambda$ from Ref 37.

TABLE XXIII (CONCLD)

SPECTRAL TRANSMISSION DATA ON DYNAQUARTZ (6.2 pcf)

Sample Thickness 0.045 inch
Sample Temperature 1073°K

λ (μ)	I_o	I	Transmission	λT	$(E_{bb})_\lambda$ Relative	trans X $(E_{bb})_\lambda$
6.6	78	0	0	.7082	.246	0
6.7	70	0.5	0.0071	.7189	.237	.0014
6.8	88	0.8	0.0091	.7296	.227	.0021
6.9	78	1.0	0.0128	.7404	.218	.0028
7.0	84	1.3	0.0155	.7511	.210	.0033
7.1	80.2	1.9	0.0237	.7618	.202	.0048
7.2	85.1	2.1	0.0247	.7726	.194	.0048
7.3	90.6	2.6	0.0287	.7833	.187	.0054
7.4	88	2.4	0.0273	.7940	.180	.0049
7.5	90.1	1.5	0.0167	.8048	.173	.0029
7.6	92	0.7	0.0076	.8155	.167	.0012
7.7	90	0	0	.8262	.160	0

Integrated transmission by graphical integration: $\frac{28}{20,324} = 0.14\%$
(See equation 31)

NOTE: Values for λT are used to obtain relative values for $(E_{bb})_\lambda$ from Ref 37.

APPENDIX IV

ERROR ANALYSIS

An error analysis was made of the values obtained for the thermal conductivity measurements using the guarded hot plate apparatus. The analysis used to determine imbalance or unbalance errors caused by main and guard heater temperature differences was taken after Woodside (Reference 50) and Woodside and Wilson (Reference 51). No error analysis was made for the absorption and scattering cross sections calculated from transmission experiments. However, an estimated uncertainty in these values could be ±25% using minimum and maximum readings for total transmission data.

1. THERMOCOUPLE DEVIATION

The following deviation was determined by the manufacturer of the thermocouple wire purchased for this investigation.

Thermocouple: C. P. Platinum vs C. P. Platinum 10%-Rhodium Standard Grade Thermocouple 0.010" diameter S. C. No. 84739.

Deviation of electromotive force from NBS Circular 561 is given below.

Temperature °C	Microvolts
600	+8
1200	+7

The elements of the thermocouple were annealed electrically in air for 15 minutes at 1400°C prior to testing. Test Number A-193. Manufacturer: Engelhard Industries, Inc.
Baker Platinum Division
113 Astor Street
Newark 14, New Jersey

2. ERROR ANALYSIS

In taking the test data, the following errors or uncertainties were estimated.

a. Temperature

In reading the potentiometer, the uncertainty is ±0.002 millivolt and the corresponding error is very small < 0.01%. The thermocouple deviation was calibrated at 600°C by the manufacturer and the error was $\frac{0.008}{5.224}$ = 0.15% and even less at 1200°C. However, the temperatures used in this investigation were averaged for two or more readings and rounded off using conversion tables for each °F, and values had to be extrapolated in most cases to the nearest 0.1°F. Considering the reproducibility of the thermocouples, potentiometer readings, and variation of the wire, a maximum error in temperature would be estimated to be ±3% and an average error of less than 2%.

b. Power

In reading the power, the wattmeter was not used directly. The uncertainty in reading the voltmeter is ±0.02 volt and the uncertainty in reading the ammeter is ±0.02 amp. The

minimum power dissipated to the sample was about 14 watts for the air experiments. Thus the error in reading the current is $\frac{0.02}{4.0} \approx 0.5\%$, and $\frac{0.02}{10.0} \approx 0.2\%$ for the voltage, resulting in a total error of 0.7%. At higher power levels the error in reading would be considerably reduced.

c. Area

In measuring the area of the main heater, a machinist's scale was used and the estimated distance was found within ±1/32 inch and the resulting uncertainty in the area is $\frac{(0.0312)^2}{(4)^2} = \frac{0.0097}{16} \approx .06\%$.

d. Thickness

The thickness of the samples was measured with a machinist's scale and the estimate of the uncertainty is ±1/32 inch. Using a micrometer caliper would decrease this uncertainty, but it would also compress the sample. The reproducibility of the sample surface is not very good, so that a maximum error in the thickness dimension would be about ±1/32 inch. The maximum error is estimated to be $\frac{0.0312}{0.500} \approx 6\%$.

e. Imbalance Errors

The error caused by imbalance of the guard and center heaters can be estimated using the analysis of Woodside (Reference 50) and Woodside and Wilson (Reference 51). They performed a theoretical analysis of the deviation from one dimensional heat flow in guarded hot plate measurements. The solution was obtained by the application of two successive Schwarz transformations and the assumptions were verified by relaxation calculations. In using Woodside's analysis the following parameters were found for this thermal conductivity apparatus:

2d = width of the gap separating the test area and guard heaters, 1/16 inch

2η = linear dimension of test area plate, 3-15/16 inches

h = thickness of test sample, 1/2 inch

The error in lateral heat flow as derived by Woodside and Wilson (Reference 51) is

$$\frac{q - q_n}{k} = \frac{\Psi}{2\pi} = \frac{(\eta + d)^2}{16h}$$

where

$$\Psi = \int_0^{\eta} \cosh^{-1}\left[2e^{\left(\exp \frac{\pi\xi}{h} - 1\right)} + 1\right] d\xi$$

and

$$e^{-1} = 1 - \exp\left(\frac{2\pi d}{h}\right)$$

The evaluation of the integral, ψ defined above, requires plotting of the function

$$y = \cosh^{-1}\left[2\alpha\left(\exp\frac{\pi x}{h} - 1\right) + 1\right]$$

and the evaluation of the area under the curve. An approximation given by Woodside is

$$\Psi = \frac{\pi\eta^2}{2h} + \eta \ln(4\alpha)$$

and the approximate value of the error in lateral heat flow is

$$\frac{q - q_0}{k} = \frac{\eta}{9\pi} \ln 4\alpha$$

Using the approximate formula above, the following values were calculated:

$$e^{-1} = 1 - e^{\frac{-2\pi d}{h}}$$

$$e^{-1} = 1 - e^{-2\pi(0.0312)2} = 1 - e^{-0.392}$$

$$e^{-1} = 1.0 - 0.6756$$

$$e^{-1} = 0.3244$$

$$\alpha = 1/e^{-1.18} = 3.0826$$

$$4\alpha = 12.3304$$

$$\ln 4\alpha = 2.512$$

$$\eta = 1.9687$$

$$\frac{q - q_0}{k} = \frac{1.9687}{9\pi}(2.512) = 0.1749$$

and the error due to lateral heat flow is

$$q - q_0 = 0.1749k \text{ BTU/hr-°F imbalanced}$$

Using the 5% value for temperature difference of 400°F across the specimen, a temperature imbalance of 20°F would be the maximum obtained for most of the measurements. At 950°F mean temperature in air

$$\text{ERROR IN HEAT FLOW } \frac{q - q_0}{q} = \frac{0.1749(0.628)(20°F)}{55.67} = 3.95\%$$

At 2350°F and 20°F imbalance

$$\text{ERROR IN } q = \frac{0.1749(20)(1.487)}{137.03} = 3.79\%$$

Therefore the maximum error deviation due to lateral heat flow is estimated to be ±4%.

The total maximum error due to uncertainties in the measurements is estimated to be ±13.95% or ±15% and the usual error in the thermal conductivity measurements is estimated to be about ±10%.

APPENDIX V

RAW DATA FOR THERMAL CONDUCTIVITY MEASUREMENTS

The tabulated raw data for the guarded hot plate measurements are shown in Table XXIV. A sample calculation of one of the thermal conductivity measurements was performed. All temperatures were determined from thermocouple readings (see Figures 16 and 17 for thermocouple locations). The raw data do not necessarily show steady-state values or low imbalance conditions. The final steady-state values (shown in Tables XII, XIII, and XIV) coupled with the best or lowest temperature imbalance conditions obtained in this investigation are indicated in Table XXIV by an asterisk. The data taken for Run 1 in air was not retained since the sample cracked during the experiment.

SAMPLE CALCULATIONS

Reduction of Data for Run 020465 - 0845 Dynaquartz in Air (Run 1)

Top specimen: 6.2 pcf Dynaquartz - no pins in main heater

Bottom specimen: 6.2 pcf Dynaquartz - zirconia pins

$(q)_{total} = Vi = (19.50)\ (4.99) = 97.3$ watts

$(q)_{total} = (97.3)\ (3.41) = 330.8$ BTU/hr

Ratio of heat flow (Power ratio): $(q)_{top}/(q)_{bot} = 0.852$

$$(q)_{bot} = \frac{330.8}{1.852} = 178.6 \text{ BTU/hr}$$

$$(q)_{top} = 330.8 - 178.6 = 152.2 \text{ BTU/hr}$$

Area of sample test section: $\frac{(4)\ (4)}{144} = 0.11\ ft^2$

Thickness of sample: 0.50 inch

$$Q_{top} = \frac{152.2}{0.11} = 1383.6 \text{ BTU/hr-ft}^2$$

$$(k)_{top} = (Q)_{top}\left(\frac{\Delta x}{\Delta T}\right) = 1383.6\ \left(\frac{0.5}{456.8}\right) = 1.514 \frac{\text{BTU-in.}}{\text{hr-ft}^2\text{-°F}}$$

$$(k)_{bot} = (Q)_{bot}\left(\frac{\Delta x}{\Delta T}\right) = \left(\frac{178.6}{0.11}\right)\left(\frac{0.5}{456.9}\right) = 1.777 \frac{\text{BTU-in.}}{\text{hr-ft}^2\text{-°F}}$$

TABLE XXIV

RAW DATA FOR THERMAL CONDUCTIVITY USING
GUARDED HOT PLATE APPARATUS

Dynaquartz in Air
Top Sample - Dynaquartz With Zirconia Pins
Bottom Sample - Sapphire Wool With Zirconia Pins

			*	*	*	*
Voltage (volts)	18.2	18.2	19.6	19.6	19.6	19.6
Current (amps)	5.25	5.25	5.5	5.5	5.5	5.5
Power (watts)	95.6	95.6	107.8	107.8	107.8	107.8
Power (Btu/hr)	326.0	326.0	367.6	367.6	367.6	367.6
Power Ratio	0.448	0.448	0.411	0.411	0.415	0.415
Top Power	101.0	101.0	107.1	107.1	107.8	107.8
Bottom Power	225.0	225.0	260.5	260.5	259.8	259.8
Top ΔT, S-C	13.0	13.0	2.7	2.7	0.4	0.4
Top ΔT, C-M	8.3	14.0	6.0	- 0 -	7.6	14.4
Top ΔT	390.0	376.8	388.7	378.3	365.2	376.4
Top Mean T	1783.0	1783.9	1878.8	1879.6	1883.0	1884.2
Top k	1.085	1.127	1.287	1.253	1.342	1.302
Bottom ΔT, S-C	22.7	22.7	11.0	11.0	9.0	9.0
Bottom ΔT, C-M	8.6	29.6	7.3	25.0	21.6	40.6
Bottom ΔT	278.3	287.3	264.3	269.7	265.3	270.0
Bottom Mean T	1781.1	1797.6	1887.1	1902.1	1882.9	1889.6
Bottom k	3.674	3.559	4.479	4.389	4.451	4.373

NOTE: The following units are used: Heat Flux, Btu/hr-ft^2; ΔT, ($^\circ$F); k, $\frac{\text{Btu-in}}{\text{hr-ft}^2{}^\circ\text{F}}$

Imbalance ΔT's are across the hot faces S-C (side to corner) and C-M (corner to main).

TABLE XXIV(CONTD)

THERMAL CONDUCTIVITY DATA AND CALCULATION SHEET

Dynaquartz in Air
Top Sample - Dynaquartz With Zirconia Pins
Bottom Sample - Sapphire Wool With Zirconia Pins

	*	*	*	*	*	
Voltage (volts)	19.6	19.6	19.6	19.6	25.4	25.4
Current (amps)	5.5	5.5	5.5	5.5	6.3	6.3
Power (watts)	107.8	107.8	107.8	107.8	160.0	160.0
Power (Btu/hr)	367.8	367.8	367.6	367.6	545.6	545.6
Power Ratio	0.430	0.430	0.415	0.415	0.377	0.377
Top Power	110.5	110.5	107.8	107.8	149.4	149.4
Bottom Power	257.1	257.1	259.8	259.8	396.2	396.2
Top ΔT, S-C	1.3	1.3	- 0 -	- 0 -	3.2	3.2
Top ΔT, C-M	6.0	12.0	16.0	- 0 -	18.0	24.9
Top ΔT	361.7	373.0	373.0	393.9	373.3	382.9
Top Mean T	1887.1	1887.1	1905.0	1911.6	2388.0	2391.0
Top k	1.389	1.347	1.314	1.244	1.819	1.678
Bottom ΔT, S-C	7.2	7.2	21.4	21.4	- 0 -	- 0 -
Bottom ΔT, C-M	20.3	38.0	5.4	12.6	42.3	61.7
Bottom ΔT	257.3	271.6	260.6	268.3	260.	26 .5
Bottom Mean T	1890.3	1907.2	1911.7	1925.8	2385.1	2400.2
Bottom k	4.541	4.466	4.531	4.401	6.901	6.681

NOTE: The following units are used: Heat Flux, Btu/hr-ft^2; ΔT, ($^\circ$F); k, $\frac{\text{Btu-in}}{\text{hr-ft}^2\,^\circ\text{F}}$

Imbalance ΔT's are across the hot faces S-C (side to corner) and C-M (corner to main).

TABLE XXIV(CONTD)

THERMAL CONDUCTIVITY DATA AND CALCULATION SHEET

Dynaquartz in Air
Top Sample - Dynaquartz With Zirconia Pins
Bottom Sample - Sapphire Wool With Zirconia Pins

	*	*	*	*	*	*
Voltage (volts)	24.3	24.3	23.5	23.5	23.6	23.6
Current (amps)	6.0	6.0	5.8	5.8	5.8	5.8
Power (watts)	145.8	145.8	136.3	136.3	136.9	136.9
Power (Btu/hr)	497.2	497.2	464.8	464.8	466.8	466.8
Power Ratio	0.378	0.378	0.399	0.399	0.410	0.410
Top Power	136.4	136.4	132.6	132.6	135.7	135.7
Bottom Power	360.8	360.8	332.2	332.2	331.1	331.1
Top ΔT, S-C	19.5	19.5	6.3	6.3	11.0	11.0
Top ΔT, C-M	1.2	3.8	1.3	4.4	6.0	1.3
Top ΔT	353.6	360.8	350.3	362.7	355.3	364.3
Top Mean T	2407.9	2406.5	2421.8	2421.3	2426.3	2426.5
Top k	1.718	1.743	1.720	1.622	1.736	1.693
Bottom ΔT, S-C	9.4	9.4	4.0	4.0	14.0	14.0
Bottom ΔT, C-M	14.6	29.3	19.3	32.7	30.0	42.3
Bottom ΔT	241.0	249.2	234.3	238.7	230.0	234.3
Bottom Mean T	2408.5	2419.1	2428.1	2439.3	2438.0	2448.1
Bottom k	6.803	6.580	6.443	6.325	6.542	6.442

NOTE: The following units are used: Heat Flux, Btu/hr-ft^2; ΔT, ($^\circ$F); k, $\frac{\text{Btu-in}}{\text{hr-ft}^2{}^\circ\text{F}}$

Imbalance ΔT's are across the hot faces S-C (side to corner) and C-M (corner to main).

TABLE XXIV(CONTD)

THERMAL CONDUCTIVITY DATA AND CALCULATION SHEET

Dynaquartz in Air (Run 1)
Top Sample - Dynaquartz Without Zirconia Pins
Bottom Sample - Dynaquartz With Zirconia Pins

Time	300365 1630	310365 1435	310365 1600	310365 1700	310365 1740	310365 2045
Voltage (volts)	7.15	12.47	12.30	12.30	12.28	12.14
Current (amps)	3.00	4.00	3.70	3.80	3.60	3.60
Power (watts)	21.50	50.00	45.5	46.7	44.3	43.9
Power (Btu/hr)	73.10	170.00	154.7	158.8	150.6	149.3
Power Ratio	0.943	0.794	0.787	0.816	0.811	0.671
Top Power	35.4	75.2	69.1	71.4	67.4	60.3
Bottom Power	37.7	94.8	86.6	87.4	83.2	89.3
Top Heat Flux	321.8	683.6	628.2	649.1	612.7	548.2
Bottom Heat Flux	342.7	861.8	787.3	749.5	766.4	811.8
Top ΔT, S-C	15.2	39.7	33.0	19.0	15.4	104.3
Top ΔT, C-M	11.8	46.5	36.2	20.8	12.2	120.7
Top ΔT	267.2	337.2	339.7	336.8	335.4	340.5
Top Mean T	391.8	1220.9	1227.4	1226.9	1224.8	1235.4
Top k	0.602	1.014	0.924	0.964	0.914	0.805
Bottom ΔT, S-C	3.8	2.4	3.4	20.1	19.6	62.0
Bottom ΔT, C-M	6.2	1.7	9.5	28.1	31.3	70.0
Bottom ΔT	249.4	339.3	336.8	333.2	327.9	331.4
Bottom Mean T	400.7	1218.0	1226.4	1227.5	1225.7	1238.8
Bottom k	0.687	1.270	1.169	1.192	1.153	1.225

NOTE: The following units are used: Heat Flux, Btu/hr-ft^2; ΔT, ($^\circ$F); k, $\frac{\text{Btu-in}}{\text{hr-ft}^2{}^\circ\text{F}}$

Imbalance ΔT's are across the hot faces S-C (side to corner) and C-M (corner to main).

TABLE XXIV(CONTD)

THERMAL CONDUCTIVITY DATA AND CALCULATION SHEET

Dynaquartz in Air (Run 1)
Top Sample - Dynaquartz Without Zirconia Pins
Bottom Sample - Dynaquartz With Zirconia Pins

Time	310365 2145	010465 1330	010465 1410	010465 1500	010465 1550	010465 1655
Voltage (volts)	12.25	17.25	17.30	17.35	17.25	17.30
Current (amps)	3.60	5.00	4.98	4.98	4.98	4.98
Power (watts)	44.30	85.90	86.20	86.4	86.2	86.2
Power (Btu/hr)	150.6	292.1	293.1	294.6	293.1	293.1
Power Ratio	0.811	0.818	0.811	0.814	0.813	0.821
Top Power	67.1	131.4	131.3	132.2	131.4	132.1
Bottom Power	83.5	160.7	161.8	162.4	161.7	161.0
Top Heat Flux	610.0	1194.5	1193.6	1201.8	1194.5	1200.9
Bottom Heat Flux	759.1	1460.9	1470.9	1476.4	1470.0	1463.6
Top ΔT, S-C	108.7	53.5	55.2	53.1	50.4	49.4
Top ΔT, C-M	123.9	78.7	81.3	44.1	69.8	68.3
Top ΔT	344.2	440.7	457.3	456.1	456.0	453.7
Top Mean T	1242.0	1630.5	1645.2	1651.2	1655.9	1656.7
Top k	0.886	1.355	1.304	1.317	1.310	1.324
Bottom ΔT, S-C	66.2	3.2	4.0	- 0 -	3.6	8.9
Bottom ΔT, C-M	75.8	10.0	10.8	2.5	4.1	5.3
Bottom ΔT	333.6	444.0	461.7	464.5	463.5	462.0
Bottom Mean T	1244.9	1629.5	1642.3	1647.8	1650.5	1652.3
Bottom k	1.138	1.645	1.593	1.589	1.587	1.584

NOTE: The following units are used: Heat Flux, Btu/hr-ft^2; ΔT, ($^\circ$F); k, $\frac{\text{Btu-in}}{\text{hr-ft}^2{}^\circ\text{F}}$

Imbalance ΔT's are across the hot faces S-C (side to corner) and C-M (corner to main).

TABLE XXIV(CONTD)

THERMAL CONDUCTIVITY DATA AND CALCULATION SHEET

Dynaquartz in Air (Run 1)
Top Sample - Dynaquartz Without Zirconia Pins
Bottom Sample - Dynaquartz With Zirconia Pins

Time	010465 2015	010465 2100	020465 0845	020465 0945	020465 1020	020465 1415
Voltage (volts)	19.40	19.40	19.50	19.50	19.45	20.20
Current (amps)	4.99	4.99	4.99	4.99	4.99	4.99
Power (watts)	96.8	96.8	97.3	97.3	97.3	100.8
Power (Btu/hr)	329.1	329.1	330.8	330.8	330.8	343.7
Power Ratio	0.862	0.846	0.852	0.857	0.847	0.786
Top Power	152.4	150.8	152.2	152.7	151.7	151.3
Bottom Power	176.7	178.3	178.6	178.1	179.1	192.4
Top Heat Flux	1385.5	1370.9	1383.6	1388.2	1379.1	1375.4
Bottom Heat Flux	1606.4	1620.9	1623.6	1619.1	1628.2	1749.1
Top ΔT, S-C	11.7	42.1	50.7	63.6	66.1	105.1
Top ΔT, C-M	52.0	74.1	76.0	91.5	93.8	27.6
Top ΔT	505.1	495.8	456.8	466.9	466.8	417.1
Top Mean T	1851.4	1847.4	1931.3	1938.1	1939.9	2122.0
Top k	1.372	1.383	1.514	1.487	1.477	1.648
Bottom ΔT, S-C	42.8	18.1	5.8	7.7	5.8	42.1
Bottom ΔT, C-M	22.0	8.5	0.8	15.3	18.1	55.7
Bottom ΔT	500.3	496.0	456.9	461.8	464.1	429.1
Bottom Mean T	1853.2	1847.4	1931.3	1937.8	1938.4	2113.2
Bottom k	1.605	1.634	1.777	1.753	1.754	2.038

NOTE: The following units are used: Heat Flux, Btu/hr-ft^2; ΔT, ($^\circ$F); k, $\frac{\text{Btu-in}}{\text{hr-ft}^2{}^\circ\text{F}}$

Imbalance ΔT's are across the hot faces S-C (side to corner) and C-M (corner to main).

TABLE XXIV (CONTD)

THERMAL CONDUCTIVITY DATA AND CALCULATION SHEET

Dynaquartz in Air (Run 1)
Top Sample - Dynaquartz Without Zirconia Pins
Bottom Sample - Dynaquartz With Zirconia Pins

Time	020465 1550	020465 1710	020465 1800	020465 1950	020465 2000	030465 1045
Voltage (volts)	20.2	20.2	20.2	20.1	20.2	22.1
Current (amps)	4.99	4.99	4.99	4.99	4.99	5.20
Power (watts)	100.8	100.8	100.8	100.3	100.8	114.9
Power (Btu/hr)	343.7	343.7	343.7	342.0	343.7	391.8
Power Ratio	0.798	0.836	0.727	0.722	0.717	0.823
Top Power	152.5	156.5	144.7	143.4	143.5	176.9
Bottom Power	191.2	187.2	199.0	198.6	200.2	214.9
Top Heat Flux	1386.4	1422.7	1315.4	1303.6	1304.5	1608.2
Bottom Heat Flux	1738.2	1701.8	1809.1	1805.4	1820.0	1953.6
Top ΔT, S-C	99.6	91.2	109.8	88.6	89.3	60.7
Top ΔT, C-M	121.0	111.6	89.0	100.4	105.4	54.5
Top ΔT	396.3	386.4	383.0	380.2	381.0	422.7
Top Mean T	2153.2	2151.5	2152.3	2150.9	2151.5	2334.0
Top k	1.749	1.841	1.717	1.714	1.712	1.902
Bottom ΔT, S-C	41.2	28.2	36.1	18.7	25.2	4.5
Bottom ΔT, C-M	42.1	18.7	22.5	17.0	16.2	6.9
Bottom ΔT	427.8	424.4	425.9	427.3	429.3	411.8
Bottom Mean T	2124.6	2128.7	2127.0	2123.7	2122.1	2315.8
Bottom k	2.032	2.005	2.124	2.145	2.119	2.372

NOTE: The following units are used: Heat Flux, Btu/hr-ft^2; ΔT, ($^\circ$F); k, $\frac{\text{Btu-in}}{\text{hr-ft}^2{}^\circ\text{F}}$

Imbalance ΔT's are across the hot faces S-C (side to corner) and C-M (corner to main).

TABLE XXIV(CONTD)

THERMAL CONDUCTIVITY DATA AND CALCULATION SHEET

Dynaquartz in Air (Run 1)
Top Sample - Dynaquartz Without Zirconia Pins
Bottom Sample - Dynaquartz With Zirconia Pins

Time	030465 1200	030465 1300	030465 1400	030465 1430	030465 1500	030465 1640
Voltage (volts)	21.9	22.4	22.4	22.3	22.3	22.3
Current (amps)	5.10	5.02	5.01	5.01	5.01	5.00
Power (watts)	111.7	112.4	112.2	111.7	111.7	111.5
Power (Btu/hr)	380.9	383.3	382.6	380.9	380.9	380.2
Power Ratio	0.810	0.851	0.832	0.820	0.821	0.839
Top Power	170.5	176.2	173.8	171.6	171.7	173.5
Bottom Power	210.4	207.1	208.8	209.3	209.2	206.7
Top Heat Flux	1550.0	1601.8	1580.0	1560.0	1560.9	1577.3
Bottom Heat Flux	1912.7	1882.7	1898.2	1902.7	1901.8	1879.1
Top ΔT, S-C	58.0	91.8	96.8	96.9	94.9	103.4
Top ΔT, C-M	82.1	150.5	150.8	149.4	140.4	154.5
Top ΔT	394.0	447.4	416.5	411.2	407.0	402.8
Top Mean T	2328.0	2434.0	2426.6	2425.4	2423.2	2422.9
Top k	1.967	1.790	1.897	1.897	1.917	1.961
Bottom ΔT, S-C	2.5	33.2	48.5	40.6	37.6	33.7
Bottom ΔT, C-M	7.0	63.2	72.2	65.6	54.1	55.3
Bottom ΔT	410.0	455.8	430.6	428.0	425.1	418.4
Bottom Mean T	2310.4	2431.7	2422.6	2419.0	2414.8	2418.3
Bottom k	2.511	2.065	2.204	2.261	2.235	2.246

NOTE: The following units are used: Heat Flux, Btu/hr-ft^2; ΔT, ($^\circ$F); k, $\frac{\text{Btu-in}}{\text{hr-ft}^2{}^\circ\text{F}}$

Imbalance ΔT's are across the hot faces S-C (side to corner) and C-M (corner to main).

TABLE XXIV(CONTD)

THERMAL CONDUCTIVITY DATA AND CALCULATION SHEET

Dynaquartz in Air (Run 2)
Top Sample - Dynaquartz Without Zirconia Pins
Bottom Sample - Dynaquartz With Zirconia Pins

Time	160665 1500	160665 1610	160665 2045	160665 2200	170665 0830	170665 1045
Voltage (volts)	7.25	7.25	7.22	7.22	10.35	10.32
Current (amps)	3.20	3.29	3.40	3.40	3.90	3.91
Power (watts)	23.2	23.85	24.55	24.50	40.37	40.35
Power (Btu/hr)	79.11	81.33	83.72	83.50	137.66	137.59
Power Ratio	1.0183	1.0731	1.242	1.318	0.818	0.8193
Top Power	39.92	41.01	46.38	47.38	61.94	61.96
Bottom Power	39.19	40.32	37.34	36.02	75.72	75.63
Top Heat Flux	362.91	372.82	421.64	431.64	563.09	563.27
Bottom Heat Flux	356.27	366.55	339.45	327.45	688.36	687.54
Top ΔT, S-C	9.4	34.2	1.2	9.8	15.5	1.5
Top ΔT, C-M	26.5	65.7	28.8	39.1	31.9	13.7
Top ΔT	219.3	183.9	186.8	183.2	297.4	292.8
Top Mean T	780.4	746.3	666.4	658.2	1089.7	1092.5
Top k	0.827	1.014	1.128	1.177	0.947	0.962
Bottom ΔT, S-C	41.2	59.8	24.8	32.7	25.3	40.2
Bottom ΔT, C-M	61.4	102.7	57.4	61.8	18.3	36.3
Bottom ΔT	207.6	171.1	140.0	140.0	309.0	311.7
Bottom Mean T	793.8	752.5	696.6	687.6	1089.1	1088.0
Bottom k	0.858	1.071	1.212	1.169	1.114	1.103

NOTE: The following units are used: Heat Flux, Btu/hr-ft^2; ΔT, ($^\circ$F); k, $\frac{\text{Btu-in}}{\text{hr-ft}^2{}^\circ\text{F}}$

Imbalance ΔT's are across the hot faces S-C (side to corner) and C-M (corner to main).

TABLE XXIV(CONTD)

THERMAL CONDUCTIVITY DATA AND CALCULATION SHEET

Dynaquartz in Air (Run 2)
Top Sample - Dynaquartz Without Zirconia Pins
Bottom Sample - Dynaquartz With Zirconia Pins

Time	170665 1245	170665 1400	170665 1550	170665 2030	180665 1030	180665 1230
Voltage (volts)	10.32	10.33	10.30	10.28	12.48	12.49
Current (amps)	3.90	3.90	3.85	3.80	3.98	4.11
Power (watts)	40.25	40.29	39.67	39.06	49.67	51.33
Power (Btu/hr)	137.25	137.39	135.27	133.19	169.37	175.04
Power Ratio	0.808	0.863	0.917	0.939	0.662	0.7512
Top Power	61.34	63.64	64.71	64.50	67.46	75.09
Bottom Power	75.91	73.75	70.56	68.69	101.91	99.95
Top Heat Flux	557.64	578.55	588.28	586.36	613.27	682.64
Bottom Heat Flux	690.09	670.45	641.45	624.45	926.46	908.64
Top ΔT, S-C	4.0	61.5	53.8	47.2	107.2	87.0
Top ΔT, C-M	15.3	81.5	78.2	74.2	170.3	88.1
Top ΔT	287.5	293.7	314.5	324.3	349.7	308.1
Top Mean T	1090.2	1092.4	1113.3	1138.7	1508.6	1444.3
Top k	0.970	0.985	0.935	0.904	0.877	1.108
Bottom ΔT, S-C	38.7	16.7	8.2	1.5	43.5	16.2
Bottom ΔT, C-M	37.3	29.5	17.2	18.9	79.6	17.4
Bottom ΔT	311.9	311.3	315.1	295.9	412.1	353.1
Bottom Mean T	1084.3	1088.9	1117.0	1149.9	1498.8	1422.5
Bottom k	1.106	1.078	1.018	1.055	1.124	1.287

NOTE: The following units are used: Heat Flux, Btu/hr-ft^2; ΔT, ($^\circ$F); k, $\frac{\text{Btu-in}}{\text{hr-ft}^2{}^\circ\text{F}}$

Imbalance ΔT's are across the hot faces S-C (side to corner) and C-M (corner to main).

TABLE XXIV(CONTD)

THERMAL CONDUCTIVITY DATA AND CALCULATION SHEET

Dynaquartz in Air (Run 2)
Top Sample - Dynaquartz Without Zirconia Pins
Bottom Sample - Dynaquartz With Zirconia Pins

Time	040965 1445	* 040965 1600	* 040965 1930	* 040965 2030	* 050965 1600	* 050965 1715
Voltage (volts)	9.82	9.72	9.80	9.80	12.00	11.92
Current (amps)	3.85	3.80	3.79	3.79	4.09	4.08
Power (watts)	37.807	36.936	37.142	37.142	49.080	48.831
Power (Btu/hr)	128.92	125.95	126.65	126.65	167.36	165.84
Power Ratio	0.760	0.7634	0.7675	0.7754	0.8232	0.8306
Top Power	55.67	54.53	55.00	55.31	75.57	75.25
Bottom Power	73.25	71.42	71.65	71.34	91.79	90.59
Top Heat Flux	506.09	495.73	500.00	502.82	687.00	684.09
Bottom Heat Flux	665.91	649.27	651.36	648.54	834.45	823.54
Top ΔT, S-C	10.0	10.4	8.4	16.0	27.1	4.0
Top ΔT, C-M	5.5	9.4	15.7	22.9	33.8	12.1
Top ΔT	402.9	409.1	406.9	409.5	451.9	454.9
Top Mean T	951.5	961.9	973.9	975.3	1259.8	1262.5
Top k	0.628	0.606	0.614	0.614	0.760	0.752
Bottom ΔT, S-C	19.7	24.0	7.5	6.4	35.5	2.3
Bottom ΔT, C-M	18.3	22.4	2.4	9.5	47.5	2.0
Bottom ΔT	417.7	426.9	424.1	426.5	457.8	460.3
Bottom Mean T	943.6	953.5	965.1	966.7	1256.9	1260.1
Bottom k	0.797	0.760	0.768	0.760	0.911	0.895

NOTE: The following units are used: Heat Flux, Btu/hr-ft^2; ΔT, ($^\circ$F); k, $\frac{\text{Btu-in}}{\text{hr-ft}^2{}^\circ\text{F}}$

Imbalance ΔT's are across the hot faces S-C (side to corner) and C-M (corner to main).

TABLE XXIV(CONTD)

THERMAL CONDUCTIVITY DATA AND CALCULATION SHEET

Dynaquartz in Air (Run 2)
Top Sample - Dynaquartz Without Zirconia Pins
Bottom Sample - Dynaquartz With Zirconia Pins

Time	* 050965 1830	* 050965 2030	* 060965 1500	* 060965 1600	* 060965 1730	060965 2100
Voltage (volts)	11.98	11.95	15.10	15.10	15.15	15.16
Current (amps)	4.08	4.10	4.34	4.30	4.37	4.33
Power (watts)	48.878	48.995	65.534	65.081	65.145	66.249
Power (Btu/hr)	166.67	167.07	223.47	221.93	222.14	225.91
Power Ratio	0.8221	0.8167	0.8161	0.8210	0.8150	0.7981
Top Power	75.20	75.11	100.42	100.06	99.75	100.27
Bottom Power	91.47	91.96	123.05	121.87	122.39	125.64
Top Heat Flux	683.64	682.82	912.91	909.64	906.82	911.54
Bottom Heat Flux	831.54	836.00	1118.64	1107.91	1112.64	1142.18
Top ΔT, S-C	2.5	3.2	4.6	1.2	2.3	60.8
Top ΔT, C-M	5.3	6.7	2.9	3.7	6.7	76.0
Top ΔT	455.9	446.6	425.1	419.9	411.8	395.0
Top Mean T	1266.2	1256.3	1749.0	1770.9	1787.0	1762.3
Top k	0.750	0.764	1.074	1.083	1.101	1.154
Bottom ΔT, S-C	8.8	4.6	0.7	2.1	0.1	65.5
Bottom ΔT, C-M	7.4	3.9	2.6	2.1	0.9	83.7
Bottom ΔT	459.6	450.3	441.8	444.5	443.0	422.4
Bottom Mean T	1265.1	1254.7	1737.0	1755.3	1768.6	1744.3
Bottom k	0.905	0.928	1.266	1.246	1.255	1.352

NOTE: The following units are used: Heat Flux, Btu/hr-ft^2; ΔT, (^{o}F); k, $\frac{\text{Btu-in}}{\text{hr-ft}^2{}^o\text{F}}$

Imbalance ΔT's are across the hot faces S-C (side to corner) and C-M (corner to main).

TABLE XXIV(CONTD)

THERMAL CONDUCTIVITY DATA AND CALCULATION SHEET

Dynaquartz in Air (Run 2)
Top Sample - Dynaquartz Without Zirconia Pins
Bottom Sample - Dynaquartz With Zirconia Pins

Time	* 070965 0945	* 070965 1100	* 070965 1330	* 070965 1430	070965 1950	070965 2115
Voltage (volts)	16.90	16.80	16.80	16.80	20.00	20.01
Current (amps)	4.33	4.32	4.33	4.35	4.80	4.79
Power (watts)	73.177	72.576	72.744	73.080	96.000	95.848
Power (Btu/hr)	249.53	247.48	248.06	249.20	327.36	326.84
Power Ratio	0.7072	0.6824	0.6651	0.6840	0.7200	0.7280
Top Power	103.37	100.38	99.08	101.22	137.03	137.70
Bottom Power	146.16	147.10	148.98	147.98	190.33	189.14
Top Heat Flux	939.73	912.54	900.73	920.18	1245.73	1251.82
Bottom Heat Flux	1328.73	1337.27	1354.36	1345.27	1730.27	1719.45
Top ΔT, S-C	15.5	3.5	6.1	2.5	14.6	6.8
Top ΔT, C-M	33.5	7.2	18.9	14.9	11.4	7.8
Top ΔT	363.7	372.7	347.0	343.9	418.8	421.0
Top Mean T	2150.1	2159.1	2155.7	2148.2	2352.5	2379.6
Top k	1.292	1.258	1.298	1.338	1.487	1.487
Bottom ΔT, S-C	16.8	7.4	0.8	1.7	16.9	9.4
Bottom ΔT, C-M	32.0	22.9	23.8	27.0	15.5	22.1
Bottom ΔT	451.5	438.3	451.2	448.5	522.2	518.0
Bottom Mean T	1999.2	2114.7	2097.2	2090.0	2293.4	2313.6
Bottom k	1.471	1.525	1.501	1.500	1.657	1.660

NOTE: The following units are used: Heat Flux, Btu/hr-ft^2; ΔT, ($^\circ$F); k, $\frac{\text{Btu-in}}{\text{hr-ft}^2{}^\circ\text{F}}$

Imbalance ΔT's are across the hot faces S-C (side to corner) and C-M (corner to main).

TABLE XXIV (CONTD)

THERMAL CONDUCTIVITY DATA AND CALCULATION SHEET

Dynaquartz in Argon (1 atm)
Top Sample - Dynaquartz Without Zirconia Pins
Bottom Sample - Dynaquartz With Zirconia Pins

Time	* 010665 0900	* 010665 1000	* 010665 1100	010665 1245	* 010665 1330	* 010665 1500
Voltage (volts)	3.40	3.40	3.40	3.40	3.40	3.40
Current (amps)	2.04	2.04	2.04	2.04	2.04	2.04
Power (watts)	6.936	6.936	6.936	6.036	6.936	6.036
Power (Btu/hr)	23.65	23.65	23.65	23.65	23.65	23.65
Power Ratio	1.0158	1.0158	0.9366	0.9730	1.0562	1.0213
Top Power	11.92	11.92	11.44	11.66	11.92	11.95
Bottom Power	11.73	11.73	12.21	11.99	11.73	11.70
Top Heat Flux	108.36	108.36	104.00	106.00	108.36	108.64
Bottom Heat Flux	106.64	106.64	111.00	109.00	106.64	106.36
Top ΔT, S-C	25.0	2.3	1.6	21.1	10.7	3.5
Top ΔT, C-M	[illegible].8	1.4	1.7	22.2	1.0	1.2
Top ΔT	156.0	158.9	162.0	149.1	145.5	159.6
Top Mean T	271.3	273.4	277.3	270.8	267.0	277.6
Top k	0.347	0.341	0.321	0.355	0.372	0.340
Bottom ΔT, S-C	25.2	1.0	0.2	16.8	4.6	- 0 -
Bottom ΔT, C-M	23.3	3.2	2.5	0.4	12.8	3.0
Bottom ΔT	146.6	149.3	152.5	124.4	136.5	152.0
Bottom Mean T	272.3	274.1	277.8	271.3	267.7	277.3
Bottom k	0.364	0.357	0.364	0.421	0.391	0.350

NOTE: The following units are used: Heat Flux, Btu/hr-ft^2; ΔT, (^{o}F); k, $\frac{\text{Btu-in}}{\text{hr-ft}^2\,^o\text{F}}$

Imbalance ΔT's are across the hot faces S-C (side to corner) and C-M (corner to main).

TABLE XXIV(CONTD)

THERMAL CONDUCTIVITY DATA AND CALCULATION SHEET

Dynaquartz in Argon (1 atm)
Top Sample - Dynaquartz Without Zirconia Pins
Bottom Sample - Dynaquartz With Zirconia Pins

Time	020665 0945	020665 1115	020665 1330	020665* 1500	020665* 1700	020665* 2030
Voltage (volts)	4.85	4.60	4.35	4.30	4.30	4.13
Current (amps)	2.60	2.48	2.40	2.40	2.39	2.30
Power (watts)	12.67	11.41	10.44	10.32	10.28	9.499
Power (Btu/hr)	43.00	38.91	35.60	35.19	35.05	32.39
Power Ratio	0.940	0.959	0.914	0.903	0.9363	0.8848
Top Power	20.84	19.05	17.00	16.70	16.95	15.21
Bottom Power	22.16	19.86	18.60	18.49	18.10	17.18
Top Heat Flux	189.45	173.18	154.55	151.82	154.09	138.27
Bottom Heat Flux	201.45	180.54	160.09	168.09	164.55	156.18
Top ΔT, S-C	2.0	0.4	0.2	3.0	10.0	11.2
Top ΔT, C-M	22.6	10.4	14.8	13.4	11.1	11.4
Top ΔT	211.6	207.7	188.9	192.9	192.1	179.7
Top Mean T	382.8	372.3	347.7	344.7	338.0	318.8
Top k	0.448	0.417	0.409	0.394	0.401	0.385
Bottom ΔT, S-C	4.3	7.4	7.0	9.0	16.2	13.1
Bottom ΔT, C-M	24.1	15.3	17.5	16.2	24.0	22.1
Bottom ΔT	197.2	187.2	177.3	182.2	181.6	169.1
Bottom Mean T	386.0	378.3	349.6	346.1	339.4	320.0
Bottom k	0.511	0.482	0.477	0.461	0.453	0.462

NOTE: The following units are used: Heat Flux, Btu/hr-ft^2; ΔT, (^{o}F); k, $\frac{\text{Btu-in}}{\text{hr-ft}^2{}^o\text{F}}$

Imbalance ΔT's are across the hot faces S-C (side to corner) and C-M (corner to main).

TABLE XXIV (CONT'D)

THERMAL CONDUCTIVITY DATA AND CALCULATION SHEET

Dynaquartz in Argon (1 atm)
Top Sample - Dynaquartz Without Zirconia Pins
Bottom Sample - Dynaquartz With Zirconia Pins

Time	030665 0845	030665 1100	030665 1320	030665* 1520	030665* 2000	030665* 2130
Voltage (volts)	10.35	8.42	8.07	7.46	7.85	7.95
Current (amps)	4.28	3.60	3.53	3.48	3.45	3.45
Power (watts)	44.30	30.31	28.49	27.70	27.08	27.43
Power (Btu/hr)	151.06	103.36	97.15	94.46	92.34	93.54
Power Ratio	0.856	0.824	0.838	0.8537	0.8759	0.8556
Top Power	69.67	46.70	44.29	43.50	43.12	43.16
Bottom Power	81.39	56.66	52.86	50.96	49.22	50.38
Top Heat Flux	633.36	424.55	402.60	395.45	392.00	392.36
Bottom Heat Flux	739.91	515.09	480.54	463.27	447.45	458.00
Top ΔT, S-C	70.0	36.5	17.4	11.0	16.9	15.6
Top ΔT, C-M	143.3	73.0	46.5	26.0	32.5	31.5
Top ΔT	429.4	370.2	352.5	372.6	370.9	369.9
Top Mean T	830.8	780.7	754.6	765.3	767.4	767.3
Top k	0.738	0.573	0.571	0.531	0.528	0.530
Bottom ΔT, S-C	129.8	45.2	27.8	21.3	27.8	25.5
Bottom ΔT, C-M	203.2	82.6	57.8	36.6	43.7	42.1
Bottom ΔT	431.9	381.6	364.6	381.1	371.5	371.9
Bottom Mean T	822.9	768.3	742.0	754.0	760.7	759.9
Bottom k	0.857	0.675	0.659	0.608	0.602	0.616

NOTE: The following units are used: Heat Flux, Btu/hr-ft^2; ΔT, (^{o}F); k, $\frac{\text{Btu-in}}{\text{hr-ft}^2{}^o\text{F}}$

Imbalance ΔT's are across the hot faces S-C (side to corner) and C-M (corner to main).

TABLE XXIV(CONTD)

THERMAL CONDUCTIVITY DATA AND CALCULATION SHEET

Dynaquartz in Argon (1 atm)
Top Sample - Dynaquartz Without Zirconia Pins
Bottom Sample - Dynaquartz With Zirconia Pins

Time	*030665 2230	*040665 1300	*040665 1400	040665 1500	*040665 1600	*040665 1700
Voltage (volts)	7.95	10.24	10.20	10.23	10.20	10.15
Current (amps)	3.45	3.60	3.56	3.57	3.55	3.55
Power (watts)	27.43	36.86	36.31	36.52	36.21	36.03
Power (Btu/hr)	93.54	125.71	123.82	124.54	123.48	122.87
Power Ratio	0.8582	0.900	0.9331	1.0278	0.8911	0.8954
Top Power	43.20	59.55	59.77	63.12	58.19	58.05
Bottom Power	50.34	66.16	64.05	61.42	65.29	64.82
Top Heat Flux	392.73	541.36	543.36	573.82	529.00	527.73
Bottom Heat Flux	457.64	601.45	582.27	558.36	593.54	589.27
Top ΔT, S-C	15.8	25.0	54.1	12.9	16.4	0.9
Top ΔT, C-M	32.0	17.6	11.6	7.1	11.1	2.5
Top ΔT	369.0	444.8	444.6	438.4	431.9	429.1
Top Mean T	766.6	1245.5	1257.6	1258.0	1257.5	1256.0
Top k	0.532	0.608	0.611	0.654	0.612	0.615
Bottom ΔT, S-C	26.2	39.5	34.0	30.3	33.0	16.5
Bottom ΔT, C-M	42.2	35.4	40.2	25.5	31.1	15.7
Bottom ΔT	370.3	434.1	432.2	422.5	415.6	413.2
Bottom Mean T	759.5	1246.3	1256.7	1259.6	1259.1	1254.1
Bottom k	0.618	0.692	0.674	0.661	0.714	0.713

NOTE: The following units are used: Heat Flux, Btu/hr-ft^2; ΔT, ($^\circ$F); k, $\frac{\text{Btu-in}}{\text{hr-ft}^2{}^\circ\text{F}}$

Imbalance ΔT's are across the hot faces S-C (side to corner) and C-M (corner to main).

TABLE XXIV(CONTD)

THERMAL CONDUCTIVITY DATA AND CALCULATION SHEET

Dynaquartz in Argon (1 atm)
Top Sample - Dynaquartz Without Zirconia Pins
Bottom Sample - Dynaquartz With Zirconia Pins

Time	040665* 1900	040665* 2000	040665* 2130	050665* 2100	050665* 2200	050665* 2230
Voltage (volts)	10.14	10.11	10.11	12.30	12.28	12.30
Current (amps)	3.52	3.51	3.50	3.80	3.80	3.80
Power (watts)	35.6	35.48	35.38	46.74	46.66	46.74
Power (Btu/hr)	121 71	121.01	120.66	159.38	159.12	159.38
Power Ratio	206	0.9195	0.9031	0.8025	0.8635	0.8725
Top Power	58.34	57.97	57.36	70.50	73.73	74.26
Bottom Power	63.37	63.04	63.40	87.85	85.39	85.12
Top Heat Flux	530.36	527.00	520.55	640.91	670.27	675.09
Bottom Heat Flux	576 09	573.09	576.36	798.64	776.27	773.82
Top ΔT, S-C	- [illegible] -	1.0	2.9	20.2	5.7	6.2
Top ΔT, C-M	5.2	3.7	2.7	10.2	16.8	17.1
Top ΔT	433.3	431.7	430.4	364.2	383.9	388.6
Top Mean T	1259 7	1259.4	1258.4	1625.2	1610.2	1603.4
Top k	0.612	0.610	0.605	0.880	0.873	0.869
Bottom ΔT, S-C	16.7	18.7	19.6	2.3	21.4	25.2
Bottom ΔT, C-M	14.1	16.3	17.1	14.3	37.7	42.3
Bottom ΔT	407.7	406.3	407.1	417.3	410.1	405.1
Bottom Mean T	1265.8	1265.7	1263.5	1594.2	1591.0	1589.5
Bottom k	0.706	0.705	0.708	0.957	0.946	0.955

NOTE: The following units are used: Heat Flux, Btu/hr-ft^2; ΔT, (^{o}F); k, $\frac{\text{Btu-in}}{\text{hr-ft}^2{}^o\text{F}}$

Imbalance ΔT's are across the hot faces S-C (side to corner) and C-M (corner to main).

TABLE XXIV(CONTD)

THERMAL CONDUCTIVITY DATA AND CALCULATION SHEET

Dynaquartz in Argon (1 atm)
Top Sample - Dynaquartz Without Zirconia Pins
Bottom Sample - Dynaquartz With Zirconia Pins

Time	050665* 2300	050665* 2330	060665* 1900	060665* 2000	060665* 2030	060665* 2100
Voltage (volts)	12.25	12.25	14.0	14.0	14.0	14.03
Current (amps)	3.80	3.80	3.97	3.90	3.96	3.93
Power (watts)	46.55	46.55	55.88	54.60	55.44	55.14
Power (Btu/hr)	158.74	158.74	189.53	186.19	189.05	189.05
Power Ratio	0.8771	0.8855	0.8571	0.9228	0.8824	0.8857
Top Power	74.17	74.55	87.47	89.36	88.63	88.32
Bottom Power	84.57	84.19	102.06	96.83	100.43	99.71
Top Heat Flux	674.27	677.73	795.18	812.36	805.64	802.91
Bottom Heat Flux	768.82	765.36	927.82	880.27	913.00	906.45
Top ΔT, S-C	4.8	8.6	18.6	15.7	10.3	1.7
Top ΔT, C-M	16.9	9.4	18.6	17.2	22.4	12.6
Top ΔT	39.33	386.6	331.2	351.8	334.3	339.7
Top Mean T	1597.4	1588.1	1913.2	1945.9	1918.6	1931.4
Top k	0.857	0.876	1.200	1.155	1.205	1.182
Bottom ΔT, S-C	22.8	22.7	0.2	6.7	23.4	15.7
Bottom ΔT, C-M	39.9	39.5	- 0 -	8.0	31.7	32.0
Bottom ΔT	400.2	396.6	382.3	409.3	387.8	396.3
Bottom Mean T	1588.5	1587.3	1887.6	1917.1	1891.9	1903.1
Bottom k	0.961	0.965	1.213	1.075	1.048	1.144

NOTE: The following units are used: Heat Flux, Btu/hr-ft^2; ΔT, ($^\circ$F); k, $\frac{\text{Btu-in}}{\text{hr-ft}^2{}^\circ\text{F}}$

Imbalance ΔT's are across the hot faces S-C (side to corner) and C-M (corner to main).

TABLE XXIV(CONTD)

THERMAL CONDUCTIVITY DATA AND CALCULATION SHEET

Dynaquartz in Vacuum
Top Sample - Dynaquartz Without Zirconia Pins
Bottom Sample - Dynaquartz With Zirconia Pins

Time	200565 1930	200565 2015	210565 1645	210565 1800	210565 2000	210565 2100
Voltage (volts)	3.0	3.0	4.70	4.68	4.68	4.68
Current (amps)	1.45	1.45	1.92	1.92	1.92	1.92
Power (watts)	4.35	4.35	9.02	8.98	8.98	8.98
Power (Btu/hr)	14.83	14.83	30.76	30.62	30.62	30.62
Power Ratio	0.972	0.976	0.933	0.935	0.942	0.933
Top Power	7.31	7.33	14.85	14.80	14.95	14.78
Bottom Power	7.52	7.50	15.91	15.82	15.77	15.84
Top Heat Flux	66.45	66.61	135.00	134.54	135.00	134.36
Bottom Heat Flux	68.36	68.18	144.64	143.82	143.30	144.0
Top ΔT, S-C	47.2	42.4	26.4	24.1	22.0	26.8
Top ΔT, C-M	45.8	40.4	18.5	15.6	13.8	17.0
Top ΔT	216.1	222.3	356.9	358.6	360.2	360.1
Top Mean T	467.5	470.7	809.0	808.9	809.9	810.2
Top k	0.154	0.150	0.189	0.187	0.187	0.186
Bottom ΔT, S-C	63.4	60.0	5.3	3.8	0.2	4.3
Bottom ΔT, C-M	57.7	54.3	4.6	3.4	1.1	4.1
Bottom ΔT	215.2	221.8	365.1	367.0	368.6	368.5
Bottom Mean T	468.1	471.4	804.5	804.5	805.3	805.7
Bottom k	0.159	0.154	0.198	0.196	0.194	0.195

NOTE: The following units are used: Heat Flux, Btu/hr-ft^2; ΔT, (^{o}F); k, $\frac{\text{Btu-in}}{\text{hr-ft}^2{}^o\text{F}}$

Imbalance ΔT's are across the hot faces S-C (side to corner) and C-M (corner to main).

TABLE XXIV(CONTD)

THERMAL CONDUCTIVITY DATA AND CALCULATION SHEET

Dynaquartz in Vacuum
Top Sample - Dynaquartz Without Zirconia Pins
Bottom Sample - Dynaquartz With Zirconia Pins

Time	* 210565 2130	220565 2130	* 230565 1445	230565 1630	* 240565 1230	* 240565 1345
Voltage (volts)	4.72	7.32	7.30	7.32	8.10	8.08
Current (amps)	1.92	2.20	2.30	2.32	2.45	2.44
Power (watts)	9.06	16.10	16.79	16.98	19.84	19.71
Power (Btu/hr)	30.89	54.90	57.25	57.90	67.65	67.20
Power Ratio	0.925	0.784	0.821	0.870	0.831	1.000
Top Power	14.84	24.13	26.81	26.44	30.70	33.60
Bottom Power	16.05	30.77	30.44	30.96	36.95	33.60
Top Heat Flux	134.91	219.36	243.72	244.91	274.09	305.45
Bottom Heat Flux	145.91	279.73	276.73	281.45	335.91	305.45
Top ΔT, S-C	21.6	8.8	0.8	0.2	12.3	10.7
Top ΔT, C-M	14.1	12.5	10.3	14.5	12.9	20.8
Top ΔT	360.1	260.3	335.9	324.8	333.6	333.8
Top Mean T	810.2	1681.4	1500.1	1482.2	1646.9	1660.0
Top k	0.187	0.421	0.363	0.377	0.418	0.457
Bottom ΔT, S-C	0.6	4.1	23.2	21.8	14.2	15.6
Bottom ΔT, C-M	0.8	11.6	31.0	30.2	2.5	0.9
Bottom ΔT	368.5	346.5	334.2	321.0	340.0	345.3
Bottom Mean T	805.7	1630.2	1499.6	1482.5	1630.3	1651.6
Bottom k	0.198	0.404	0.414	0.438	0.494	0.442

NOTE: The following units are used: Heat Flux, Btu/hr-ft^2; ΔT, ($^\circ$F); k, $\frac{\text{Btu-in}}{\text{hr-ft}^2{}^\circ\text{F}}$

Imbalance ΔT's are across the hot faces S-C (side to corner) and C-M (corner to main).

TABLE XXIV(CONTD)

THERMAL CONDUCTIVITY DATA AND CALCULATION SHEET

Dynaquartz in Vacuum
Top Sample - Dynaquartz Without Zirconia Pins
Bottom Sample - Dynaquartz With Zirconia Pins

Time	240565 1445	240565* 1545	240565* 2000	240565* 2100	250565* 1100	250565* 1145
Voltage (volts)	8.1	8.1	8.07	8.05	10.19	10.12
Current (amps)	2.41	2.41	2.40	2.40	2.72	2.70
Power (watts)	19.52	19.52	19.37	19.32	27.72	27.32
Power (Btu/hr)	66.56	66.56	66.05	66.22	94.52	93.16
Power Ratio	0.855	0.797	0.818	0.777	0.862	0.794
Top Power	30.68	29.52	29.71	28.96	43.76	41.23
Bottom Power	35.88	37.04	36.34	37.26	50.76	51.93
Top Heat Flux	278.91	268.36	270.09	263.27	397.82	374.82
Bottom Heat Flux	321.64	336.73	330.36	338.73	461.45	472.09
Top ΔT, S-C	1.2	29.4	13.2	15.0	34.3	39.0
Top ΔT, C-M	17.8	14.4	6.8	9.2	35.2	41.9
Top ΔT	337.0	342.3	331.4	333.5	345.8	334.1
Top Mean T	1674.5	1688.4	1706.5	1709.8	2063.0	2055.0
Top k	0.414	0.392	0.407	0.395	0.575	0.561
Bottom ΔT, S-C	25.1	4.1	42.9	28.0	3.8	13.7
Bottom ΔT, C-M	4.9	6.3	28.7	30.1	9.4	8.7
Bottom ΔT	349.5	342.1	346.3	349.9	396.7	405.6
Bottom Mean T	1655.2	1672.0	1694.6	1695.4	2021.0	2009.8
Bottom k	0.460	0.492	0.471	0.484	0.582	0.582

NOTE: The following units are used: Heat Flux, Btu/hr-ft^2; ΔT, ($^\circ$F); k, $\frac{\text{Btu-in}}{\text{hr-ft}^2{}^\circ\text{F}}$

Imbalance ΔT's are across the hot faces S-C (side to corner) and C-M (corner to main).

TABLE XXIV(CONTD)

THERMAL CONDUCTIVITY DATA AND CALCULATION SHEET

Dynaquartz in Vacuum
Top Sample - Dynaquartz Without Zirconia Pins
Bottom Sample - Dynaquartz With Zirconia Pins

Time	250565* 1500	250565* 1625	250565 1845	250565* 2040	270565 0900	270565 1045
Voltage (volts)	10.05	10.05	10.05	10.05	8.74	8.79
Current (amps)	2.70	2.72	2.70	2.70	2.36	2.41
Power (watts)	27.14	27.14	27.14	27.14	20.63	21.18
Power (Btu/hr)	92.55	92.55	92.55	92.55	70.35	72.22
Power Ratio	0.782	0.808	0.794	0.818	0.850	0.811
Top Power	40.61	41.36	40.96	41.64	32.32	32.34
Bottom Power	51.94	51.19	51.59	50.91	38.03	39.88
Top Heat Flux	369.2	376.0	372.4	378.5	293.82	294.0
Bottom Heat Flux	472.2	465.4	469.0	462.8	345.73	362.5
Top ΔT, S-C	52.0	9	2.8	0.9	22.1	16.8
Top ΔT, C-M	43.9	.8	11.5	7.2	9.1	7.0
Top ΔT	318.0	322.3	329.2	340.9	357.2	356.5
Top Mean T	2071.8	2017.0	2021.0	2027.0	1981.0	1931.7
Top k	0.581	0.583	0.566	0.555	0.411	0.412
Bottom ΔT, S-C	75.8	46.2	27.1	19.8	44.5	38.6
Bottom ΔT, C-M	79.7	39.1	18.5	10.2	16.1	30.4
Bottom ΔT	375.7	369.7	366.3	365.8	375.1	351.4
Bottom Mean T	1979.8	1979.8	1993.6	2004.4	1974.8	1921.7
Bottom k	0.628	0.629	0.640	0.633	0.461	0.516

NOTE: The following units are used: Heat Flux, Btu/hr-ft^2; ΔT, ($^\circ$F); k, $\frac{\text{Btu-in}}{\text{hr-ft}^2{}^\circ\text{F}}$

Imbalance ΔT's are across the hot faces S-C (side to corner) and C-M (corner to main).

TABLE XXIV(CONTD)

THERMAL CONDUCTIVITY DATA AND CALCULATION SHEET

Dynaquartz in Vacuum
Top Sample - Dynaquartz Without Zirconia Pins
Bottom Sample - Dynaquartz With Zirconia Pins

Time	* 270565 1300	270565 1600	270565 1700	270565 2000	* 270565 2100	270565 2145
Voltage (volts)	8.72	8.80	8.80	8.80	8.80	8.80
Current (amps)	2.45	2.48	2.48	2.48	2.48	2.48
Power (watts)	21.36	21.82	21.82	21.82	21.82	21.82
Power (Btu/hr)	72.84	74.41	74.41	74.41	74.41	74.41
Power Ratio	0.781	0.8097	0.826	0.8594	0.8381	8.308
Top Power	31.94	33.29	33.66	34.39	33.93	33.77
Bottom Power	40.90	41.12	40.75	40.02	40.48	40.64
Top Heat Flux	290.36	302.64	306.00	312.62	308.45	307.00
Bottom Heat Flux	371.82	373.82	370.45	363.82	368.00	369.45
Top ΔT, S-C	9.3	9.0	17.7	23.5	20.7	12.6
Top ΔT, C-M	4.8	9.5	2.3	5.3	2.3	14.6
Top ΔT	333.6	335.5	340.4	344.5	343.5	333.4
Top Mean T	1913.8	1992.5	1894.8	1896.5	1894.5	1889.2
Top k	0.435	0.451	0.449	0.454	0.449	0.460
Bottom ΔT, S-C	29.0	29.3	39.5	43.3	33.1	32.0
Bottom ΔT, C-M	34.6	11.4	20.6	28.6	18.0	13.5
Bottom ΔT	346.4	352.7	352.2	341.2	332.2	339.3
Bottom Mean T	1895.2	1872.3	1876.1	1886.6	1888.9	1880.7

NOTE: The following units are used: Heat Flux, Btu/hr-ft^2; ΔT, ($^\circ$F); k, $\frac{\text{Btu-in}}{\text{hr-ft}^2{}^\circ\text{F}}$

Imbalance ΔT's are across the hot faces S-C (side to corner) and C-M (corner to main).

TABLE XXIV(CONCLD)

THERMAL CONDUCTIVITY DATA AND CALCULATION SHEET

Dynaquartz in Vacuum
Top Sample - Dynaquartz Without Zirconia Pins
Bottom Sample - Dynaquartz With Zirconia Pins

Time	* 280565 1115	* 280565 1230	* 280565 1330	* 280565 1430	* 280565 1530	* 280565 1630
Voltage (volts)	6.16	6.15	6.15	6.19	6.18	6.19
Current (amps)	2.12	2.11	2.12	2.12	2.11	2.12
Power (watts)	13.06	12.97	13.04	13.12	13.04	13.14
Power (Btu/hr)	44.53	44.25	44.47	44.74	44.46	44.82
Power Ratio	0.9289	0.9535	0.9333	0.8648	0.933	0.9438
Top Power	21.45	21.60	21.47	20.75	21.46	21.76
Bottom Power	23.08	22.65	23.00	23.99	23.00	23.06
Top Heat Flux	195.00	196.36	195.18	188.64	195.09	197.82
Bottom Heat Flux	209.82	205.91	209.09	218.09	209.09	209.62
Top ΔT, S-C	10.6	4.8	8.2	9.2	14.5	15.5
Top ΔT, C-M	11.8	3.5	8.4	7.3	16.4	11.9
Top ΔT	316.7	336.8	340.5	345.4	350.5	351.6
Top Mean T	1295.1	1293.4	1287.3	1285.8	1282.8	1281.1
Top k	0.308	0.292	0.287	0.273	0.278	0.281
Bottom ΔT, S-C	21.6	5.4	1.4	1.0	2.5	4.8
Bottom ΔT, C-M	25.9	9.8	8.4	8.5	1.9	3.5
Bottom ΔT	297.9	307.9	308.0	314.1	321.1	318.8
Bottom Mean T	1295.4	1308.4	1294.0	1292.0	1287.5	1287.4
Bottom k	0.352	0.334	0.339	0.347	0.326	0.328

NOTE: The following units are used: Heat Flux, Btu/hr-ft^2; ΔT, ($^\circ$F); k, $\frac{\text{Btu-in}}{\text{hr-ft}^2{}^\circ\text{F}}$

Imbalance ΔT's are across the hot faces S-C (side to corner) and C-M (corner to main).

APPENDIX VI

CORRECTION FOR ZIRCONIA PINS IN THERMAL CONDUCTIVITY MEASUREMENTS

The raw data for the guarded hot plate measurements was corrected for the conduction through the zirconia pins which was usually in the bottom sample. There was one exception where two different materials were used in one run (sapphire wool and Dynaquartz) and in that case the Dynaquartz was the top sample with zirconia pins in the metered area. The magnitude of the corrections is shown in Table XXV. The subject is discussed in Section III.5 and graphically shown in Figures 19, 20, and 21.

Correction for Zirconia pins in Bottom Specimen for Run 020465-0845 Dynaquartz in Air (Run 1):

Assume:

$$(q_{bot})_{total} = q_D + q_{pins}$$

$$q_{pins} = k_{pins} A_{pins} \frac{\Delta T}{\Delta x}$$

and

$$(q_{bot})_{total} = k_{total} A_T \frac{\Delta T}{\Delta x}$$

Since ΔT and Δx are for the same experimental conditions

$$q_{pins} = \left[\left(\frac{k_{pins}}{k_{total}}\right)\left(\frac{A_{pins}}{A_{total}}\right)\right] (q_{bot})_{total}$$

and

$$q_D = (q_{bot})_{total} - \left[\left(\frac{k_{pins}}{k_{total}}\right)\left(\frac{A_{pins}}{A_{total}}\right)\right](q_{bot})_{total}$$

finally

$$k_D = (q_{bot})_{total} \left[1-\left(\frac{k_{pins}}{k_{total}}\right)\left(\frac{A_{pins}}{A_{total}}\right)\right] \frac{\Delta x}{\Delta T} \left(\frac{1}{A_D}\right)$$

Calculating using the data:

$(q_{bot})_{total}$ = 178.6 BTU/hr

k_{pins} = 6.5 $\frac{\text{BTU-in.}}{\text{hr-ft}^2\text{-°F}}$ (References 42 and 43)

k_{total} = 1.777 $\frac{\text{BTU-in.}}{\text{hr-ft}^2\text{-°F}}$ Calculated previously (see Appendix V)

A_{pins} = (1/4) (1/4) 5 = 5/16 = 0.3125 in^2

$$A_{total} = (4)\ (4) = 16\ in^2$$

$$\left(\frac{k_{pins}}{k_{total}}\right)\left(\frac{A_{pins}}{A_{total}}\right) = \left(\frac{6.5}{1.777}\right)\left(\frac{0\ 3125}{16}\right) = 0.07144$$

$$1 - 0.07144 = 0.92856$$

$$(q_{bot})_{total}\ (0.92856) = (178.6)\ (0.92856) = 165.84\ \frac{BTU}{hr}$$

$$k_D = (165.84)\ \left(\frac{\Delta x}{\Delta T}\right)\ \left(\frac{1}{A_D}\right)$$

$$\left(\frac{1}{A_D}\right) = \left(\frac{144}{15.6875}\right) - 9.179\ ft^{-2}$$

$$k_D = (165.84)\ \left(\frac{0.5}{456.9}\right)\ (9.179)$$

$$k_D = (0.18148)\ (9.179) = 1.666\ \frac{BTU\text{-}in.}{hr\text{-}ft^2\text{-}°F}$$

TABLE XXV

CORRECTION FOR ZIRCONIA PINS IN
GUARDED HOT PLATE MEASUREMENTS

Dynaquartz in Air (Run 1)
Top Sample - Dynaquartz Without Zirconia Pins
Bottom Sample - Dynaquartz With Zirconia Pins

Bottom Power (Btu/HR)	Thermal Conductivity Pins	Total Thermal Conductivity Sample	Corrected Power (Btu/HR)	Corrected Heat Flux Btu/HR ft^2	ΔT Bottom (^oF)	Corrected Conductivity $\frac{Btu\ in}{HR\ ft^2\ ^oF}$	Mean Temperature (^oF)
37.7	4.88	0.687	32.47	149.02	249.4	0.597	400.7
94.8	4.98	1.270	87.54	401.76	333.3	1.184	1218.0
86.6	4.98	1.169	79.39	364.36	336.8	1.082	1226.4
87.4	4.98	1.192	80.27	368.40	333.2	1.106	1227.5
83.2	4.98	1.153	76.19	349.68	327.9	1.066	1255.7
89.3	4.98	1.225	82.21	377.30	331.4	1.138	1238.8
83.5	4.98	1.138	76.36	350.45	333.6	1.050	1244.9
160.7	5.14	1.645	150.90	692.55	444.0	1.560	1629.5
161.8	5.14	1.593	151.60	695.75	461.7	1.507	1642.3
162.4	5.14	1.589	152.14	698.25	464.5	1.503	1647.8
161.7	5.14	1.587	151.46	695.13	463.2	1.501	1650.5
161.0	5.14	1.584	150.79	692.05	462.0	1.498	1652.3
176.7	5.28	1.605	165.34	758.83	500.3	1.517	1853.2
178.3	5.28	1.634	167.05	766.68	496.0	1.546	1847.4
178.6	5.32	1.777	168.15	771.72	456.9	1.689	1931.3
178.1	5.32	1.753	167.54	768.92	461.8	1.665	1937.8
179.1	5.32	1.754	168.50	773.33	464.1	1.666	1938.4
192.4	5.52	2.038	187.22	836.30	429.1	1.949	2113.2
191.2	5.52	2.032	181.07	831.02	427.8	1.942	2124.6
187.2	5.52	2.005	177.13	812.94	424.4	1.915	2128.7
199.0	5.52	2.124	188.90	866.95	425.9	2.035	2127.0
198.6	5.52	2.145	188.61	865.63	427.3	2.026	2123.7
200.2	5.72	2.119	190.01	872.05	429.3	2.031	2122.1
214.9	5.72	2.372	204.78	939.84	411.8	2.282	2415.8
210.4	5.85	2.511	201.04	922.67	410.0	2.250	2310.6
208.8	5.85	2.204	197.78	908.63	430.6	2.110	2422.6
209.3	5.85	2.261	198.73	913.86	428.0	2.135	2419.0
209.2	5.85	2.235	198.51	911.06	425.4	2.142	2414.8
206.7	5.85	2.246	196.18	900.37	418.4	2.152	2418.3

TABLE XXV(CONTD)

CALCULATION CORRECTION FOR ZIRCONIA PINS

Dynaquartz in Air (Run 2)
Top Sample - Dynaquartz Without Zirconia Pins
Bottom Sample - Dynaquartz With Zirconia Pins

Bottom Power (Btu/HR)	Thermal Conductivity Pins	Total Thermal Conductivity Sample	Corrected Power (Btu/HR)	Corrected Heat Flux Btu/HR ft^2	ΔT Bottom °F	Corrected Conductivity Btu in / HR ft^2 °F	Mean Temperature (°F)
71.42	4.70	0.760	62.79	288.17	426.9	0.675	953.5
71.65	4.70	0.768	63.09	289.55	424.1	0.683	965.1
71.34	4.70	0.760	62.72	287.85	426.5	0.675	966.7
91.79	5.10	0.911	81.76	375.24	457.8	0.820	1256.9
90.59	5.10	0.895	80.51	369.50	460.3	0.803	1260.1
91.47	5.10	0.905	81.40	373.59	459.6	0.813	1265.1
91.96	5.10	0.928	82.09	376.75	450.3	0.837	1254.7
123.05	5.60	1.266	112.42	515.95	441.8	1.168	1737.0
121.87	5.60	1.246	111.17	510.21	444.5	1.148	1755.3
122.39	5.60	1.255	111.73	512.78	433.0	1.157	1768.6
146.16	6.00	1.471	134.51	617.33	451.5	1.367	1999.2
147.10	6.10	1.525	135.61	622.38	438.3	1.420	2114.7
148.98	6.10	1.501	137.15	629.45	451.2	1.395	2097.2
147.98	6.10	1.500	136.23	625.23	448.5	1.394	2090.0
190.33	6.40	1.657	175.98	807.66	522.5	1.547	2293.4
189.14	6.40	1.660	174.90	802.70	518.0	1.550	2313.6

TABLE XXV(CONTD)

CALCULATION CORRECTION FOR ZIRCONIA PINS

Dynaquartz in Air
Top Sample - Dynaquartz With Zirconia Pins
Bottom Sample - Sapphire Wool With Zirconia Pins

Top Power (Btu/HR)	Thermal Conductivity Pins	Total Thermal Conductivity Sample	Corrected Power (Btu/HR)	Corrected Heat Flu Btu/HR ft^2	ΔT Top (^oF)	Corrected Conductivity $\frac{Btu\text{-}in}{HR\ FT^2\ ^oF}$	Mean Temperature (^oF)
101.0	5.20	1.177	92.28	423.52	390.0	1.085	1783.0
107.1	5.28	1.287**	98.52	452.16	378.3	1.195	1878.8
107.1	5.28	1.253**	98.28	451.06	388.7	1.160	1879.6
107.8	5.28	1.302**	99.26	455.55	376.4	1.210	1884.2
110.5	5.28	1.347**	102.05	468.36	373.0	1.255	1887.1
107.8	5.28	1.342**	99.52	456.75	365.2	1.250	1883.0
110.5	5.28	1.389**	102.30	469.51	361.7	1.298	1887.1
101.0	5.20	1.218	92.58	424.90	376.8	1.127	1783.9
107.8	5.29	1.314**	99.33	455.87	373.0	1.222	1905.0
107.8	5.29	1.244**	98.85	453.67	393.9	1.151	1911.6
149.4	5.72	1.819**	140.23	643.58	373.3	1.724	2388.0
149.4	5.72	1.774	140.00	642.53	382.9	1.678	2391.1
136.4	5.73	1.718**	127.52	585.25	360.8	1.622	2407.9
136.4	5.73	1.743**	127.69	586.03	353.6	1.657	2406.5
132.6	5.74	1.720**	123.95	568.87	350.3	1.623	2421.8
132.6	5.74	1.662**	123.66	567.54	362.7	1.564	2421.3
135.7	5.74	1.736**	126.93	582.55	355.3	1.639	2426 3
135.7	5.74	1.693**	126.72	581.58	364.3	1.596	2426.5

** Corrected data are tabulated in Table 11 of text.

TABLE XXV (CONTD)

CALCULATION CORRECTION FOR ZIRCONIA PINS

Dynaquartz in Argon (1 atm)
Top Sample - Dynaquartz Without Zirconia Pins
Bottom Sample - Dynaquartz With Zirconia Pins

Bottom Power (Btu/HR)	Thermal Conductivity Pins	Total Thermal Conductivity Sample	Corrected Power (Btu/HR)	Corrected Heat Flux (Btu/HR ft^2)	ΔT Bottom °F	Corrected Conductivity $\frac{Btu\,in}{HR\,ft^2\,°F}$	Mean Temperature °F
11.73	4.50	0.364	8.897	40.833	146.6	0.2785	272.3
11.73	4.50	0.357	8.842	40.580	149.3	0.2718	274.1
12.21	4.50	0.364	9.261	42.503	152.5	0.2787	277.8
11.99	4.50	0.421	9.488	43.545	129.4	0.3365	271.3
11.73	4.50	0.391	9.093	41.732	136.5	0.3057	267.7
11.70	4.50	0.350	8.762	40.213	152.0	0.2645	277 3
18.60	4.50	0.477	15.184	69.641	177.3	0.393	349.6
18.49	4.50	0.461	14.96	68.686	182.2	0.377	346.1
18.10	4.50	0.453	14.59	66.952	181.6	0.368	339.4
17.18	4.50	0.462	13.92	63.849	169.1	0.377	320.0
50.96	4.50	0.608	43.59	200.08	381.1	0.525	754.0
49.22	4.50	0.602	42.03	192.92	371.5	0.519	760.7
50.38	4.50	0.616	43.19	198.22	371.9	0.533	759.9
50.34	4.50	0.618	43.18	198.18	370.3	0.535	759.6
66.16	5.10	0.693	56.65	260.00	434.1	0.599	1246.3
64.05	5.10	0.674	54.58	250.51	432.2	0.579	1256.7
65.29	5.10	0.714	56.18	257.84	415.6	0.620	1259.1
64.82	5.10	0.713	55.76	255.93	413.2	0.619	1254.1
63.37	5.15	0.706	54.33	249.39	407.7	0.612	1265.8
63.04	5.15	0.705	53.96	247.63	406.3	0.609	1265.7

TABLE XXV (CONTD)

CALCULATION CORRECTION FOR ZIRCONIA PINS

Dynaquartz in Argon (1 atm)
(Continued)
Top Sample - Dynaquartz Without Zirconia Pins
Bottom Sample - Dynaquartz With Zirconia Pins

Bottom Power (Btu/HR)	Thermal Conductivity Pins	Total Thermal Conductivity Sample	Corrected Power (Btu/HR)	Corrected Heat Flux (Btu/HR ft^2)	ΔT Bottom °F	Corrected Conductivity $\frac{Btu\text{-}in}{HR\ ft^2\ °F}$	Mean Temperature °F
63.40	5.15	0.708	54.39	249.63	407.1	0.613	1263.5
87.85	5.50	0.957	77.99	357.45	417.4	0.858	1594.2
85.39	5.50	0.946	75.69	347.42	410.1	0.847	1591.0
85.12	5.50	0.955	75.54	346.71	405.1	0.856	1589.5
84.57	5.50	0.961	75.11	344.74	400.2	0.861	1588.6
84.19	5.50	0.965	74.82	343.38	396.6	0.866	1587.3
101.58	5.95	1.369	92.95	426.62	377.3	1.131	1976.6
101.71	5.95	1.186	91.74	421.05	389.7	1.080	1961.8
102.06	5.90	1.213	92.36	423.90	382.3	1.108	1887.6
96.83	5.90	1.075	86.45	396.76	409.3	0.969	1917.1
100.43	5.90	1.048	89.39	410.27	387.8	1.058	1891.9
99.73	5.95	1.144	89.58	411.12	396.3	1.037	1903.1

TABLE XXV (CONTD)

CALCULATION CORRECTION FOR ZIRCONIA PINS

Dyraquartz in Vacuum
Top Sample - Dynaquartz Without Zirconia Pins
Bottom Sample - Dynaquartz With Zirconia Pins

Bottom Power (Btu/HR)	Thermal Conductivity Pins	Total Thermal Conductivity Sample	Corrected Power (Btu/HR)	Corrected Heat Flux (Btu/HR ft^2)	ΔT Bottom (°F)	Corrected Conductivity $\frac{Btu\text{-}in}{HR\ ft^2\ °F}$	Mean Temperature (°F)
7.52	4.88	0.154	3.013	13.828	215.2	0.0642	468.1
7.50	4.88	0.154	2.858	13.117	221.8	0.0591	471.4
15.91	4.90	0.198	8.221	37.730	365.1	0.1033	804.5
15.82	4.90	0.196	8.095	37.152	367.0	0.1012	804.5
15.77	4.90	0.194	7.991	36.675	368.6	0.0995	805.3
15.84	4.90	0.195	8.066	37.019	368.5	0.1004	805.7
16.05	4.90	0.198	8.293	38.06	368.5	0.103	805.7
23.08	5.00	0.352	16.678	76.54	297.9	0.257	1295.4
22.65	5.00	0.334	16.027	73.55	307.9	0.239	1308.4
23.00	5.00	0.339	16.374	75.15	308.0	0.244	1294.0
23.99	5.00	0.347	17.239	79.12	314.1	0.252	1292.0
23.00	5.00	0.326	16.111	73.94	321.1	0.230	1287.5
23.06	5.00	0.328	16.195	74.33	319.8	0.232	1287.4
30.44	5.08	0.414	23.147	106.23	334.2	0.318	1499.6
30.96	5.08	0.438	23.947	109.91	321.0	0.342	1482.5
32.24	5.08	0.453	25.179	115.56	323.7	0.357	1477.1
33.27	5.08	0.466	26.187	120.18	324.4	0.370	1469.7
32.73	5.08	0.469	25.808	118.45	317.0	0.374	1454.5
36.95	5.16	0.494	29.412	134.99	340.0	0.397	1630.3
37.16	5.16	0.489	29.501	135.39	345.3	0.392	1651.6
37.88	5.16	0.460	28.019	128.60	349.5	0.368	1655.2
37.04	5.16	0.492	29.454	135.18	342.1	0.395	1672.0

TABLE XXV(CONCLD)

CALCULATION CORRECTION FOR ZIRCONIA PINS

Dynaquartz in Vacuum
(Continued)
Top Sample - Dynaquartz Without Zirconia Pins
Bottom Sample - Dynaquartz With Zirconia Pins

Bottom Power (Btu/HR)	Thermal Conductivity Pins	Total Thermal Conductivity Sample	Corrected Power (Btu/HR)	Corrected Heat Flux (Btu/HR ft^2)	ΔT Bottom (^oF)	Corrected Conductivity $\frac{Btu\text{-}in}{HR\ ft^2\ ^oF}$	Mean Temperature (^oF)
36.34	5.16	0.477	28.661	131.54	346.3	0.380	1694.6
37.26	5.16	0.484	29.502	135.39	349.9	0.387	1695.4
40.90	5.40	0.537	32.867	150.84	346.4	0.435	1895.2
41.25	5.40	0.533	33.087	151.85	351.9	0.432	1879.4
41.12	5.40	0.530	32.937	151.16	352.7	0.428	1872.3
40.75	5.40	0.526	32.580	149.53	352.2	0.424	1876.1
40.02	5.40	0.533	32.100	147.32	341.7	0.432	1886.6
40.48	5.40	0.554	32.773	150.41	332.2	0.453	1888.9
40.64	5.40	0.544	32.760	150.35	339.3	0.443	1880.7
50.76	5.44	0.582	41.491	190.42	396.7	0.480	2021.0
51.93	5.44	0.582	42.447	194.81	405.6	0.480	2009.8
51.94	5.44	0.628	43.152	198.05	375.7	0.527	1979.8
51.19	5.44	0.629	42.544	195.25	369.7	0.528	1979.8
51.59	5.44	0.640	43.026	197.47	366.3	0.539	1993.6
50.91	5.44	0.633	42.367	194.44	365.8	0.531	2004.4

REFERENCES

1. Wechsler, A. E., and Glaser, P. E., Investigation of the Thermal Properties of High Temperature Insulation Materials, ASD-TDR-63-574, Aeronautical Systems Division, Wright-Patterson Air Force Base, Ohio (July 1963).

2. Minges, M. L., "Thermal Transport Properties of Materials," Air Force Materials Laboratory Symposium, AFML-TR-65-29, Air Force Materials Laboratory, Wright-Patterson Air Force Base, Ohio (June 1965). See also Minges, M. L., Thermal Insulations for Aerospace Applications -423° to +3000°F, ASD-TDR-63-699, Aeronautical Systems Division, Wright-Patterson Air Force Base, Ohio (September 1963).

3. Collins, J. A., and Moodie, D. M., "Thermal Insulation for Lifting Re-Entry Vehicles," Paper Presented at the Lifting Re-Entry Vehicles Conference, Palm Springs, California, (4-7 April 1961).

4. Hurley, J., and Traiger, H., in Lightweight Thermal Protection System Development, AFML-TR-65-26, Vol II, Air Force Materials Laboratory, Wright-Patterson Air Force Base, Ohio (June 1965) (see Reference 5).

5. Ryan, J. M., et al, Lightweight Thermal Protection System Development, AFML-TR-65-26, Volume II, Air Force Materials Laboratory, Wright-Patterson Air Force Base, Ohio (June 1965).

6. Ryan, J. M., Cross, R. F., Paulsen, J. J., and Black, W. E., Research on the Optimization of Thermal Composites, AFML-TR-65-244, Air Force Materials Laboratory, Wright-Patterson Air Force Base, Ohio (June 1965).

7. Cross, R. I., and Black, W. E., Optimization of Insulation and Mechanical Supports for Hypersonic and Entry Vehicles, AFML-TR-66-414, Air Force Materials Laboratory, Wright-Patterson Air Force Base, Ohio (April 1967).

8. Shields, S., Investigation of Insulative Heat Shield Attachment Systems, AFFDL-TR-65-55, Air Force Flight Dynamics Laboratory, Wright-Patterson Air Force Base, Ohio (April 1965).

9. Johns-Manville Company, Bulletin No. IN-475A, New York, New York (June 1963).

10. Speil, S., and Collins, J., Personal Communication (September 1966).

11. Campbell, M. D., Hertz, J., O'Barr, G. L., and Haskins, J. F., Thermophysical Properties of Plastic Materials and Composites to Liquid Hydrogen Temperature (-423°F), ML-TDR-64-33, Part II, Materials Laboratory, Wright-Patterson Air Force Base, Ohio (March 1965).

12. Purcell, G. V., Personal Communication (June 1966).

13. Rolinski, E. J., and Purcell, G. V., "Thermal Conductivity Measurements of Fibrous Insulations up to 2500°F," Paper No. 128, Third International Heat Transfer Conference, Volume IV, Chicago (August 1966).

14. Strong, H. M., Bundy, F. P., and Bovenkerk, H. P., "Flat Panel Vacuum Thermal Insulation," Jour. Appl. Physics, 31, No. 1, (January 1960), pp 39-50.

REFERENCES (CONT)

15. Glaser, P. E., et al, Investigation of Materials for Vacuum Insulation up to 4000°F, ASD-TDR-62-88, Aeronautical Systems Division, Wright-Patterson Air Force Base, Ohio (January 1962).

16. Schotte, W., "Thermal Conductivity of Packed Beds," AIChE Journal, 6 (1960) p 63.

17. Svehla, R. A., Estimated Viscosities and Thermal Conductivities of Gases at High Temperatures, NASA TR R-132, Cleveland, Ohio (1962).

18. Verschoor, J. D., and Greebler, P., "Heat Transfer by Gas Conduction and Radiation in Fibrous Insulations," Trans. ASME, 74 (1952), pp 961-968.

19. Scott, R. B., Cryogenic Engineering, D. Van Nostrand Company, Inc., Princeton, New Jersey (October 1959), pp 142-215.

20. Wang, D., I-J., "Multiple Layer Insulation," Aerodynamically Heated Structures, Edited by P. E. Glaser, Prentice Hall, Inc., Englewood Cliffs, New Jersey (1962).

21. Chen, J. C., and Churchill, S. W. "Radiant Heat Transfer in Packed Beds," AIChE Journal, 9, No. 1, (1963), pp 35-41.

22. Chen, J. C., Ph.D. Thesis, University of Michigan, Ann Arbor, Michigan (1961).

23. Russell, H. W., "Principles of Heat Flow in Porous Insulators," Journal of Amer. Ceramic Soc., 18 (1935), p 1.

24. Bosworth, R. L. C., Heat Transfer Phenomena, John Wiley and Sons, Inc., New York (1952).

25. Argo, W. B., and Smith, J. M., "Heat Transfer in Packed Beds," "Prediction of Radial Rates in Gas-Solid Beds," Chem. Eng. Progress, 49 (1953), pp 443-451.

26. Kunii, D., and Smith, J. M., "Heat Transfer Characteristics of Porous Rocks," AIChE Journal, 6 (1960), pp 71-78.

27. Laubitz, M. J., "Thermal Conductivity of Powders," Canadian Journ. Phys., 37, No. 7 (July 1959), pp 798-808.

28. Schuster, A., "The Influence of Radiation on the Transmission of Heat," Philosophical Magazine Series, G. 5 (1903), pp 243-257.

29. Hamaker, H. C., "Radiation and Heat Conduction in Light Scattering Material," I. "Reflection and Transmission" R-36, Philips Res. Rep., 2, R-36 (1947), pp 55-67.

30. Hamaker, H. C., "Radiation and Heat Conduction in Light Scattering Material," II. "General Equations Including Heat Conduction," R-38, Philips Res., Rep 2 (1947), pp 103-111.

31. Hamaker, H. C., "Radiation and Heat Conduction in Light Scattering Material," III. "Application of the Theory," R-39, Philips Res., Rep. 2 (1947), pp 112-125.

REFERENCES (CONT)

32. Hamaker, H. C., "Radiation and Heat Conduction in Light Scattering Material," IV. "Various Extensions and a Generalized Theory," R-61, Philips Res., Rep. 2 (1947), pp 420-425.

33. Chu, C. M., and Churchill, S. W., "Numerical Solution of Problems in Multiple Scattering of Electromagnetic Radiation," J. Phys. Chem 59, (1955), pp 855-863.

34. Larkin, B. K., Ph.D. Thesis, "A Study of the Rate of Thermal Radiation Through Porous Insulating Materials," University of Michigan, Ann Arbor, Michigan (June 1957).

35. Larkin, B. K., and Churchill, S. W., "Heat Transfer by Radiation Through Porous Insulations," AIChE Journal, 5, No. 4 (December 1959), pp 467-474.

36. Viskanta, R., "Heat Transfer by Conduction and Radiation in Absorbing and Scattering Materials," Journal of Heat Transfer Paper 64-HT-33, Trans. of ASME (September 1964).

37. Stevenson, G. T., "Black Body Radiation Functions," NOTS TP 2623 NAWEPS 7621, U.S. Naval Ordnance Test Station, China Lake, California (May 1963) AD 407 307.

38. Wechsler, A. E., and Kritz, M., Investigation and Development of High Temperature Insulation Systems, AFML-TR-65-138, Air Force Materials Laboratory, Wright-Patterson Air Force Base, Ohio (April 1965).

39. Wolfe, W. L., and Ballard, S. S., "Optical Materials, Films and Filters for Infrared Instrumentation," Proc. Inst. Radio Engrs., 47 (September 1959), pp 1540-1546.

40. Sparrell, J. K., et al, An Instrument for Measuring the Thermal Conductance of High Temperature Structural Materials, ASD-TDR-63-359, Aeronautical Systems Division, Wright-Patterson Air Force Base, Ohio (May 1963).

41. American Society for Testing Materials, Designation C-177-63 "Standard Method of Test for Thermal Conductivity of Materials by Means of the Guarded Hot Plate," ASTM Standards on Thermal Insulating Materials Sponsored by ASTM Committee C-16, Third Edition (1963).

42. Whittemore, O. J., "Properties and Uses of Pure Oxide Heavy Refractories," Journal of American Ceramic Society, 32 (1949), pp 48-53.

43. Jones, N. C., "A Note on Fused Stabilized Zirconia, A Modern High Temperature Refractory," Journal Inst. Fuel, 25 (1952), pp 66-67

44. Ryshkewitch, E., Journal of the American Ceramic Society, 36, 65 (February 1953).

45. Plunkett, J. D., in Lightweight Thermal Protection System Development, ASD-TDR-63-596, Volume II - Materials - Existing Data and Recommended Data Acquisition, Aeronautical Systems Division, Wright-Patterson Air Force Base, Ohio (June 1963).

46. Rolinski, E. J., and Purcell, Lt. G. V., "Elevated Temperature Thermal Conductivity Measurements of Fibrous Insulations," Paper V-B, Presented at the Fifth Thermal Conductivity Conference, Denver, Colorado (October 1965).

REFERENCES (CONT)

47. Corning Glass Works, Materials Handbook, 6th Edition, Section 3, "Corning 7940 Fused Silica," Corning, New York (April 1963).

48. Bird, R. B., Stewart, W. E., and Lightfoot, E. N., Transport Phenomena, John Wiley and Sons, Inc., New York (January 1962), pp 426-444.

49. Shortley, G., and Williams, D., Elements of Physics, Prentice Hall, Inc., Englewood Cliffs, New Jersey (1955), pp 437-445.

50. Woodside, W., "Deviations from One Dimensional Heat Flow in Guarded Hot Plate Measurements," Rev. Scientific Instruments, 28, No. 12 (December 1957), pp 1033-1037.

51. Woodside, W., and Wilson, A. G., "Unbalance Errors in Guarded Hot Plate Measurements," Presented at ASTM Symposium on Thermal Conductivity Measurements, Philadelphia, Pa., ASTM Special Publication 217 (February 1957).

BIBLIOGRAPHY

Adams, J. J., and Sterry, P. J., Zirconia Fibrous Insulations, ASD-TDR-63-725, Aeronautical Systems Division, Wright-Patterson Air Force Base, Ohio (December 1963).

Adams, J. J., and Sterry, P. J., High Temperature Fibrous Insulations, ML-TDR-64-156, Materials Laboratory, Wright-Patterson Air Force Base, Ohio (October 1964).

Baschiere, R. J., Lis, S. J., and Engholm, G. "Thermal Transport and Radiative Properties of Fibrous Structural Materials," Paper Presented at the Sixth National Heat Transfer Conference AIChE/ASME, Boston, Massachusetts (11-14 August 1963).

Churchill, S. W., Evans, L. B., Tien, LiChiu, and Pang, Sing-Chin, "Exact Solutions for Anisotropic, Multiple Scattering by Parallel Plane Dispersions, DASA-1257, University of Michigan, AD 272 325, (September 1961).

Clark, G. C., Chu, C. M., and Churchill, S. W., "Angular Distribution Coefficients for Radiation Scattered by a Spherical Particle," Journal Opt. Soc. Am., 47, (1957), pp 81-84.

Deissler, R. G., and Eian, C. S., "Investigation of Effective Thermal Conductivities of Powders," NACA RM E52C05, Washington, D.C. (June 1952).

Farmer, R. W., Air Aging of Inorganic Fibrous Insulations, ML-TDR-64-137, Materials Laboratory, Wright-Patterson Air Force Base, Ohio (June 1964).

Folweiler, R. C., et al, Thermal Radiation Characteristics of Transparent, Semi-Transparent, and Translucent Materials Under Non-Isothermal Conditions," ASD-TDR-62-719, Part I (April 1964), and Part II (June 1964), Aeronautical Systems Division, Wright-Patterson Air Force Base, Ohio.

Glaser, P. E., Editor, Aerodynamically Heated Structures, Prentice Hall, Inc., Englewood Cliffs, New Jersey (1962).

Gorring, R. L., and Churchill, S. W., "The Thermal Conductivity of Heterogeneous Materials," Chem. Eng. Prog., 57, No. 7 (July 1961), p 53.

Greebler, P., "Thermal Properties and Applications of High Temperature Aircraft Insulations," Jet Propulsion, 24, (1954), pp 374-378.

Hill, F. B., and Wilhelm, R. H., "Radiative and Conductive Heat Transfer in a Quiescent Gas-Solid Bed of Particles: Theory and Experiment," AIChE Journal, 5, No. 4 (December 1959), pp 486-496.

Johnson, V. J., Editor, A Compendium of the Properties of Materials at Low Temperature (Phase I), Part I, Properties of Fluids, WADD-TR-60-56, Part I, Wright Air Development Division, Wright-Patterson Air Force Base, Ohio (July 1960) pp 3.001 and 3.006.

Kingery, W. D., Property Measurements at High Temperatures, "Heat Conduction and Radiation," John Wiley and Sons, Inc., New York (1959) pp 88-129.

Kingery, W. D., and McQuarrie, M. C., "Thermal Conductivity I. Concepts of Measurement and Factors Affecting Thermal Conductivity of Ceramic Materials," Journal of America Ceramic Soc., 37, (1954), p 67.

BIBLIOGRAPHY (CONT)

Larkin, B. K., and Churchill, S. W., "Scattering and Absorption of Electromagnetic Radiation by Infinite Cylinders," Journal of Opt. Soc. Am., 49, (1959), pp 188-190.

Lee, D. W., and Kingery, W. D., "Radiation Energy Transfer and Thermal Conductivity of Ceramic Oxides," Jour. Amer. Ceramic Soc., 43, No. 11 (November 1960), pp 594-607.

Loser, J. B., Moeller, C. E., and Thompson, M. B., Thermophysical Properties of Thermal Insulating Materials, ML-TDR-64-5, Materials Laboratory, Wright-Patterson Air Force Base, Ohio (April 1964), pp 257-258.

Reeder, Charles M., and Co., Catalog 1963-1965, Detroit, Michigan (1963).

Rolinski, E. J., et al, "Development of High Temperature Insulation Systems," Paper 66-43, Presented at AIAA Third Aerospace Sciences Meeting, New York (January 1966).

Schumann, T. E. W., and Voss, V., "Heat Flow Through Granulated Material," Fuel in Science and Practice, 13, No. 8, (August 1934), pp 249-256.

Van De Hulst, H. C., Light Scattering by Small Particles, John Wiley and Sons, Inc., New York (1957), pp 3-10, 383-390.

van der Held, E. F. M., "The Contribution of Radiation to the Conduction of Heat" II. Boundary Conditions, Applied Sci. Res. A 4, No. 2, (1953), pp 77-99.

van der Held, E. F. M., "The Contribution of Radiation to the Conduction of Heat," Applied Sci. Res., Section A, 3, (1952), pp 237-249.

Viskanta, R., and Grosh, R. J., "International Developments in Heat Transfer," Part IV, Am. Soc. Mech. Eng., New York (1961), pp 820-829.

Ward, J. M., "Reliability and Reproducibility of Leached Glass-Silica Fabrics," Paper Presented at the Fourth Annual Reliability and Maintainability Conference (ASME/AIAA/SAE/ASTME/AIChE/ASTM/EIA), Los Angeles, California (28-30 July 1965).

Wechsler, A. E., "Advances in High Temperature Thermal Protection Systems," Aerodynamically Heated Structures, Edited by P. E. Glaser, Prentice Hall, Inc., Englewood Cliffs, New Jersey (1962).

Wechsler, A. E., Kritz, M. A., and Glaser, P. E., "Thermal Conductivity of High Temperature Heterogeneous Insulations," Paper III-B, Proceedings of the 4th Conference on Thermal Conductivity, San Francisco, California, (October 1964).

UNCLASSIFIED
Security Classification

DOCUMENT CONTROL DATA - R&D

(Security classification of title, body of abstract and indexing annotation must be entered when the overall report is classified)

1 ORIGINATING ACTIVITY (Corporate author)	2a REPORT SECURITY CLASSIFICATION
Air Force Materials Laboratory Wright-Patterson Air Force Base, Ohio 45433	UNCLASSIFIED
	2b GROUP

3 REPORT TITLE

INVESTIGATION OF RADIATION AND CONDUCTION HEAT TRANSFER IN FIBROUS HIGH TEMPERATURE INSULATIONS

4 DESCRIPTIVE NOTES (Type of report and inclusive dates)

Final Report September 1965 - August 1967

5 AUTHOR(S) (Last name, first name, initial)

Rolinski, Edmund J., and Purcell, George V., Capt, USAF

6 REPORT DATE	7a TOTAL NO. OF PAGES	7b NO. OF REFS
December 1967	158	51

8a CONTRACT OR GRANT NO.	9a ORIGINATOR'S REPORT NUMBER(S)
b PROJECT NO. 7381, 7360	AFML-TR-67-251
c Task No. 738103, 736001	9b OTHER REPORT NO(S) (Any other numbers that may be assigned this report)
d	

10 AVAILABILITY/LIMITATION NOTICES This document is subject to special export controls and each transmittal to foreign governments or foreign nationals may be made only with prior approval of Air Force Materials Laboratory (MAYT), Wright-Patterson Air Force Base, Ohio 45433

11 SUPPLEMENTARY NOTES	12 SPONSORING MILITARY ACTIVITY
N/A	Air Force Materials Laboratory Air Force Systems Command Wright-Patterson AFB, Ohio 45433

13 ABSTRACT

The experimental investigation was concerned with understanding the mechanisms by which fibrous insulations attenuate the transfer of thermal energy. Three fibrous insulation materials, Dynaquarts, Sapphire Wool, and Dynaflex, were evaluated for their usefulness in the high temperature environment. Effective thermal conductivities were measured in air, argon, and vacuum up to 2500°F. Transmission experiments were carried out to evaluate the relative contribution of radiation attenuation parameters for Dynaquarts.

(Distribution of this abstract is unlimited.)

DD FORM 1 JAN 64 1473

UNCLASSIFIED
Security Classification

UNCLASSIFIED

Security Classification

14 KEY WORDS	LINK A		LINK B		LINK C	
	ROLE	WT	ROLE	WT	ROLE	WT
Thermal Conductivity **Fibrous Silica** **Heat Transfer** **High Temperature Insulations:** **Dynaquartz** **Sapphire Wool** **Dynaflex**						

INSTRUCTIONS

1. **ORIGINATING ACTIVITY:** Enter the name and address of the contractor, subcontractor, grantee, Department of Defense activity or other organization *(corporate author)* issuing the report.

2a. **REPORT SECURITY CLASSIFICATION:** Enter the overall security classification of the report. Indicate whether "Restricted Data" is included. Marking is to be in accordance with appropriate security regulations.

2b. **GROUP:** Automatic downgrading is specified in DoD Directive 5200.10 and Armed Forces Industrial Manual. Enter the group number. Also, when applicable, show that optional markings have been used for Group 3 and Group 4 as authorized.

3. **REPORT TITLE:** Enter the complete report title in all capital letters. Titles in all cases should be unclassified. If a meaningful title cannot be selected without classification, show title classification in all capitals in parenthesis immediately following the title.

4. **DESCRIPTIVE NOTES:** If appropriate, enter the type of report, e.g., interim, progress, summary, annual, or final. Give the inclusive dates when a specific reporting period is covered.

5. **AUTHOR(S):** Enter the name(s) of author(s) as shown on or in the report. Enter last name, first name, middle initial. If military, show rank and branch of service. The name of the principal author is an absolute minimum requirement.

6. **REPORT DATE:** Enter the date of the report as day, month, year, or month, year. If more than one date appears on the report, use date of publication.

7a. **TOTAL NUMBER OF PAGES:** The total page count should follow normal pagination procedures, i.e., enter the number of pages containing information.

7b. **NUMBER OF REFERENCES:** Enter the total number of references cited in the report.

8a. **CONTRACT OR GRANT NUMBER:** If appropriate, enter the applicable number of the contract or grant under which the report was written.

8b, 8c, & 8d. **PROJECT NUMBER:** Enter the appropriate military department identification, such as project number, subproject number, system numbers, task number, etc.

9a. **ORIGINATOR'S REPORT NUMBER(S):** Enter the official report number by which the document will be identified and controlled by the originating activity. This number must be unique to this report.

9b. **OTHER REPORT NUMBER(S):** If the report has been assigned any other report numbers *(either by the originator or by the sponsor)*, also enter this number(s).

10. **AVAILABILITY/LIMITATION NOTICES:** Enter any limitations on further dissemination of the report, other than those imposed by security classification, using standard statements such as:

(1) "Qualified requesters may obtain copies of this report from DDC."

(2) "Foreign announcement and dissemination of this report by DDC is not authorized."

(3) "U. S. Government agencies may obtain copies of this report directly from DDC. Other qualified DDC users shall request through _____."

(4) "U. S. military agencies may obtain copies of this report directly from DDC. Other qualified users shall request through _____."

(5) "All distribution of this report is controlled. Qualified DDC users shall request through _____."

If the report has been furnished to the Office of Technical Services, Department of Commerce, for sale to the public, indicate this fact and enter the price, if known.

11. **SUPPLEMENTARY NOTES:** Use for additional explanatory notes.

12. **SPONSORING MILITARY ACTIVITY:** Enter the name of the departmental project office or laboratory sponsoring *(paying for)* the research and development. Include address.

13 **ABSTRACT:** Enter an abstract giving a brief and factual summary of the document indicative of the report, even though it may also appear elsewhere in the body of the technical report. If additional space is required, a continuation sheet shall be attached.

It is highly desirable that the abstract of classified reports be unclassified. Each paragraph of the abstract shall end with an indication of the military security classification of the information in the paragraph, represented as *(TS)*, *(S)*, *(C)* or *(U)*.

There is no limitation on the length of the abstract. However, the suggested length is from 150 to 225 words.

14 **KEY WORDS:** Key words are technically meaningful terms or short phrases that characterize a report and may be used as index entries for cataloging the report. Key words must be selected so that no security classification is required. Identifiers, such as equipment model designation, trade name, military project code name, geographic location, may be used as key words but will be followed by an indication of technical context. The assignment of links, rules, and weights is optional.

UNCLASSIFIED

Security Classification

√ AD-827 107 Air Force Materials Lab., Wright-Patterson AFB, Ohio. Final rept. Sep 65-Aug 67. Rept. no. TR-67 251 Dec 67	No Foreign without approval of Air Force Materials Lab., Attn: MAYT, Wright-Patterson AFB, Ohio.	No limitation	AFML ltr, 14 Jan 69